Draft Manuscript for Review

Pyroxenite Layers in the Northern Apennines' Upper Mantle (Italy) – Generation by Pyroxenite Melting and Melt-infiltration

Journal:	*Journal of Petrology*
Manuscript ID	JPET-Sep-14-0127.R2
Manuscript Type:	Original Manuscript
Date Submitted by the Author:	n/a
Complete List of Authors:	Borghini, Giulio; University of Milano, Dipartimento di Scienze della Terra Ardito Desio; Università degli Studi Di Genova, Dipartimento di Scienze della Terra, dell'Ambiente e della Vita; Columbia University, Lamont Doherty Earth Observatory Rampone, Elisabetta; Università degli Studi Di Genova, Dipartimento di Scienze della Terra, dell'Ambiente e della Vita Zanetti, Alberto; Consiglio Nazionale delle Ricerche (CNR), Istituto di Geoscienze e Georisorse Class, Cornelia; Columbia University, Lamont Doherty Earth Observatory Cipriani, Anna; University of Modena and Reggio Emilia, Dipartimento di Scienze Chimiche e Geologiche; Columbia University, Lamont Doherty Earth Observatory Hofmann, Albrecht; Max Plank Institute of Chemistry, ; Columbia University, Lamont Doherty Earth Observatory Goldstein, Steven; Columbia University, Department of Earth and Environmental Sciences; Columbia University, Lamont Doherty Earth Observatory
Keyword:	pyroxenite, mantle heterogeneity, melt-rock reaction, mantle geochemistry, trace element, isotopes, External Liguride ophiolites, mafic layers, ultramafic

Pyroxenite Layers in the Northern Apennines' Upper Mantle (Italy) – Generation by Pyroxenite Melting and Melt-infiltration

GIULIO BORGHINI[1,2,3], ELISABETTA RAMPONE[2], ALBERTO ZANETTI[4], CORNELIA CLASS[3], ANNA CIPRIANI[3,5], ALBRECHT W. HOFMANN[3,6], STEVEN L. GOLDSTEIN[3,7]

[1]DIPARTIMENTO DI SCIENZE DELLA TERRA, UNIVERSITÀ DI MILANO, VIA BOTTICELLI 23, 20133 MILANO, ITALY
[2]DIPARTIMENTO DI SCIENZE DELLA TERRA, DELL'AMBIENTE E DELLA VITA, UNIVERSITÀ DI GENOVA, CORSO EUROPA 26, 16132 GENOVA, ITALY
[3]LAMONT-DOHERTY EARTH OBSERVATORY OF COLUMBIA UNIVERSITY, 61 ROUTE 9W, PALISADES, NY 10964, USA
[4]CNR-ISTITUTO DI GEOSCIENZE E GEORISORSE, SEZIONE DI PAVIA, VIA FERRATA 1, I-27100 PAVIA, ITALY
[5]DIPARTIMENTO DI SCIENZE CHIMICHE E GEOLOGICHE, UNIVERSITÀ DEGLI STUDI DI MODENA E REGGIO EMILIA, LARGO S. EUFEMIA 19, 41100 MODENA, ITALY
[6]MAX PLANCK INSTITUTE FOR CHEMISTRY, P.O. BOX 3060, 55020 MAINZ, GERMANY
[7]DEPARTMENT OF EARTH AND ENVIRONMENTAL SCIENCES OF COLUMBIA UNIVERSITY, LAMONT-DOHERTY EARTH OBSERVATORY, 61 ROUTE 9W, PALISADES, NY 10964, USA

http://dx.doi.org/10.1093/petrology/egv074

Corresponding Author:

Giulio Borghini
Dipartimento di Scienze della Terra "Ardito Desio"
Università degli Studi di Milano
Via Botticelli 23
20133 Milano (Italy)

Tel. 0039 02 50315600
Fax. 0039 02 50314597
Email: giulio.borghini@unimi.it

Keywords:

Pyroxenites, mantle heterogeneity, melt-rock reaction, mantle geochemistry, trace element, isotopes, External Ligurides ophiolites, mafic layers, ultramafic

Abstract

Pyroxenite layers embedded within peridotite represent wide-spread lithological mantle heterogeneities and are potential components in the mantle source of many oceanic basalts. Pyroxenites can be generated by several magmatic and metamorphic processes. However, in most natural samples (especially in ultramafic massifs), their primary characteristics are partially or completely erased by later petrologic evolution (e.g. metamorphism, metasomatism or partial melting). Here we investigate a suite of pyroxenites from the External Liguride Jurassic ophiolites (Northern Apennines, Italy). They are spinel-bearing websterites and clinopyroxenites, partially recrystallized under plagioclase-facies conditions, and occur as cm-scale layers parallel to the tectonite foliation of their host peridotites. Pyroxenites have bulk Mg-numbers from 74 to 88 and display rather constant LREE depletion over the MREE (La_N/Sm_N = 0.15-0.35), but variable MREE-HREE fractionation, with some of them having markedly positive HREE slopes (Sm_N/Yb_N=0.30-0.96). The HREE enrichment coupled with high Zr and Sc contents in clinopyroxene porphyroclasts from spinel-bearing domains provides strong evidence that garnet was present in the precursor mineral associations. Mass balance calculations suggest that the pyroxenites originally contained up to about 40 vol% of garnet, indicating they originated by segregation of melts at rather high pressure (P > 1.5 GPa). Parental melts of pyroxenites have reacted to some extent with the host peridotite during mantle infiltration. Lack of olivine in the primary mineral assemblage and orthopyroxene-rich rims along the contact with wall-rock peridotites indicate that pyroxenites have crystallized from silica-rich melts. These, likely, had REE patterns and Sr-Nd isotope compositions similar to enriched MORB. We propose that the pyroxenites originated from melts derived from a hybrid eclogite-bearing peridotite source, and then reacted with the host peridotite to form “secondary pyroxenites”. Their existence has been invoked in current models of basalts petrogenesis. During later decompression, they experienced an intermediate recrystallization at spinel-facies conditions, at 1.2-1.5 GPa and minimum temperature of 950-1000°C, and partial re-equilibration at low-pressure plagioclase-facies. The latter is dated by internal Sm-Nd isochrons at 178 (±8) Ma and is associated with Mesozoic exhumation, during extension of the Tethys lithosphere.

INTRODUCTION

Geochemical studies on oceanic basalts have documented that their upper mantle sources are chemically and isotopically heterogeneous (e.g. Hofmann, 2003). The nature, distribution and scale of such mantle heterogeneities are of fundamental importance for the understanding of the dynamics and long-term evolution of the upper mantle. Direct observations on mantle rocks, such as mantle xenoliths, abyssal peridotites and tectonically exhumed mantle sectors (Alpine-type peridotite massifs), have indicated that pyroxenite/mafic layers, commonly embedded within peridotite, represent wide-spread lithological mantle heterogeneities (e.g. Bodinier & Godard, 2003; Downes, 2007). Whether or not pyroxenite components occur in the upper mantle has been hotly debated during the last decades, mostly because of their potential involvement in mantle partial melting and generation of basalt (e.g. Hirschmann and Stolper 1996; Stracke et al., 1999; Salters & Dick, 2002; Kogiso et al., 2004a,b; Sobolev et al., 2005; Lambart et al., 2013).

Experimental studies (e.g. Yaxley & Green, 1998; Hirschmann et al., 2003; Pertermann & Hirschmann, 2003; Kogiso et al., 2004a; Sobolev et al., 2007; Lambart et al., 2009, 2012) have shown that the partial melting of mafic components, occurring at mantle depths as pyroxenites and eclogites, can produce highly variable melt compositions and, together with melts from depleted peridotite, reproduce the wide compositional range documented in oceanic basalts. On this basis, geochemical models have highlighted the role of a mixed pyroxenite-peridotite mantle source in the genesis of mid-ocean ridge (MORB) and ocean island (OIB) basalts (e.g. Allegre & Turcotte, 1986; Hirschmann & Stolper, 1996; Kogiso et al., 2004b; Sobolev et al., 2005; Stracke & Bourdon, 2009; Herzberg, 2011; Mallik & Dasgupta, 2012; Lambart et al., 2012).

The nature of mantle pyroxenites, however, remains a controversial subject, mostly because their origin has been related to a variety of magmatic and metamorphic processes, including: i) recycling of subducted oceanic crust stirred by mantle convection and incorporated into the lithosphere (e.g. Allègre & Turcotte, 1986; Kornprobst et al., 1990; Morishita & Arai, 2001; Morishita et al., 2003, Yu et al., 2010), ii) moderate- to high-pressure crystal segregation from magmas derived by melting of asthenospheric sources (Bodinier et al., 1987a,b; Vannucci et al., 1993; Rivalenti et al., 1995; Kempton et al., 1997; Takazawa et al., 1999; Mukasa & Shervais, 1999; Keshav et al., 2007; Dantas et al., 2007; Warren et al., 2009; Gysi et al., 2011) or subducted oceanic crust (Davies et al., 1993; Pearson et al., 1993; Becker, 1996; Pearson & Nowell, 2004), iii) refertilization of ‘infertile’ or ‘depleted’ upper mantle via melt-peridotite reactions (Garrido & Bodinier, 1999; Bodinier et al., 2008; Dantas

et al., 2009, van Acken et al., 2010). An additional difficulty in characterizing the role of pyroxenites in melting is associated with their reactivity within the mantle, causing them to be easily modified by magmatic and metamorphic processes subsequent to their emplacement at depth (e.g. Takazawa et al., 1999; Morishita & Arai, 2001; Morishita et al., 2003), interaction with transient melts (e.g. Garrido & Bodinier, 1999; Chazot et al., 2005; Kaeser et al., 2009), and decompressional partial melting (e.g. Pearson et al., 1993; Blichert-Toft et al., 1999; Montanini et al., 2012).

Orogenic and ophiolitic massifs offer the possibility to observe structural, spatial and geochemical relations between pyroxenites and host peridotites at different stages of their evolution (Bodinier & Godard, 2003). They are also important as the only locations with the possibility to gain insights on the distribution and extent of small-scale heterogeneities in the upper mantle through direct field observations. In this paper, we present petrographic, chemical and Sm-Nd isotope data on spinel pyroxenite samples from three, hundred-meter-sized ultramafic bodies from the western sector of the External Liguride Jurassic ophiolites (Northern Apennines, Italy; Fig. 1). Our microstructural and geochemical combined approach allows us to infer primary characteristics of pyroxenites, conditions and timing of their emplacement, geochemical affinities of their parental melts, and the later petrologic evolution. Our results impact the fundamental question of how pyroxenite components originate in the upper mantle, and provide further evidence of a "secondary-type" pyroxenite (also called "2stage" pyroxenite, Sobolev et al., 2005, 2007; Lambart et al., 2013) emplacement at rather deep mantle levels.

GEOLOGICAL BACKGROUND

Alpine-Apennine ophiolites represent lithospheric remnants of the Piemont-Ligurian ocean basin, a branch of the Mesozoic Tethys separating the European and Adriatic passive margins (Rampone & Hofmann, 2012, and references therein). The Middle Jurassic opening of the basin led to uplift and denudation of the subcontinental lithospheric mantle, the dominant lithotype exposed in Alpine-Apennine ophiolite sequences. Most of these mantle bodies have been affected by thermochemical erosion and refertilization processes, related to asthenospheric upwelling during rifting and oceanization (e.g. Rampone et al., 1997, 2004, 2008; Müntener et al., 2004; Piccardo et al., 2007). However, some of the mantle sequences from the Northern Apennines, namely the ultramafic massifs from the External Liguride Unit, have escaped these melt-rock interaction processes and preserved their old subcontinental signature (Beccaluva et al., 1984; Rampone et al., 1995; Montanini et al., 2006; Borghini et

al., 2011). The External Liguride (EL) ophiolites consist of large slide-blocks (up to km-scale) of ultramafic rocks, and minor MORB-type gabbros and basalts, within Cretaceous sedimentary melanges that were obducted during the closure of the Ligurian Tethys oceanic basin (Rampone et al., 1993, 1995; Tribuzio et al., 2004; Montanini et al., 2008). These mantle sequences consist mostly of fertile spinel-plagioclase lherzolites with disseminated Ti-rich amphibole and widespread spinel pyroxenite layers (Beccaluva et al., 1984). Lherzolites locally retain extremely "depleted" Nd-Sr isotopic compositions (Rampone et al., 1995) coupled with ancient Os model ages (1.6 Ga, Snow et al., 2000), which have been interpreted to reflect long residence times in the subcontinental mantle. The External Liguride ophiolitic mantle sequences have therefore been inferred to represent remnants of a fossil ocean-continent transition, where exhumed subcontinental mantle was associated with embryonic oceanic crust and rocks of continental origin (Marroni et al., 1998; Tribuzio et al., 2004; Montanini et al., 2008), an analogue to the modern Iberian passive margin (e.g. Whitmarsh et al., 2001).

Garnet pyroxenite layers from the northern sector of the External Liguride Unit have been recently investigated by Montanini et al. (2006, 2012) and consist of thin websterites and meter-scale thick garnet clinopyroxenites recording equilibration in the subcontinental lithosphere at T = 1100°C and P = 2.8 GPa. Sm-Nd and Lu-Hf geochronology on garnet-plagioclase pairs yielded 186±2 Ma and 220±13 Ma ages, interpreted as cooling ages that reflect the rifting-related exhumation of these mantle sectors (Montanini et al., 2006, 2012). Pyroxenites investigated in this study are from the southern sector of the Western External Liguride Unit (Suvero, La Spezia; Fig. 1). Borghini et al. (2011) recently showed that the peridotites from this mantle sector experienced a rather cold spinel- to plagioclase-facies decompressional tectonic evolution (T=870-930°C), thus confirming that this pyroxenite-peridotite association escaped melt-rock interaction and re-fertilization processes widely documented in most Alpine-Apennine ophiolitic peridotites (e.g. Müntener & Hermann, 1996; Rampone et al., 1997, 2004, 2008; Rampone & Borghini, 2008; Piccardo et al., 2004, 2007).

FIELD OCCURRENCE AND PETROGRAPHY

A summary of the location and description of samples is presented in Table 1. Pyroxenites occur as layers within the host mantle peridotites, mostly ranging in thickness from several millimetres to about 15 centimetres (Fig. 2). Samples GV12 and GV14 occur as lenses about 30 cm thick. Layers are parallel to the foliation plane of the host peridotites,

showing sharp contacts, and can be weakly boudinaged (Fig. 2d). In outcrop, pyroxenite layers are recognised by their pinkish or dark-grey colour (Fig. 2a,b,c) and by the occurrence of coarse black spinel grains. Pyroxenite abundance is variable, and in some outcrops can be as high as 50% (Fig. 2a,b). In some places, pyroxenite layers alternate with harzburgite portions within the peridotite, thus forming a compositional layering parallel to the tectonite foliation (Fig. 2a,d).

Most of the pyroxenites are characterized by a porphyroclastic texture defined by coarse-grained (up to 10-12 mm) porphyroclasts of pyroxenes and spinels, stretched along the tectonite foliation. Porphyroclastic minerals are partially substituted by a plagioclase-bearing granoblastic assemblage (Fig. 3a,b,c,d), indicating a retrograde evolution from spinel- to plagioclase-facies. The low-P metamorphic recrystallization is recorded by the development of i) millimeter and sub-millimeter bands of plagioclase and olivine (±amphibole) crystallized around coarse porphyroclasts of greenish spinels and pyroxenes (Fig. 3a,b), ii) orthopyroxene plus plagioclase exsolutions in large clinopyroxene porphyroclasts (Fig. 3b), iii) fine-grained (~200–300 μm) granoblastic aggregates made of plagioclase, olivine, newly formed pyroxenes and occasionally dark-brown spinel and brownish amphibole, partially replacing the spinel-facies pyroxene porphyroclasts (Fig. 3c,d). Amphibole is heterogeneously distributed in the pyroxenite samples and is always associated with the plagioclase-bearing neoblastic assemblage (Fig. 3d). In the most altered samples (GV14 and GV17), granoblastic olivine and plagioclase are almost completely substituted by low-T alteration products (chlorite and sausurrite, respectively).

Most of the pyroxenite samples are characterized by two alternating mineralogical domains: i) spinel-rich portions, where green spinel relics are rimmed by plagioclase and olivine (±amphibole), ii) pyroxene-bearing domains in which the large pyroxene porphyroclasts are partially substituted by neoblastic aggregates of new pyroxenes and plagioclase. The latter mineralogical feature is clearly observable in the thickest pyroxenite layers, whereas the two domains are usually stretched and boudinaged in the thinner bands (discussed further below). Most of the pyroxenite bands show irregular orthopyroxene-rich borders along the contact with the hosting peridotite (Fig. 3e). This is the result of interaction between the melt from which the pyroxenite crystallized and the host mantle peridotite during the pyroxenite emplacement (Borghini et al., 2013).

Olivine and amphibole are totally absent in pyroxenite GV12; this sample is texturally distinct and characterized by few small relics of clinopyroxene porphyroclasts that are strongly substituted by a fine-grained equigranular metamorphic texture consisting of

clinopyroxene, dark-green spinel and plagioclase (completely replaced by low-T alteration minerals, Fig. 3f). This granoblastic assemblage often forms clusters and seams stretched along the foliation (Fig. 3f).

ANALYTICAL METHODS

Whole-rock major and trace element analyses of pyroxenites were made by lithium metaborate/tetraborate fusion ICP-OES (for major elements) and ICP/MS (for trace elements) at the Actlabs Laboratories (Western Ontario, Canada; http://www.actlabs.com).

Mineral major element compositions were analyzed using: (1) a Philips SEM 515 equipped with an X-ray dispersive analyzer (accelerating potential 15 kV, beam current 20 nA), at the Dipartimento di Scienze della Terra, dell'Ambiente e della Vita, University of Genova, and (2) a JEOL JXA 8200 Superprobe equipped with five wavelength-dispersive (WDS) spectrometers, an energy dispersive (EDS) spectrometer, and a cathodoluminescence detector (accelerating potential 15 kV, beam current 15 nA), at the Dipartimento di Scienze della Terra "Ardito Desio", University of Milano. *In situ* trace element mineral analyses were carried out by laser ablation inductively coupled plasma mass spectrometry (LA-ICP-MS) at IGG-CNR in Pavia. A detailed description of analytical procedures is given in Miller et al. (2007).

Sm and Nd isotopic compositions were measured on clinopyroxene and plagioclase separates and on whole rock powders from pyroxenite samples. Clinopyroxenes and plagioclases (90-150 μm sized) were separated by grinding, sieving, electromagnetic separation and handpicking under a microscope. Weights of unleached mineral concentrates were 25-82 mg for clinopyroxenes and 54-132 mg for plagioclases. Minerals were leached in at least three steps using a solution of 5% HF + 6.2M HCl. Nd isotopic compositions, together with elemental abundances of Sm and Nd by isotope dilution, were measured by thermal ionization mass spectrometry (TIMS) on a VG Sector 54-30 at the Lamont-Doherty Earth Observatory of Columbia University (Palisades, NY, USA). The $^{143}Nd/^{144}Nd$ ratios were normalized to $^{146}Nd/^{144}Nd$ =0.7219, and reported relative to JNdi $^{143}Nd/^{144}Nd$ =0.512115 (Tanaka et al., 2000). Samples were analyzed during the course of 6 analytical sessions. Individual sample data were corrected to the standard values measured during the individual time intervals. Analyses of the JNdi-1 standard during the 6 sessions yielded $^{143}Nd/^{144}Nd$ ratios of 0.512080±9 (2σ, mean of n=7 analyses, 34 ppm external reproducibility), 0.512074±10 (n=10, 18 ppm), 0.512075±12 (n=13, 23 ppm), 0.512088±14 (n=5, 27 ppm),

0.512096±13 (n=26, 25 ppm), 0.512095±10 (n=5, 20 ppm). Total Sr and Nd blanks did not exceed 150 pg.

RESULTS

Bulk-rock chemistry

The bulk-rock major and trace element data of the pyroxenite samples (Table 2) display a large total range of Mg-numbers [molar $Mg/(Mg+Fe^{2+}_{tot})*100$] (74-88 mol%), although most values are concentrated between 83-85. Conversely, pyroxenites cover a large range of Al_2O_3 and CaO contents (10.6-16.5 wt% and 6.8-19.5 wt%, respectively; Fig. 4), mostly reflecting their modal variation between clinopyroxenite and websterite assemblages. In Figure 4, selected major and trace elements are plotted against Mg-number, together with the compositional fields of garnet pyroxenites and spinel-bearing websterites from orogenic and ophiolitic massifs (details and references in Fig. 4 caption).

Major element compositions of most samples lie in the fields of overlap between garnet-pyroxenites and spinel-bearing websterites from orogenic massifs at intermediate Mg-numbers (Fig. 4). However, they diverge from literature data by having generally higher CaO and lower Na_2O contents. Samples GV14 and GV17 have unusual, very low SiO_2 abundances (Table 2). Petrographic observations indicate that this is likely due to a high extent of low-temperature hydrothermal alteration, mostly dominated by chloritization of pyroxenes and olivine, as observed for many oceanic and ophiolitic mafic rocks (e.g. Alt et al., 1998). Pyroxenite lens GV12 plots within the compositional field of garnet pyroxenites, but with slightly higher CaO content (Fig. 4). Garnet-pyroxenites from other EL ultramafic massifs, recently studied by Montanini et al. (2012), show lower Mg-numbers and higher Na_2O, Al_2O_3 contents relative to our samples, but similar SiO_2 and CaO compositional variations (Fig. 4). In terms of Cr, Ni, V, Sc abundances, the pyroxenites also lie in the compositional field of overlap between garnet pyroxenites and websterites in the literature, except for samples GV12 and GV14, which plot within the compositional field of garnet-pyroxenites, at lower Mg values (Fig. 4). Our pyroxenites have low Cr, Ni (560-1530 ppm, 210-860 ppm, respectively) and moderate Sc, V (31-51 ppm, 163-280 ppm, respectively) concentrations. EL garnet-pyroxenites studied by Montanini et al. (2012) show similar values, at lower Mg-numbers (Fig. 4).

The CI-normalized REE and other refractory elements (Fig. 5) of most of the pyroxenites (BG3, BG4, BG5, BG13, BG14, BG22, GV10, GV17, MC3, MC5) display rather constant LREE depletion over the MREE (La_N/Sm_N = 0.15-0.35), but variable MREE-HREE

fractionation. In fact, the HREE slopes range from flat (GV17) to markedly positive (BG13) (Sm_N/Yb_N=0.30-0.96), with absolute concentrations varying from 3 to 20 x CI. In particular, samples BG13, GV10, MC3 and MC5 display HREE enriched patterns as observed in some garnet pyroxenites (e.g. Pearson et al., 1993; Gysi et al., 2011; Montanini et al., 2012). Spinel-rich clinopyroxenite GV12 has an overall lower REE content, showing a LREE-depleted pattern combined with slightly fractionated MREE to HREE (Sm_N/Yb_N=0.77). The pyroxenite GV14 shows a convex-upward pattern with HREE depletion over MREE (Sm_N/Yb_N=1.66). Finally, pyroxenite GV8 displays a nearly flat pattern at 3-4 x CI. Zr and Hf show a rather flat trend between Nd and Sm, with some small positive Zr anomalies. In contrast, Sr is highly enriched compared to the LREE. These "spikes" probably derived from later fluid-driven contamination as evidenced by very thin whitish veins orthogonal to the layer direction not completely eliminated from the samples during powder preparation for bulk-rock analysis. This is further supported by the absence of positive Sr anomalies in any of the porphyroclasts. Our samples have MREE-HREE abundances within the compositional field defined by the External Liguride garnet-pyroxenites studied by Montanini et al. (2012) (Fig. 5). However, they have higher LREE content, with the exception of sample GV12, which is consistent with literature data.

Mineral chemistry

Pyroxenes and spinel have Mg-numbers varying according to the Mg-number of their bulk-rock, and within each sample they show systematic major element variations according to the different mineral generations (porphyroblast vs. neoblast). Clinopyroxene porphyroclasts have Mg-numbers varying in agreement with their bulk-rock Mg-number, from 0.77 in the olivine-free clinopyroxenite GV12, to 0.88 in the high Mg-number websterites MC3 and MC5 (Table 3 and Fig. 6a). They also have rather high Al_2O_3 contents (6.21-10.12 wt%) and low Cr_2O_3 and Na_2O abundances (≤0.36 wt% and ≤1.0 wt% respectively; Table 3). A chemical profile on a representative pyroxenite layer shows that clinopyroxene porphyroclasts have Mg-numbers increasing from the center of the pyroxenite layer towards its margins (Suppl. Fig.1, and Suppl. Table 1), where Mg-numbers approach those of clinopyroxene of the host peridotite. As shown in Figure 6a, clinopyroxene neoblasts in each sample exhibit systematically lower Al_2O_3 concentrations (3.16-6.62 wt%) and higher Mg-numbers relative to corresponding clinopyroxene porphyroclasts. In the orthopyroxene porphyroclasts, the Mg-number varies from 0.82 to 0.88, and Al_2O_3 and CaO contents range between 4.33-7.56 wt% and 0.52-1.19 wt%, respectively (Table 4). Similar to clinopyroxenes,

orthopyroxene neoblasts display lower Al_2O_3 concentrations (1.17-3.43 wt%) and increased Mg-numbers (Fig. 6b); CaO abundance does not exceed 0.79 wt% (Table 4).

Coarse, millimeter-sized green spinels are characterized by very low Cr-numbers [molar Cr/(Cr+Al)] (average Cr-number between 0.01 and 0.03), Mg-numbers between 0.61-0.78, and TiO_2 lower than 0.24 wt% (Table 5). Small-sized, dark-brown spinels, associated with fine-grained plagioclase-bearing aggregates, show higher Cr-numbers (0.10-0.29) and TiO_2 contents (0.21-0.89 wt%), coupled to lower Mg-numbers (Fig. 7a,b).

Olivines have rather homogeneous compositions within each sample. Overall, olivine Mg-numbers vary between 0.80-0.87, in agreement with the bulk-rock Mg-number (Table 6). Plagioclase has anorthite contents [An = Ca/(Ca+Na)*100] of An_{55-68} in the cores of neoblasts; a few analyses on rims of plagioclase neoblasts gave significantly higher anorthite values (An_{74-83}; Table 7). Amphibole compositions range between kaersutite and Ti-rich pargasite (according to Leake classification 1997) with low K_2O (≤0.3 wt%) and Cr_2O_3 abundance not exceeding 1.37 wt% (Table 8).

In situ LA-ICP-MS trace element analyses have been performed mostly on clinopyroxene porphyroclasts and a few representative clinopyroxene, plagioclase and amphibole neoblasts (Table 9). Consistent with the bulk-rock REE variability described above, clinopyroxene porphyroclasts display heterogeneous trace element composition in the different samples (Fig. 8). LREE depletion (La_N/Sm_N=0.11-0.24) of clinopyroxene within a single sample is comparatively uniform, similar to the bulk-rock REE composition. However, the MREE to HREE are variably fractionated. Samples with the greatest bulk-rock MREE-HREE fractionation (BG13, GV10, MC3, MC5, Table 2) locally show marked HREE enrichment over the MREE in their clinopyroxenes (Sm_N/Yb_N=0.25-0.94; Yb_N=17.3-87.6) (Fig. 8a). Clinopyroxene porphyroclasts from pyroxenites with moderate bulk-rock HREE enrichment (BG4, BG5, BG14, BG22, GV17, Table 2) are similarly characterized by rather variable MREE-HREE fractionation, but with less pronounced HREE enrichment (Sm_N/Yb_N=0.60-1.20; Yb_N=10.2-42; Fig. 8b). Clinopyroxenes from the other pyroxenites show more homogeneous REE patterns (GV8, GV12, GV14, Fig. 8c), similar to their respective bulk-rock REE abundances (Fig. 5).

As described above, the thickest pyroxenite layer (sample GV10, Fig. 9) is characterized by two mineralogical domains, namely a spinel-rich and a pyroxene-rich domain. A trace element chemical profile within this single sample shows grain-to-grain (thin section scale, <5 cm) REE variability in clinopyroxene porphyroclasts, related to their microstructural location, i.e. in the spinel-rich versus pyroxene-rich domains (Suppl. Table 2).

We found that clinopyroxene porphyroclasts with the highest MREE-HREE fractionation are systematically located in the spinel-rich zone, and this HREE enrichment is coupled with higher Zr and Sc abundance relative to those in clinopyroxenes from the pyroxene-rich domains (Fig. 9). As discussed below, this peculiar chemical feature was likely inherited by metamorphic breakdown of precursor garnet in the primary assemblage.

Figure 8d shows the REE spectra of neoblasts from the plagioclase-bearing mineral assemblage of a representative sample (BG13). Compared to clinopyroxene porphyroclasts, clinopyroxene neoblasts always exhibit overall higher REE absolute concentrations and development of negative Eu anomalies. Amphiboles have REE patterns similar in shape to those of clinopyroxene neoblasts, but with higher absolute concentrations. Plagioclases have low REE abundances and LREE enrichment (La_N/Sm_N=3.55-5.41), as well as marked positive Eu anomalies.

Geothermometry

Conventional geothermometers, mostly based on Ca-Mg exchange between the two pyroxenes, have been applied to both spinel-facies porphyroclasts and plagioclase-bearing neoblasts (Table 10), in order to constrain the thermal evolution during the tectonic exhumation. For the spinel-facies pyroxenes, the two-pyroxene thermometers provide similar temperature ranges, between 830-940°C (Taylor, 1998) and 860-980°C ($T_{Opx-Cpx}$; Brey & Kohler, 1990), which are in good agreement with temperature estimated by the single-clinopyroxene thermometer of Nimis & Taylor (2000), between 820-960°C (Table 10). Systematically higher temperatures are obtained using the Ca-in-Opx thermometer of Brey & Kohler (1990), ranging between about 930 and 1100°C. As discussed by Nimis & Grutter (2010), the Ca-in-Opx thermometer is affected by a positive bias at temperatures lower than 1000°C; however, we observe (Table 10) that this overestimation of calculated T persists even after the empirical correction proposed by Nimis & Grutter (2010). Temperatures estimated for spinel-facies pyroxenes partially overlap the temperature range documented by Borghini et al. (2011) in the associated peridotites (940-1000°C), though extending to lower values. This is probably due to the higher extent of recrystallization shown by the pyroxenites relative to the host peridotites. The occurrence of thin (2-10 μm) exsolution in both clinopyroxene and orthopyroxene porphyroclasts of the pyroxenites suggests that the spinel-bearing porphyroclasts are likely affected by low-P re-equilibration. Accordingly, temperatures obtained for the spinel-facies stage must be considered as minimum T estimates.

Systematically lower temperature estimates have been calculated for the plagioclase-bearing neoblasts with four different thermometers: 830-890°C and 790-860°C with the Brey & Kohler (1990) thermometers (Ca-in Opx and Opx-Cpx, respectively), 770-860°C with the Taylor (1998) thermometer and 780-900°C with Nimis & Taylor (2000) thermometer. As observed for the spinel-facies minerals, Borghini et al. (2011) found temperatures up to 950°C in the plagioclase-facies recrystallization in the associated peridotites, about 50°C higher than those of the pyroxenites (Table 10).

Sr-Nd isotope compositions and Sm-Nd geochronology

Sr and Nd isotopic compositions of clinopyroxenes from pyroxenites investigated in this work have been reported by Borghini et al. (2013), together with spatially associated host rocks and distal peridotites, i.e. peridotite sampled in pyroxenite-free outcrops. In Figure 10a, the present-day Sr and Nd isotope ratios of pyroxenites are plotted along with isotopic data previously documented in orogenic and ophiolitic massifs (references reported in caption of Fig. 10), and the compositional field of global MORB (Class & Lehnert, 2012: PetDB Expert MORB, Mid-Ocean Ridge Basalt, Compilation. EarthChem Library. http://dx.doi.org/10.1594/IEDA/100060) and OIB (GEOROC database: http://georoc.mpch-mainz.gwdg.de/georoc/).

Our pyroxenites have MORB-type Sr and Nd isotopic compositions, and when compared to the data of pyroxenites from orogenic and ophiolitic massifs, they plot among the samples with the lowest $^{87}Sr/^{86}Sr$ and highest $^{143}Nd/^{144}Nd$ ratios (Fig. 10a). Initial εNd values computed at the inferred age of pyroxenite emplacement (433 ±51 Ma; Borghini et al., 2013) range between +3 and +8, consistent with enriched MORB compositions.

Here, we present new Sm-Nd isotopic data on plagioclase separates and whole-rock powders of selected pyroxenite samples that, together with clinopyroxene data from Borghini et al. (2013), are used to construct internal isochrons. The Sm-Nd isotopic compositions of whole-rocks and leached clinopyroxene and plagioclase mineral separates of selected pyroxenites are listed in Table 11, together with elemental abundances of Nd and Sm determined by isotope dilution. The latter are largely within 10% of the bulk-rock analyses (Table 2), and most of Sm and Nd concentrations in clinopyroxenes and plagioclases obtained by ID are within the variability shown by corresponding *in situ* LA-ICP-MS data (Table 9).

Sm-Nd internal isochrons have been defined by whole rock, plagioclase and clinopyroxene for pyroxenites BG13, BG14 and GV8, and by plagioclase and clinopyroxene for sample BG5 (Fig. 11). Age calculations have been performed using Isoplot (Ludwig,

2003). The strong Sm-Nd fractionation between plagioclase and clinopyroxene in the four pyroxenite samples provides for well-constrained ages of 177±13, 178±11, 174±25 and 183±14 Ma. According to petrographic features, these ages date the event of partial metamorphic recrystallization at low-pressure plagioclase-facies conditions, as temperature estimates for plagioclase-facies neoblasts (Table 10) are largely higher than the closure temperature for the Sm-Nd system (Mezger et al., 1992). Considering that the ages are indistinguishable within uncertainty, and given the field and geochemical evidence of the decompressional evolution, documented also in the associated host peridotites (Borghini et al., 2011), we conclude that the EL pyroxenite-peridotite mantle experienced subsolidus recrystallization in a single event. The age of this event is given by the weighted average of the individual internal isochrons, at 178±8 Ma.

DISCUSSION

Reconstruction of the precursor mineral assemblage

The pyroxenites investigated in this study contain an older spinel-bearing mineral assemblage partially replaced by subsequent plagioclase-bearing neoblastic aggregates (Fig. 3). However, some microstructural and chemical features shown by several pyroxenite samples suggest that variable modal amounts of garnet were present in the precursor mineral associations. The most important evidence is that clinopyroxene porphyroclasts from spinel-rich domains systematically show HREE enrichment coupled to high Zr and Sc contents (Fig. 9). These compositional features can be explained by the replacement of previously existing garnet, which preferentially partitions HREE over the MREE. Moreover, the Zr and Sc Kd values of garnet/melt are much higher than those of clinopyroxene/melt (e.g. Hauri et al., 1994; Johnson, 1998, Ionov et al., 2002). Conversely, experimentally determined Kds (spinel/melt) for HFSE are about an order of magnitude lower than those of both garnet and clinopyroxene (Horn et al., 1994). Similar trace element characteristics of precursor garnets have been previously documented by Vannucci et al. (1993) in pyroxenes of spinel+plagioclase-bearing pyroxenites from Zabargad (Red Sea). They also observed that this garnet imprint has been partially erased by subsequent metamorphic recrystallization at lower pressure and is only evident in a few relicts. Low pressure overprinting could also explain the variability of HREE-MREE fractionation of clinopyroxene porphyroclasts in spinel-rich domains of our pyroxenites (Fig. 9). Zr and Sc enrichments seem to be better preserved, as shown by the kink in the chemical profile of Figure 9, even though Zr and Sc contents could have been higher in the early garnet and later partially smoothed by chemical

diffusion during subsequent spinel- and plagioclase-facies partial re-equilibration. It is remarkable that Sc contents observed in clinopyroxene porphyroclasts from spinel-rich and pyroxene-rich domains match very well with the range of Sc variations in garnet and its equilibrium clinopyroxene, respectively, documented by Müntener et al. (2010) in garnet pyroxenite from Totalp and Malenco (Fig. 9).

The CMAS projection in the garnet-pyroxene plane of pyroxenite bulk-rock compositions is usually considered as evidence of primary crystallization of a mineral assemblage dominated by garnet and pyroxene (e.g. Garrido & Bodinier, 1999; Takazawa et al., 1999). Accordingly, in the CaTs-Fo-Qz triangle of Figure 12, most pyroxenites plot close to the enstatite-garnet-CaTs line.

HREE enrichment over the MREE shown by some pyroxenite bulk-rock REE spectra (samples BG13, GV10, MC3, MC5; Fig. 5) is comparable to that observed in garnet-bearing pyroxenites from orogenic ultramafic massifs (e.g. Beni Bousera, Pearson et al., 1991, 1993; Kumar et al., 1996; Gysi et al., 2011; Ronda, Garrido & Bodinier, 1999; Pyrenees, Bodinier et al., 1987a), and has been interpreted as indicative of high-pressure magmatic segregation of garnet (e.g. Kornprobst et al., 1969, 1970; Loubet & Allegre 1982). Similar bulk HREE-MREE fractionation indicating precursor garnet has been documented in low-pressure recrystallized pyroxenites from Zabargad and Horoman (Vannucci et al., 1995; Takazawa et al., 1999).

In order to test the hypothesis of a precursor garnet-bearing assemblage in some of our pyroxenites, we performed a mass balance calculation to derive an estimate of the original modal compositions, in two separate steps. First, we calculated the modal abundances of a potential garnet-bearing assemblage by using whole-rock major element data of the studied pyroxenites (Table 2) and mineral compositions of garnet pyroxenites having similar bulk-rock chemistry from the literature (see details below). Mass balance calculations, performed by weighted least-squares minimization, included seven major element oxides (SiO_2, TiO_2, Al_2O_3, Cr_2O_3, FeO, MgO, CaO and Na_2O), and were computed by using the software Wolfram Mathematica 8. The quality of the fit was evaluated based on the sum of the squares of the residuals (R2 in Table 12); we considered as realistic only the computed garnet-bearing assemblages with errors well below 1.

In the second step, we derived the hypothetical Sm_N/Yb_N ratios of bulk-rocks from the Sm_N/Yb_N ratios of minerals used to calculate the primary garnet-bearing assemblage.

Results of the first step of the mass balance calculation are reported in Table 12, together with the spinel-facies modes computed using the whole rock major element

abundances and the compositions of spinel-facies porphyroclasts in each pyroxenite. We estimated garnet-bearing modes by adopting the mineral compositions of selected garnet pyroxenite samples from the Beni Bousera (Gysi et al., 2011) and Pyrenees (Bodinier et al., 1987a) ultramafic massifs, with bulk-rock compositions similar to our pyroxenites (sample B7, B9 and B15 with Mg-numbers ranging from 78-85, Gysi et al., 2011; sample 70-379 Mg-number = 86, Bodinier et al., 1987a; Figure 4, Suppl. Table 3 and Suppl. Fig. 2). Beni Boussera pyroxenites cover a broader range in both whole-rock and mineral chemistry, thus providing a larger choice of compositions that can better simulate our samples, particularly in terms of major element contents of garnet and pyroxenes (Gysi et al., 2011). Garnet websterites from the Pyrenees have minerals with Mg-numbers comparable with our samples MC3 and MC5 (Fig. 4 and Suppl. Table 3).

In addition to pyroxene, garnet and spinel compositions from literature garnet pyroxenites, we used, in the mass balance calculation, the average composition of olivine measured in each sample, as it strongly depends on bulk-rock Mg-number and it is not expected to change composition in the different mineral assemblages within a single sample.

The mass balance shows that all the bulk pyroxenite compositions characterized by HREE enrichment over the MREE are consistent with primary garnet-bearing assemblages, with modal garnet varying between 20-40 vol% (samples BG13, GV8, GV10, GV12, MC3, MC5, Table 12). Moreover, our calculations show that lower garnet modal abundances (generally_<17 vol%) could have been present in the precursor assemblage also for other pyroxenites with nearly flat MREE-HREE spectra (samples BG4, BG5, BG14, Table 12). This is, for example, documented in some garnet pyroxenites from Beni Bousera, characterized by bulk-rock REE patterns lacking MREE-HREE fractionation (Gysi et al., 2011).

The reliability of the computed garnet-bearing mineral modes has then been checked by comparing calculated bulk $(Sm/Yb)_N$ ratios with measured values (Fig. 13). Except for sample BG14, good agreement is generally observed between the two values. Pyroxenites with Mg-numbers between 74 and 84 are well modelled by major and trace element data of minerals from Beni Bousera garnet pyroxenites (sample B7, B9 and B15; Gysi et al., 2011), whereas pyroxenites MC3 and MC5, with slightly higher Mg-numbers (86-87), yield a better fit using data from Pyrenean garnet websterites (Bodinier et al., 1987a). For samples GV14 and GV17 with very low SiO_2 bulk-rock abundances, we could not compute realistic garnet-bearing assemblages, and their spinel-bearing modal compositions have also the highest errors (R2, Table 12). In terms of the estimated REE patterns (Suppl. Fig. 2), our mass balance

modelling is able to simulate the overall MREE-HREE fractionation, but does not reproduce the kink between Sm and Gd. It must be noted that modelling is very sensitive to the MREE-to-HREE compositions of garnet and pyroxenes used in the calculation. However, selective Gd_N-Yb_N enrichment in whole-rock chemistry has been documented also in garnet pyroxenite from the literature (e.g. Gysi et al., 2011; Marchesi et al., 2013).

We are well aware that the above mass balance calculations do not constitute absolute proof of the occurrence of garnet in the precursor assemblage. They do, however, demonstrate that this is a highly plausible explanation for the otherwise rather difficult-to-explain abundance patterns of the HREE. Garnet has important implications for the chemistry of melts formed in its presence, and for the depth of melting, and we will explore some of the consequences of this in the remainder of this paper.

Origin of pyroxenites by deep melt infiltration

Garnet pyroxenites have been described in orogenic and ophiolitic ultramafic massifs (Downes, 2007, and references therein; Montanini et al., 2006, 2012; Gysi et al., 2011, Marchesi et al., 2013), and in mantle xenoliths (e.g. Jacob, 2004; Bizimis et al., 2005; Gonzaga et al., 2009), and their origin has been related to a range of processes. Garnet is the typical high-pressure metamorphic Al-rich mineral in both mantle peridotites and pyroxenites (Herzberg, 1978; Gasparik, 1984). In addition, a garnet-bearing assemblage can result from high-pressure crystallization of a mafic magma or by complete high-pressure metamorphic recrystallization of mafic rocks with primary low-pressure mineral assemblages (i.e., "eclogites").

Garnet pyroxenites of both origins can be present in a single ultramafic massif, as documented in Lherz (Bodinier et al., 1987a,b), Ronda (Garrido & Bodinier, 1999) and Beni Boussera (Kornpbrost et al., 1990). In some garnet pyroxenites, whole-rock trace element compositions with positive Eu and Sr anomalies, relatively low HREE and MREE, and high LREE/HREE, reflect high modal abundances of primary plagioclase, and thus they have been considered of crustal origin (e.g. Kornpbrost et al., 1990; Garrido & Bodinier, 1999; Morishita et al., 2003, Marchesi et al., 2013). In some garnet pyroxenites from Beni Boussera, a low-P crustal imprinting is also supported by peculiar Nd-Hf-O isotopic compositions (Pearson et al., 1993; Pearson & Nowell, 2004). Based on geochemical and isotopic data, a similar conclusion has also been inferred for a few garnet pyroxenites from other sectors of the External Liguride ophiolites by Montanini et al. (2006, 2012). When compared to our pyroxenites, the latter have significantly lower bulk Mg-numbers and higher Al_2O_3 and Na_2O

contents (Fig. 4). Montanini et al. (2012) inferred that these garnet pyroxenites represent either melt residues of precursor eclogites, or high-pressure segregation products of eclogite-derived melts. Pyroxenites investigated in our study are not consistent with these origins. First, they lack the trace element bulk-rock compositions indicative of plagioclase-rich gabbros characterized by positive Sr and Eu anomalies, rather high LREE and very low HREE, thus, ruling out an origin as recrystallization products from low-pressure magmatic protoliths (Fig. 5). Second, almost flat or weakly LREE-depleted bulk REE spectra (La_N/Sm_N= 0.15-0.66; Table 2) do not support an origin as melting residues of precursor mafic rocks (Fig. 5).

Instead, the inferred occurrence of primary garnet in most samples (Table 12) indicates that the pyroxenites likely originated by segregation of melts at rather high pressure, as garnet is stable at P >1.5 GPa in pyroxenitic assemblages (e.g. Kogiso et al., 2004, Downes 2007). Garnet-bearing assemblages have been obtained by crystallization of a hydrous primitive magma in experiments at 1.2 GPa and variable T (Müntener et al., 2001). However, the bulk compositions of these experimental magmatic products do not match the compositions of our pyroxenites (Fig. 4), and the lack of evidence of primary amphibole in the pyroxenites does not support the origin from a hydrous melt.

Geochemical affinity of the parental melts

In this section we discuss the nature of the parental melts to the pyroxenites, but note two major limitations: i) the primary garnet-facies mineral assemblage has been completely obliterated by metamorphic recrystallization events, most likely related to the tectonic exhumation of the pyroxenite-peridotite mantle sequence (Borghini et al., 2011), ii) magmatic interaction and/or subsolidus diffusion between pyroxenite and host peridotite have likely partially modified the original chemical signatures of the melts (e.g. the Mg-number). This precludes the possibility to compute equilibrium melts by using the present trace element mineral composition. Therefore, the nature of pyroxenite parental melts can only be inferred by combining available microstructural and chemical observations.

The bulk-rock Mg-numbers vary from 74-88, and are inversely correlated with the thickness of layers and lenses, and positively correlated with the bulk Ni contents (Fig. 14). An inverse relationship between dyke thickness and bulk Mg-number has been documented in pyroxenitic layers from the Lherz ultramafic massif and explained as the result of local chemical re-equilibration with the adjacent peridotite (Bodinier et al., 1987b; Fabries et al., 2001). Bodinier et al. (2008) have investigated in detail this process by studying some

pyroxenites from Ronda (Spain). These authors performed numerical modeling demonstrating that interaction between the host peridotite and variably evolved melts can generate pyroxenites with Mg-numbers intermediate between those of the peridotite and melts.

The chemical profile along the GV10 pyroxenite (9 cm-long, Fig. 9 and Suppl. Fig. 1), where data were acquired only in cores of large clinopyroxene porphyroclasts, shows a significant zonation across the pyroxenite layer, with Mg-numbers of clinopyroxenes at the margins of the layer close to those of clinopyroxenes in the surrounding peridotite (a complete data set of this profile is provided in Suppl. Tables 1 and 2). Similar chemical gradients have been described across mafic-peridotite associations from orogenic massifs (e.g. Pearson et al., 1993; Takazawa et al., 1999; Mazzucchelli et al., 2010). They indicate that most of these pyroxenites, having a thickness of only a few centimetres, do not reflect equilibrium with the infiltrating parental melts but rather show a modified Mg-number due to the interaction with the surrounding peridotite. Accordingly, the composition of clinopyroxene porphyroclasts from the core of our thickest pyroxenite layer, GV10 and lens GV12, are likely to be the least affected by interaction with the peridotite. We thus used their compositions to calculate the Mg-number of the equilibrium parental melt, with the equation $Mg\#_{melt} = (K^{cpx}{}_{Fe\text{-}Mg} * Mg\#_{cpx})/(1\text{-}Mg\#_{cpx} + Mg\#_{cpx} * K^{cpx}{}_{Fe\text{-}Mg})$ proposed by Wood and Blundy (1997).

We assume that primary garnet-bearing clinopyroxenes had Mg-numbers similar to those of spinel-facies clinopyroxenes, because Mg-number is not expected to be significantly modified by subsequent lower-pressure recrystallization (e.g. Robinson & Wood, 1998). Computed Mg-numbers of the melt vary between 52-56 for layer GV10 and 44-50 for lens GV12. Melts with such values, significantly lower than the Mg-number of melts in equilibrium with mantle minerals, must have been very reactive with the surrounding peridotite. This is consistent with the occurrence of orthopyroxene-rich rims at the pyroxenite-peridotite boundary, as well as the orthopyroxene blebs and orthopyroxene modal enrichment in the wall rocks documented by Borghini et al. (2013).

Orthopyroxene enrichment at the pyroxenite-peridotite boundaries has been documented in other ultramafic massifs (e.g. Bodinier et al., 1987a; Varfalvy et al., 1996; Takazawa et al., 1999), and interpreted as the result of either solid-state reaction (e.g. Kogiso et al., 2004b; Herzberg et al., 2011) or reaction between high-silica activity melts, coming from the pyroxenites, and the surrounding peridotite (e.g. Varfalvy et al., 1996; Yaxley & Green, 1998; Sobolev et al., 2005; Lambart et al., 2012). In the studied pyroxenites, Borghini et al. (2013) have documented that clinopyroxenes in the first few (<5) centimetres of the host peridotite, at the contact with the pyroxenite layer (i.e. our so-called “wall-rock” peridotite),

have been chemically modified. In particular, the cm-scale progressive REE enrichment observed in clinopyroxene porphyroclasts of wall-rock peridotite points to reactive percolation of the pyroxenite-derived melt into the adjacent mantle. This is also consistent with the complete isotopic resetting observed in the first centimeters of the wall-rock peridotite (Borghini et al., 2013).

Lack of evidence for precursor garnet in the host peridotites suggests that this melt-rock reaction process occurred under spinel-facies mantle conditions, at pressures below garnet-lherzolite stability (P <2.8 GPa, e.g. O'Neill et al., 1981; Robinson & Wood, 1998), but likely above 1.5 GPa, to account for the garnet-bearing primary modes reconstructed for the pyroxenites. Spinel-facies clinopyroxene porphyroclasts in the wall-rock peridotites, thus, retain a trace element signature acquired by the interaction with the pyroxenite-derived melts (Borghini et al., 2013), and their REE composition can be used to obtain information on the geochemical signature of the pyroxenite parental melts.

Computed melts in equilibrium with wall-rock clinopyroxene porphyroclasts in the three profiles investigated by Borghini et al. (2013) are shown in Figure 15. We note here that a large set of trace element data has been filtered in order to select only the clinopyroxene porphyroclasts not affected by the subsequent plagioclase-bearing recrystallization, for example by checking Sr-Zr elemental variations (Rampone et al., 1993). However, the effect of a partial subsolidus plagioclase-facies re-equilibration would tend to slightly increase the REE absolute contents in clinopyroxene, without causing significant change of the LREE/HREE fractionation (Rampone et al., 1993; Hellebrand et al., 2005). Equilibrium melts are characterized by enrichment of LREE over HREE (La_N/Yb_N = 4-7.6) and moderate MREE-HREE fractionation (Dy_N/Yb_N = 1.2-1.4). The resulting melts have LREE significantly higher than a normal MORB and, rather, they resemble the REE compositions of enriched MORBs (E-type MORB) sampled in oceanic settings (Hemond et al., 1993, 2006; Hoernle et al., 2011; Waters et al., 2011). This is consistent with the initial epsilonNd values of clinopyroxenes in the pyroxenites, ranging from +3.29 to +8.25 (Borghini et al., 2013).

In summary, based on our microstructural and chemical observations, we conclude that the studied pyroxenites have originated from the segregation of low-Mg-number E-MORB melts. Moreover, very low alkali abundances of the bulk-rock pyroxenite compositions (Fig. 4 and Table 2), suggest a tholeiitic affinity of the parental melts.

Borghini et al. (2013) showed that interaction of EL pyroxenites with wall-rock peridotites reset the Nd isotopic compositions of the wall-rocks. They demonstrated that Sm-Nd isotopic investigations on clinopyroxene from pyroxenite-wall rock peridotite pairs

provide linear correlations yielding ages of 424-452 Ma, which are in good agreement with the age resulting from the errorchron defined by all pyroxenites (433±51 Ma), thus indicating the most likely timing of melt infiltration and pyroxenite emplacement. The ages indicate that this event significantly predated the Mesozoic evolution of this mantle sector (discussed below), and may have been related to Late Ordovician-Silurian lithosphere extension that led to the opening of the PaleoTethys oceanic basin (e.g. Stampfli & Borel 2002; von Raumer & Stampfli, 2008; Murphy et al., 2008).

Inferences on the nature of mantle source

The computed Mg-numbers of the parental melt (44-56) of the pyroxenites are too low to represent a primitive basaltic melt from a peridotitic mantle source (e.g. Walter, 1998). This indicates that pyroxenites originated either from i) a peridotite-derived melt that experienced significant chemical evolution, or ii) a melt derived by melting of a low-Mg-number hybrid source. The first hypothesis has been inferred for garnet pyroxenites from xenoliths (e.g. Frey et al., 1980; Keshav et al., 2007) and orogenic massifs (e.g. Bodinier et al., 1987a,b), and requires processes of liquid-crystal separation. A commonly invoked mechanism of high-pressure crystal segregation and melt differentiation is the dynamic flow crystallization in conduits described by Irving (1980). This model provides a possible alternative to the cumulus processes requiring the settling of crystals by gravity in magma chambers, a process difficult to be envisaged at pressures above 1.5 GPa within a plastically-deforming peridotite. However, how hydraulic fractures can form at such depth is unknown, because the deep mantle is not expected to be brittle enough to fracture (e.g. Kelemen et al., 1995, 1997). Moreover, it is noteworthy that the lowest Mg-number computed for our pyroxenite parental melts (around 44-50) would require more than 60% of fractional crystallization of a primitive melt with a Mg-number of 70 (Villiger et al., 2004). This would imply that a large amount of magmatic products should have been created in the mantle, before generating the evolved melt parental to the observed pyroxenites. Although there is no evidence of such large fractionation processes, we cannot exclude that this process played a role in the origin of our pyroxenites.

An alternative hypothesis calls for the involvement of a low-MgO mafic source component, as proposed for some pyroxenites from orogenic and ophiolitic massifs (e.g. Garrido & Bodinier, 1999; van Acken et al., 2010; Montanini et al., 2012; Marchesi et al., 2013; Montanini & Tribuzio, 2015). This means that low-Mg-number melts parental to pyroxenites can be the result of partial melting of a precursor mafic/pyroxenitic component or

a mixed pyroxenite-peridotite source. Several experimental studies have been dedicated to the melting behaviour of mafic lithologies at variably high pressure, and they have shown that a wide range of melt compositions can be produced, depending on the choice of starting bulk composition (e.g. Kogiso et al., 2004; Lambart et al., 2013).

In a review study on the composition of melts produced by pyroxenite melting at high pressure (>2 GPa), Kogiso et al. (2004) suggested that silica-deficient (SD) pyroxenites can be involved in the genesis of alkalic OIB lavas, whereas mixing of silica-excess (SE) pyroxenite melts with MgO-rich peridotitic melts would account for the genesis of tholeiitic OIB. Lack of olivine in the primary garnet-bearing assemblage of our pyroxenites (Table 12), together with the occurrence of orthopyroxene-rich rims along the contact with wall-rock peridotites, indicate that the observed pyroxenites have crystallized from melts with high silica activity, suggesting the involvement of a silica-excess pyroxenite component (e.g. Sobolev et al., 2005, 2007). Conversely, olivine-rich websterite and wehrlite are expected to form by reaction between melts produced by melting of SD pyroxenites and a peridotite (Lambart et al., 2012). Furthermore, the compositions of the pyroxenites in the proximity of the thermal divide in the pseudo-ternary CaTs-Fo-Qz diagram (see Fig. 12), suggest that they could have formed by partial melting of mantle sources with mixed eclogite-peridotite lithologies (Yaxley and Green, 1998; Kogiso et al., 1998; Takahashi & Nakajima, 2002; Mallik and Dasgupta, 2012; Fig. 12). Mallik and Dasgupta (2012) have recently demonstrated that saturated tholeiitic melts, with Mg-numbers as low as about 56, can form through reaction between eclogite-derived partial melts and a fertile peridotite. Remarkably, the compositions of such melts cover the range defined by our pyroxenites in the CMAS system (Fig. 12).

We propose that the EL pyroxenites originated from melts produced by a hybrid eclogite-peridotite mantle source, further modified through reaction with the host peridotite after their infiltration. The E-MORB signature inferred for the parental melts is consistent with this origin, given that similar E-MORB melts from modern mid-ocean-ridge settings are often interpreted to be the products of partial melting of a mantle peridotite source enriched by a pyroxenitic/mafic component (e.g. Hémond et al., 2006; Waters et al., 2011; Hoernle et al., 2011).

The major limitation of this hypothesis is that these low-Mg-number melts are highly reactive in the mantle; indeed, if their migration occurs by pervasive porous flow, then the compositions of these melts are expected to be rapidly buffered by reaction with the host peridotite (e.g. Daines & Kohlstedt, 1994). However, the occurrence of residues of precursor

eclogites within the EL mantle sector, in the form of garnet pyroxenites (Montanini et al., 2012), may support the scenario of a pristine eclogite-bearing mantle affected by partial melting. This could also indicate that such melts, after their production, migrated only over short distances, thus, preventing significant re-equilibration with the surrounding peridotite. The migration of these melts could have been enhanced by stress-driven melt segregation along shear zones, a mechanism able to produce high-permeability pathways within partially molten ductile rocks (e.g. Holtzman et al., 2003; Havlin et al., 2013). This is consistent with some field and geochemical evidence (Borghini unpublished), suggesting that the pyroxenite emplacement occurred within an already plastically deformed mantle. Part of the evolved signature of parental melts to the pyroxenites, such as the low Mg-numbers, could have been acquired by crystal segregation and melt evolution along these high-porosity magma conduits.

In summary, a possible scenario is that low-Mg-number melts produced by moderate degrees of SE pyroxenite/eclogite melting were mixed with low-degree peridotitic melts, which infiltrated and reacted with the overlying mantle to form the Suvero suite of pyroxenites layers.

This scenario is in agreement with recent models of basalt petrogenesis that invoke the generation of secondary pyroxenites in the upper mantle by interaction between peridotites and silica-rich melts derived by deeper melting of mafic components prior to major basalt production with larger degrees of melting (Sobolev et al., 2005, 2007; Lambart et al., 2012). According to our petrological reconstruction, the EL pyroxenites represent an excellent natural example of such secondary pyroxenites. We argue that partial melting of mafic components within a rising heterogeneous mantle, and the infiltration of the resulting melts, reacting with the host mantle peridotites, are efficient processes to generate additional heterogeneities in the upper mantle (Garrido & Bodinier, 1999; Borghini et al., 2013; Marchesi et al., 2013; Montanini & Tribuzio, 2015).

Metamorphic evolution and timing of exhumation

The mass balance modelling in this work accounts for the fractionation of HREE over the MREE shown by the bulk composition of many of the pyroxenites, thus supporting the hypothesis that they originally contained a primary garnet-bearing mineral assemblage, which is not preserved. The oldest mineral assemblage observed in the pyroxenites consists of coarse porphyroclasts of green spinel, clinopyroxene ± orthopyroxene, partially replaced by plagioclase-bearing neoblasts. The occurrence of plagioclase+olivine coronas around spinel porphyroclasts suggests that plagioclase did not originate directly from the breakdown of the

garnet-bearing assemblage. Rather, textural observations indicate that the plagioclase-bearing neoblastic assemblage replaced a previous spinel-bearing association, thus suggesting that plagioclase appeared at lower pressure than the spinel+pyroxenes assemblage. This is in agreement with experimental results on a low-Na garnet-spinel websterite (pyroxenite R394 from Irving, 1974) and computed subsolidus phase relations for a low-Na, high-Mg websterite from Ronda ultramafic massif (southern Spain, Hidas et al., 2013). A similar mineralogical evolution has been documented in Mg-rich clinopyroxenites and websterites from other External Liguride Units, and related to progressive mantle exhumation, from garnet- to spinel- to plagioclase-facies conditions (Montanini et al., 2006).

Thermometric estimates on cores of coarse spinel-facies pyroxenes indicate temperatures around 950-1000°C, which must be considered as minimum temperatures, given the occurrence of exsolution textures in both pyroxenes. According to experimental results on a garnet-spinel websterite, the spinel-bearing assemblage observed in the pyroxenites should record a recrystallization stage within the P-T range of 1.2-1.5 GPa and T <1200°C, as this is expected to be the solidus temperature at 1.5 GPa (Irving 1974).

Continued pressure decrease led to crystallization of a plagioclase-bearing neoblastic assemblage at the expense of spinel-facies porphyroclasts. This process is accompanied by systematic changes in mineral compositions, including lower Al content in pyroxenes (Fig. 6) and higher Cr-number and TiO_2 content at lower Mg-number in the small relicts of spinel (Fig. 7), similar to what is observed in plagioclase peridotites of metamorphic origin (e.g. Gasparik, 1984; Rampone et al., 1993; Montanini et al., 2006; Borghini et al., 2010, 2011). Borghini et al. (2011) previously traced the exhumation of mantle peridotite hosting the pyroxenites from 0.7 to 0.3 GPa by applying thermometric estimates on neoblastic pyroxenes and experimentally-derived An-isopleths of plagioclase. Therefore, we infer that associated pyroxenites reasonably followed the same P-T path as the host peridotites. Average compositions of plagioclase in pyroxenites (core: An = 0.58-0.64; rim: An = 0.76-0.82; Table 6) are very close to those documented in the associated peridotites (core: An = 0.56-0.59; rim: An = 0.74-0.79; Borghini et al., 2011). This may indicate that the plagioclase composition does not depend on the bulk-rock chemistry even in pyroxenite bulks, which are significantly different from peridotite lithologies (Borghini et al., 2010), however, this needs to be confirmed by further experimental data. As a consequence, according to the An in plagioclase geobarometer proposed by Borghini et al. (2011), the similarity of An contents would constitute robust evidence that plagioclase crystallized contemporaneously in both pyroxenites and peridotites during their decompressional evolution.

Internal Sm-Nd isochrons, based on clinopyroxene-plagioclase-whole rocks analyses performed on four samples, give an average age of 178 (±8) Ma (Fig. 11) for the plagioclase-facies recrystallization event, which dates the exhumation of this mantle sector at relatively shallow depth. This age is slightly younger than the ages obtained by internal Sm-Nd isochrons documented in garnet pyroxenites investigated by Montanini et al. (2006). They proposed a Middle to Late Triassic age for the near-isothermal spinel- to plagioclase-facies decompression recorded by the External Liguride mantle section. Sm-Nd ages provided by this study indicate that exhumation of this EL mantle sector occurred in the Early Jurassic, which is coeval with the first syn-rift MOR-type intrusions in the subcontinental mantle of the Piedmont-Ligurian oceanic basin (Tribuzio et al., 2004, Rampone et al., 2014).

CONCLUDING REMARKS

Pyroxenites form centimetre-thick layers and lenses in peridotite from the External Liguride ultramafic massif (Northern Apennines, Italy); they range from websterites to clinopyroxenites, and are characterized by a porphyroclastic spinel-facies assemblage partially replaced by a low-pressure plagioclase-bearing neoblastic association.

Microstructural and chemical features shown by several pyroxenite samples suggest that variable modal amounts of garnet were present in the primary mineral association, thus indicating that pyroxenites likely originated by segregation of melts at rather high pressure (above 1.5 GPa).

Chemical and Sr-Nd isotopic compositions indicate that pyroxenites crystallized from a E-MORB-type melt, similar to those documented in modern mid-ocean-ridge settings. Low Mg-numbers together with the lack of olivine in most of the primary mineral assemblages suggest that their parental melts were produced by partial melting of a hybrid pyroxenite-bearing mantle, which then reacted with the host peridotite during high-pressure infiltration. The EL pyroxenites studied in this work are an example of a "secondary pyroxenite" component in the upper mantle, which has been proposed in recent models of basalt petrogenesis at oceanic intra-plate and mid-ocean ridge settings.

Finally, later decompressional metamorphic evolution from spinel- to plagioclase-facies followed the same P-T path defined for the host peridotites (Borghini et al., 2011). Low-P plagioclase-facies re-equilibration is dated by internal (clinopyroxene-plagioclase-whole rocks) Sm-Nd isochrons at 178±8 Ma, indicating that the exhumation of this mantle sector can be attributed to the Mesozoic continental rifting that led to the opening of the Jurassic Tethys.

ACKNOWLEDGEMENTS

This study was supported by the University of Genova (grant PRA2011 and PRA2013), the U.S. National Science Foundation grant ANT10-43540 (to Class and Goldstein), and the Storke Endowment of the Department of Earth and Environmental Sciences of Columbia University. L. Negretti and A. Risplendente are greatly thanked for assistance with the EDS and WDS analyses. L. Bolge, Y. Cai, P. Montagna and N. Rollins are acknowledged for their laboratory and analytical help. Reviews by J.-L. Bodinier, O. Müntener and an anonymous referee are gratefully acknowledged for constructive criticisms and suggestions, which improved an early version of the paper. We thank M. Wilson for the editorial handling. This is Lamont-Doherty Earth Observatory (LDEO) Contribution # XXXX (number to be filled in if accepter for publication).

REFERENCES

Adam, J., Green, T. H. & Day, R.A. (1992). An experimental study of two garnet pyroxenite xenoliths from the Bullenmerri and Gnotuk Maars of western Victoria, Australia. *Contributions to Mineralogy and Petrology* **111**, 505–514.

Allègre, C.J. & Turcotte, D.L. (1986). Implications of a two-component marble-cake mantle: *Nature* **323**, 123–127.

Alt, J.C., Teagle, D.A.H., Brewer, T., Shanks, W.C. & Halliday, A. (1998). Alteration and mineralization of an oceanic forearc and ophiolite-oceanic crust analogy. *Journal of Geophysical Research* **103**, 12365-12380.

Anders, E. & Grevesse, N. (1989). Abundances of the elements: meteoric and solar: *Geochimica et Cosmochimica Acta* **53**, 197–214.

Beccaluva, L., Macciotta, G., Piccardo, G. B. & Zeda, O. (1984). Petrology of lherzolitic rocks from the Northern Apennine ophiolites. *Lithos* **17**, 299–316.

Becker, H. (1996). Crustal trace element and isotopic signatures in garnet pyroxenites from garnet peridotite massifs from Lower Austria. *Journal of Petrology* **37**, 785-810.

Bizimis, M., Sen, G., Salters, V.J.M. & Keshav, S. (2005). Hf–Nd–Sr isotope systematics of garnet pyroxenites from Salt Lake Crater, Oahu, Hawaii: evidence for a depleted component in Hawaiian volcanism. *Geochimica et Cosmochimica Acta* **69**, 2629-2646.

Blichert-Toft, J., Albare`de, F. & Kornprobst, J. (1999). Lu–Hf isotope systematics of garnet pyroxenites from Beni Bousera, Morocco: implications for basalt origin. *Science* **283**, 1303–1306.

Bodinier, J.-L., Guiraud, M., Fabries, J., Dostal, J. & Dupuy, C. (1987a). Petrogenesis of layered pyroxenites from the Lherz, Freychinede and Prades ultramafic bodies (Ariege, French Pyrenees). *Geochimica et Cosmochimica Acta* **51**, 279-290.

Bodinier, J.-L., Fabries, J., Lorand, J.-P., Dostal, J. & Dupuy, C. (1987b). Geochemistry of amphibole pyroxenite veins from the Lherz and Freychinede ultramafic bodies (Ariege, French Pyrenees). *Bull. Mineral.* **110**, 345-358.

Bodinier, J.-L. & Godard, M. (2003). Orogenic, ophiolitic and abyssal peridotites: Treatise on Geochemistry, v. 2, H.D. Holland and K.K. Turkian (eds). Oxford, UK, Elsevier Science.

Bodinier, J.-L., Garrido, C.J., Chanefo, I., Bruguier, O. & Gervilla, F. (2008). Origin of pyroxenite-peridotite veined mantle by refertilization reactions: Evidence from the Ronda peridotite (Southern Spain). *Journal of Petrology* **49**, 999-1025.

Borghini, G., Fumagalli, P. & Rampone, E. (2010). The stability of plagioclase in the upper mantle: subsolidus experiments on fertile and depleted lherzolite. *Journal of Petrology* **51**, 229-254.

Borghini, G., Fumagalli, P. & Rampone, E. (2011). The geobarometric significance of plagioclase in mantle peridotites: A link between nature and experiments: *Lithos* **126**, 42–53.

Borghini, G., Rampone, E., Zanetti, A., Class, C., Cipriani, A., Hofmann, A.W. & Goldstein, S. (2013). Meter-scale Nd isotopic heterogeneity in pyroxenite-bearing Ligurian peridotites encompasses global-scale upper mantle variability. *Geology* **41**, 1055-1058.

Brey, G.P. & Köhler, T. (1990). Geothermobarometry in four-phase lherzolites II. New thermobarometers, and practical assessment of existing thermobarometers. *Journal of Petrology* **31**, 1353-1378.

Chazot, G., Charpentier, S., Kornprobst, J., Vannucci, R. & Luais, B. (2005). Lithospheric mantle evolution during continental break-up: the West Iberia non-volcanic passive margin. *Journal of Petrology* **46**, 2527-2568.

Class, C. & Lehnert, K. (2012). PetDB Expert MORB, Mid-Ocean Ridge Basalt, Compilation. EarthChem Library. http://dx.doi.org/10.1594/IEDA/100060.

Daines, M.J. & Kohlstedt, D.L. (1994). The transition from porous to channelized flow due to melt/rock reaction during melt migration. *Geophys. Res. Lett.* **21**, 145-148.

Dantas, C., Ceuleneer, G., Gregoire, M., Python, M., Freydier, R., Warren, J. & Dick, H.J.B. (2007). Pyroxenites from the Southwest Indian Ridge, 9–16°E: cumulates from incremental melt fraction produced at the top of a cold melting regime. *Journal of Petrology* **48**, 647-660.

Dantas, C., Gregoire, M., Koester, E., Conceicao, R.D. & Rieck Jr., N. (2009). The lherzolite-websterite xenolith suite from Northern Patagonia (Argentina): evidence of mantle-melt reaction processes. *Lithos* **107**, 107-120.

Davies, G. R., Nixon, P. H., Pearson, D. G. & Obata, M. (1993). Tectonic implications of graphitized diamonds from the Ronda peridotite massif, southern Spain. *Geology* **21**, 471–474.

Downes, H. (2007). Origin and significance of spinel and garnet pyroxenites in the shallow lithospheric mantle: Ultramafic massifs in orogenic belts in Western Europe and NW Africa. *Lithos* **99**, 1-24.

Fabries, J., Lorand, J.-P. & Guiraud, M. (2001). Petrogenesis of the amphibole-rich veins from Lherz orogenic lherzolite massif (Easter Pyrenees, France): a case study for the origin of orthopyroxene-bearing amphibole pyroxenites in the lithospheric mantle. *Contribution to Mineralogy and Petrology* **140**, 383-403.

Frey, F.A. (1980). The origin of pyroxenites and garnet pyroxenites from Salt Lake Crater, OAHU, Hawaii: trace element evidence. *American Journal of Science* **280**, 427-449.

Garrido, C.J. & Bodinier, J.L. (1999). Diversity of mafic rocks in the Ronda peridotite: evidence for pervasive melt–rock reaction during heating of subcontinental lithosphere by upwelling asthenosphere. *Journal of Petrology* **40**, 729-754.

Gasparik, T. (1984). Two-pyroxene thermobarometry with new experimental data in the system CaO-MgO-Al_2O_3-SiO_2. *Contribution to Mineralogy and Petrology* **87**, 87-97.

Green, D.H. & Falloon, T.J. (1998). Pyrolite: A Ringwood concept and its current expression. In: The Earth's Mantle, edited by I. Jackson, 311-378, Cambridge University Press, Cambridge.

Gonzaga, R.G., Lowry, D., Jacob, D.E., LeRoex, A., Schulze, D. & Menzies, M.A. (2009). Eclogites and garnet pyroxenites: similarities and differences. *J. Volcanol. Geotherm. Res.* **190**, 235-247.

Gysi, A.P., Jagoutz, O., Schmidt, M.W. & Targuisti, K. (2011). Petrogenesis of pyroxenites and melt infiltrations in the ultramafic complex of Beni Boussera, Northern Morocco. *Journal of Petrology* **52**, 1676-1735.

Hauri, E.H., Wagner, T.P. & Grove, T.L. (1994). Experimental and natural partitioning of Th, U, Pb and other trace elements between garnet, clinopyroxene and basaltic melts. *Chemical Geology* **117**, 149-166.

Havlin, C., Parmentier, E.M. & Hirth, G. (2013). Dike propagation driven by melt accumulation at the lithosphere-asthenosphere boundary. *Earth and Planetary Sciences Letters* **376**, 20-28.

Hellebrand, E., Snow, J.E., Mostefaoui, S. & Hoppe P. (2005). Trace element distribution between orthopyroxene and clinopyroxene in peridotites from Gakkel Ridge: a SIMS and NanoSIMS study. *Contribution to Mineralogy and Petrology* **150**, 486-504.

Hémond, C., Arndt, N.T., Lichtenstein, U. & Hofmann, A.W. (1993). The heterogeous Iceland plume: Nd-Sr-O isotopes and trace element constraints. *Journal of Geophysical Research* **98**, 15833-15850.

Hémond, C., Hofmann, A.W., Vlastelic, I. & Nauret, F. (2006). Origin of MORB enrichment and relative trace element compatibilities along the Mid-Atlantic Ridge between 10° and 24°N. *Geochemistry Geophysics Geosystems* **7**, Q12010.

Herzberg, C.T. (1978). Pyroxene geothermometry and geobarometry: experimental and thermodynamic evaluation of some subsolidus phase relations involving pyroxenes in the system CaO-MgO-Al_2O_3-SiO_2. *Geochimica et Cosmochimica Acta* **42**, 945-957.

Herzberg, C. (2011). Identification of source lithology in the Hawaiian and Canary Island: implications for origins. *Journal of Petrology* **52**, 113-146.

Hidas, K., Garrido, C., Tommasi, A., Padron-Navarta, J.A., Thielmann, M., Konc, Z., Frets, E. & Marchesi, C. (2013). Strain localization in pyroxenite by reaction-enhanced softening in the shallow subcontinental lithospheric mantle. *Journal of Petrology* **54**, 1997-2031.

Hirschmann, M.M. & Stolper, E.M. (1996). A possible role for garnet pyroxenite in the origin of the 'garnet signature' in MORB. *Contributions to Mineralogy and Petrology* **124**, 185-208.

Hirschmann, M. M., Kogiso, T., Baker, M. B. & Stolper, E. M. (2003). Alkalic magmas generated by partial melting of garnet pyroxenite. *Geology* **31**, 481-484.

Hoernle, K., Hauff, F., Kokfelt, T.F., Haase, K., Garbe-Shonberg, D. & Werner, R. (2011). On- and off-axis chemical heterogeneities along the South Atlantic Mid-Ocean-Ridge (5–11°S): shallow or deep recycling of ocean crust and/or intraplate volcanism? *Earth and Planetary Science Letters* **306**, 86-97.

Hofmann, A.W. (1988). Chemical differentiation of the earth: the relationships between mantle, continental crust and oceanic crust. *Earth and Planetary Science Letters* **90**, 297-314.

Hofmann, A.W. (2003). Sampling mantle heterogeneity through oceanic basalts: Isotopes and trace elements, in Carlson, R.W., ed., The Mantle and Core: Treatise on Geochemistry, v. 2, 61-101.

Holtzman, B., Groebner, N., Zimmerman, M., Ginsberg, S. & Kohlstedt, D. (2003). Stress-driven melt segregation in partially molten rocks. *Geochem. Geophys. Geosyst.* **4**, 8607.

Horn, I., Foley, S.F., Jackson, S.E. & Jenner, G.A. (1994). Experimentally determined partitioning of high field strength- and selected transition elements between spinel and basaltic melt. *Chemical Geology* **117**, 193-218.

Ionov, D. A., Bodinier, J. L., Mukasa, S. B. & Zanetti, A. (2002). Mechanisms and sources of mantle metasomatism: major and trace element conditions of peridotite xenoliths from Spitzbergen in the context of numerical modelling. *Journal of Petrology* **43**, 2219-2259.

Irving, A.J. (1974). Geochemical and high pressure experimental studies on garnet pyroxenite and pyroxene granulite xenoliths from the Delegate basaltic pipes. Australia. *Journal of Petrology* **15**, 1-40.

Jacob, D.E. (2004). Nature and origin of eclogite xenoliths from kimberlites. *Lithos* **77**, 295-316.

Jacobsen, S.B. & Wasserburg, G.J. (1980). Sm-Nd isotopic evolution of chondrites. *Earth and Planetary Science Letters* **50**, 139-155.

Johnson, K.T.M. (1998). Experimental determination of partition coefficient for rare earth and high-field-strenght elements between clinopyroxene, garnet, and basaltic melt at high pressures. *Contributions to Mineralogy and Petrology* **133**, 60-68.

Kelemen, P.B., Whitehead, J.A., Aharonov, E. & Jordahl, K.A. (1995). Experiments on flow focusing in soluble porous-media, with applications to melt extraction from the mantle. *Journal of Geophysical Research* **100**, 475-496.

Kelemen, P.B., Hirth, G., Shimizu, N., Spiegelman, M. & Dick, H.J.B. (1997). A riview of melt migration processes in the adiabatically upwelling mantle beneath oceanic spreading ridges. *Philosophical Transactions: Mathematical, Physical and Engineering Sciences* **355**, 283-318.

Kempton, P.D. & Stephens, C.J. (1997). Petrology and geochemistry of nodular websterites inclusions in harzburgite, Hole 920D, in Karson, J.A., et al., eds., Proceedings of the Ocean Drilling Program, Scientific results **153**: College Station, Texas, Ocean Drilling Program, p. 321-331.

Kaeser, B., Olker, B., Kalt, A., Altherr, R. & Pettke, T. (2009). Pyroxenite xenoliths from Marsabit (Northern Kenya): evidence for different magmatic events in the lithospheric mantle and interaction between peridotite and pyroxenite. *Contributions to Mineralogy and Petroogy* **157**, 453-472.

Keshav, S., Sen, G. & Presnall, D.C. (2007). Garnet-bearing xenoliths from Salt Lake Crater,

Oahu, Hawaii: high-pressure fractional crystallisation in the oceanic mantle. *Journal of Petrology* **48**, 1681-1724.

Kogiso, T., Hirose, K. & Takahashi, E. (1998). Melting experiments on homogeneous mixtures of peridotite and basalt: application to the genesis of ocean island basalts. *Earth and Planetary Science Letters* **162**, 45-61.

Kogiso, T., Hirschmann, M. M. & Frost, D. J. (2003). High-pressure partial melting of garnet pyroxenite: possible mafic lithologies in the source of ocean island basalts. *Earth and Planetary Science Letters* **216**, 603-617.

Kogiso, T., Hirschmann, M.M. & Pertermann, M. (2004a). High-pressure partial melting of mafic lithologies in the mantle. *Journal of Petrology* **45**, 2407-2422.

Kogiso, T., Hirschmann, M.M. & Reiners, W. (2004b). Length scales of mantle heterogeneities and their relationship to ocean island basalt geochemistry. *Geochimica et Cosmochimica Acta* **68**, 345-360.

Kornprobst, J., Piboule, M., Roden, M. & Tabit, A. (1990). Corundum-bearing garnet clinopyroxenites at Beni Bousera (Morocco): original plagioclase-rich gabbros recrystallized at depth within the mantle? *Journal of Petrology* **31**, 717-745.

Kumar, N., Reisberg, L. & Zindler, A. (1996). A major and trace element and strontium, neodymium, and osmium isotopic study of a thick pyroxenite layer from the Beni Bousera ultramafic complex of northern Morocco. *Geochimica et Cosmochimica Acta* **60**, 1429-1444.

Lambart, S., Laporte, D. & Schiano, P. (2009). An experimental study of pyroxenite partial melts at 1 and 1·5 GPa: implications for the major-element composition of mid-ocean ridge basalts. *Earth and Planetary Science Letters* **288**, 335-347.

Lambart, S., Laporte, D., Provost, A. & Schiano, P. (2012). Fate of pyroxenite-derived melts in the peridotitic mantle: thermodynamic and experimental constraints. *Journal of Petrology* **53**, 451-476.

Lambart, S., Laporte, D., and Schiano, P. (2013). Markers of the pyroxenite contribution in the major-element compositions of oceanic basalts: Review of the experimental constraints. *Lithos* **160-161**, 14-36.

Leake, B.E. (1997). Nomenclature of amphiboles: report of the subcommittee on amphiboles of the international mineralogical association, commission on new minerals and mineral names. *American Mineralogists* **82**, 1019-1037.

Lehnert, K., Su, Y., Langmuir, C., Sarbas, B. & Nohl, U. (2000). A global geochemical database structure for rocks. *Geochemistry Geophysics Geosystems* **1**, 1012-1025.

Loubet, M. & Allègre, C.J. (1982). Trace elements in orogenic lherzolites reveal the complex history of the upper mantle. *Nature* **298**, 809.

Mallik, A. & Dasgupta, R. (2012). Reaction between MORB-eclogite derived melts and fertile peridotite and generation of ocean island basalts. *Earth and Planetary Science Letters* **329-330**, 97-108.

Marchesi, C., Garrido, C.J., Bosch, D., Bodinier, J-L., Hidas, K., Padron-Navarta, A. & Gervilla, F. (2012). A late Oligocene suprasubduction setting in the Westernmost Mediterranean revealed by intrusive pyroxenite dikes in th Ronda peridotite (Southern Spain). *Journal of Geology* **120**, 237-247.

Marchesi, C., Garrido, C.J., Bosch, D., Bodinier, J-L., Gervilla, F. & Hidas, K. (2013). Mantle refertilization by melts of crustal-derived garnet pyroxenite: Evidence from the Ronda peridotite massif, southern Spain. *Earth and Planetary Science Letters* **362**, 66-75.

Marroni, M., Molli, G., Montanini, A. & Tribuzio, R. (1998). The association of continental crust rocks with ophiolites in the Northern Apennines (Italy): implications for the continent-ocean transition in the Western Tethys: *Tectonophysics* **292**, 43-66.

Mazzucchelli, M., Zanetti, A., Rivalenti, G., Vannucci, R., Correia, C.T. & Tassinari, C.C.G. (2010). Age and geochemistry of mantle peridotites and diorite dykes from the Baldissero body: Insights into the Paleozoic-Mesozoic evolution of the Southern Alps. *Lithos* **119**, 485-500.

Mezger, K., Essene, E.J. & Halliday, A.N. (1992). Closure temperature of the Sm-Nd system in metamorphic garnets. *Earth Planetary Sciences Letters* **113**, 397-409.

Miller, C., Zanetti, A., Thoni, C. & Konzett, J. (2007). Eclogitisation of gabbroic rocks: redistribution of trace elements and Zr in rutile thermometry in an Eo-Alpine subduction zone (Eastern Alps). *Chemical Geology* **239**, 96-123.

Montanini, A., Tribuzio, R. & Anczkiewicz, R. (2006). Exhumation history of a garnet pyroxenite-bearing mantle section from a continent-ocean transition (Northern Apennine ophiolites, Italy). *Journal of Petrology* **47**, 1943-1971.

Montanini, A., Tribuzio, R. & Thirlwall, M. (2012). Garnet clinopyroxenite layers from the mantle sequences of the Northern Apennine ophiolites (Italy): Evidence for recycling of crustal material. *Earth and Planetary Science Letters* **351-352**, 171-181.

Montanini, A. & Tribuzio, R. (2015). Evolution of recycled crust within the mantle: constraints from the garnet pyroxenites of the External Ligurian ophiolites (northern Apennines, Italy). *Geology* **43**, 911-914.

Morishita, T. & Arai, S. (2001). Petrogenesis of corundum-bearing mafic rock in the

Horoman Peridotite Complex, Japan. *Journal of Petrology* **42**, 1279-1299.

Morishita, T., Arai, S., Gervilla, F. & Green, D. H. (2003). Closed-system geochemical recycling of crustal materials in the upper mantle. *Geochimica et Cosmochimica Acta* **67**, 303-310.

Mukasa, S.B. & Shervais, J.W. (1999). Growth of sub-continental lithosphere: Evidence from repeated injections in the Balmuccia lherzolite massif, Italian Alps. *Lithos* **48**, 287-316.

Müntener, O., Hermann, J. (1996). The Val Malenco lower crust – Upper mantle complex and its field relations (Italian Alps). *Schweizerische Mineralogishe und Petrographische Mitteilungen* **76**, 475-500.

Müntener, O., Kelemen, P.B. & Grove, T.L. (2001). The role of H2O during crystallization of primitive arc magmas under uppermost mantle conditions and genesis of igneous pyroxenites: an experimental study. *Contributions to Mineralogy and Petrology* **141**, 643-658.

Müntener, O., Pettke, T., Desmurs, L., Meier, M. & Schaltegger. U. (2004). Refertilization of mantle peridotite in embryonic ocean basins: trace element and Nd-isotopic evidence and implications for crust-mantle relationships. *Earth and Planetary Science Letters* **221**, 293-308.

Müntener, O., Manatschal, G., Desmurs, L. & Pettke, T. (2010). Plagioclase peridotites in Oceanic-Continent transitions: refertilized mantle domains generated by melt stagnation in the shallow mantle lithosphere. *Journal of Petrology* **51**, 255-294.

Murphy, B.J., Gutierrez-Alonso, G., Fernandez-Suarez, J. & Braid, J.A. (2008). Probing crustal and mantle lithosphere origin through Ordovician volcanic rocks along the Iberian passive margin of Gondwana. *Tectonophysics* **461**, 166-180.

Nimis, P., Taylor, W.R. (2000). Single-clinopyroxene thermobarometry for garnet peridotites. Part I. Calibration and testing of a Cr-in- Cpx barometer and an enstatite-in-Cpx thermometer. *Contributions to Mineralogy and Petrology* **139**, 541-554.

Nimis, P. & Grutter, H. (2010). Internally consistent geothermometers for garnet peridotites and pyroxenites. *Contributions to Mineralogy and Petrology* **159**, 411-427.

O'Hara, M.J. (1968). The bearing of phase equilibria studies in synthetic and natural systems on the origin and evolution of basic and ultrabasic rocks. *Earth-Science Reviews* **4**, 69-133.

O'Neill, H. St. C. (1981). The transition between spinel lherzolite and garnet lherzolite, and its use as a geobarometer. *Contributions to Mineralogy and Petrology* **77**, 185-194.

Pearson, D.G., Davies, G.R. & Nixon, P.H. (1993). Geochemical constraints on the petrogenesis of diamond facies pyroxenites from the Beni Bousera peridotite massif, North Morocco. *Journal of Petrology* **34**, 125-172.

Pearson, D.G. & Nowell, G.M. (2004). Re-Os and Lu-Hf isotope constraints on the origin and age of pyroxenites from the Beni Bousera peridotite massif: implications for mixed peridotite-pyroxenite mantle source. *Journal of Petrology* **45**, 439-455.

Pertermann, M. & Hirschmann, M. M. (2003). Anhydrous partial melting experiments on MORB-like eclogite: phase relations, phase compositions and mineral–melt partitioning of major elements at 2– 3 GPa. *Journal of Petrology* **44**, 2173–2201.

Piccardo, G.B., Zanetti, A., Poggi, E., Spagnolo, G. & Müntener, O. (2007). Melt/peridotite interaction in the Lanzo South peridotite: field, textural and geochemical evidence. *Lithos* **94**, 181-209.

Rampone, E., Piccardo, G.B., Vannucci, R., Bottazzi, P. & Ottolini, L. (1993). Subsolidus reactions monitored by trace element partitioning: the spinel- to plagioclasi-facies transition in mantle peridotites. *Contribution to Mineralogy and Petrology* **115**, 1-17.

Rampone, E., Hofmann, A.W., Piccardo, G.B., Vannucci, R., Bottazzi, P. & Ottolini, L. (1995). Petrology, mineral and isotope geochemistry of the External Liguride peridotites (Northern Appennine, Italy). *Journal of Petrology* **123**, 61-76.

Rampone, E., Piccardo, G.B., Vannucci, R. & Bottazzi, P. (1997). Chemistry and origin of ted melts in ophiolitic peridotites. *Geochimica et Cosmochimica Acta* **61**, 4557-4569.

Rampone, E., Hofmann, A.W. & Raczek, I. (1998). Isotopic contrasts within the Internal Liguride ophiolite (N. Italy): the lack of a genetic mantle-crust link. *Earth and Planetary Science Letters* **163**, 175-189.

Rampone, E., Romairone, A. & Hofmann, A.W. (2004). Contrasting bulk and mineral chemistry in depleted peridotites: evidence for reactive porous flow. *Earth and Planetary Science Letters* **218**, 491-506.

Rampone, E., Piccardo, G.B. & Hofmann, A.W. (2008). Multi-stage melt-rock interaction in the Mt. Maggiore (Corsica, France) ophiolitic peridotites: microstructural and geochemical records. *Contribution to Mineralogy and Petrology* **156**, 453-475.

Rampone, E. & Hofmann, A.W. (2012). A global overview of isotopic heterogeneities in the oceanic mantle. *Lithos* **148**, 247-261.

Rampone, E., Borghini, G., Romairone, A., Abouchami, W., Class, C. & Goldstein, S.L. (2014). Sm-Nd geochronology of the Erro-Tobbio gabbros (Ligurian Alps, Italy): insights on the evolution of the Alpine Tethys. *Lithos* **205**, 236-246.

Rivalenti, G., Mazzucchelli, M., Vannucci, R., Hofmann, A.W., Ottolini, L. & Obermiller, W. (1995). The relationship between websterite and peridotite in the Balmuccia peridotite massif (NW Italy) as revealed by trace element variations in clinopyroxene. *Contributions to Mineralogy and Petrology* **121**, 275-288.

Robinson, J.A.C. & Wood, B.J. (1998). The depth of the spinel to garnet transition at the peridotite solidus. *Earth and Planetary Science Letters* **164**, 277-284.

Salters, V.J.M. & Dick, H.J.B. (2002). Mineralogy of the mid-ocean-ridge basalt source from neodymium isotopic composition of abyssal peridotites. *Nature* **418**, 68-72.

Sinigoi, S., Comin-Chiaramonti, P., Demarchi, G. & Siena, F. (1983). Differentiation of partial melts in the mantle: evidence from the Balmuccia peridotite, Italy. *Contributions to Mineralogy and Petrology* **82**, 351-359.

Snow, J. E., Schmidt, G. & Rampone, E. (2000). Os isotopes and highly siderophile elements (HSE) in the Ligurian ophiolites, Italy. *Earth and Planetary Science Letters* **175**, 119-132.

Sobolev, A.V., Hofmann, A.W., Sobolev, S.V. & Nikogosian, I.K. (2005). An olivine-free mantle source of Hawaiian shield basalts. *Nature* **434**, 590-597.

Sobolev, A.V., Hofmann, A.W. & Kuzmin, D.W. (2007). The amount of recycled crust in sources of mantle-derived melts. *Science* **316**, 412-417.

Stampfli, G.M. & Borel, G.D. (2002). A plate tectonic model for the Paleozoic and Mesozoic constrained by dynamic plate boundaries and restored synthetic oceanic isochrons. *Earth and Planetary Science Letters* **196**, 17-33.

Stracke, A., Salters, V.J.M. & Sims, K.W.W. (1999). Assessing the presence of garnet–pyroxenite in the mantle sources of basalts through combined hafnium–neodymium–thorium isotope systematics. *Geochemistry Geophysics Geosystems* **1**.

Stracke, A. & Bourdon, B. (2009). The importance of melt extraction for tracing mantle heterogeneity. *Geochimica et Cosmochimica Acta* **73**, 218-238.

Suen, C.J. & Frey F.A. (1987). Origin of the mafic and ultramafic rocksin the Ronda peridotite. *Earth and Planetary Science Letters* **85**, 183-202.

Takahashi, E., Nakajima, K. & Wright, T. L. (1998). Origin of the Columbia River basalts: melting model of a heterogeneous plume head. *Earth and Planetary Science Letters* **162**, 63-80.

Takahashi, E. & Nakajima, K. (2002). Melting process in the Hawaiian plume: an experimental study. In: Takahashi, E., Lipman, P. W., Garcia, M. O., Naka, J. & Aramake, S. (eds) Hawaiian Volcanoes: Deep Underwater Perspectives. Geophysical

Mono-graph, American Geophysical Union **128**, 403-418.

Takazawa, E., Frey, F.A., Shimizu, N., Saal, N. & Obata, M. (1999). Polybaric petrogenesis of mafic layers in the Horoman peridotite complex, Japan. *Journal of Petrology* **40**, 1827-1831.

Tanaka, T., Togashi, S., Kamioka, H. et al. (2000). JNdi-1: a neodymium isotopic reference in consistency with LaJolla neodymium. *Chemical Geology* **168**, 279-281.

Taylor, W.R. (1998). An experimental test of some geothermometer an geobarometer formulation for upper mantle peridotites with application to the thermobarometry of fertile lherzolite and garnet websterite. *N. Jb. Min. Abh.* **172**, 381-408.

Thirlwall, M.F. (1991). Long-term reproducibility of multicollector Sr and Nd isotope ratio analysis. *Chemical Geology* **94**, 85-104.

Tribuzio, R., Thirwall, M.F. & Vannucci, R. (2004). Origin of the gabbro-peridotite association from the Northern Apennine ophiolites (Italy). *Journal of Petrology* **45**, 1109-1124.

Tsuruta, K. & Takahashi, E. (1998). Melting study of an alkali basalt JB-1 up to 12.5GPa: behavior of potassium in the deep mantle. *Physics of the Earth and Planetary Interiors* **107**, 119-130.

Van Acken, D., Becker, H., Walker, R.J., McDonough, W.F., Wombacher, F., Ash, R.D. & Piccoli, P.M. (2010). Formation of pyroxenite layers in the Totalp ultramafic massif (Swiss Alps) – Insights from highly siderophile elements and Os isotopes. *Geochimica et Cosmochimica Acta* **74**, 661-683.

Vannucci, R., Shimizu, N., Piccardo, G.B., Ottolini, L. & Bottazzi, P. (1995). Distribution of trace-elements during breakdown of mantle garnet: an example from Zabargad. *Contributions to Mineralogy and Petrology* **113**, 437-449.

Villiger, S., Ulmer, P., Müntener, O. & Thompson, A.B. (2004). The liquid line of descent of anhydrous, mantle-derived, tholeiitic liquids by fractional and equilibrium crystallization – an experimental study at 1.0 GPa. *Journal of Petrology* **45** 2369-2388.

von Raumer, J. & Stampfli, G.M. (2008). The birth of the Rheic Ocean-Early Paleozoic subsidence patters and tectonic plate scenario. *Tectonophysics* **461**, 9-20.

Voshage, H., Sinigoi, S., Mazzucchelli, M., Demarchi, G., Rivalenti, G. & Hofmann, A.W. (1988). Isotopic constraints on the origino f ultramafic and mafic dikes in the Balmuccia peridotite (Ivrea Zone). *Contributions to Mineralogy and Petrology* **100**, 261-267.

Walter, M.J. (1998). Melting of garnet peridotite and the origin of komatiite and depleted lithosphere. *Journal of Petrology* **39**, 29-60.

Warren, J.M., Shimizu, N., Sakaguchi, C., Dick, H.J.B. & Nakamura, E. (2009). An assessment of upper mantle heterogeneity based on abyssal peridotite isotopic compositions. *Journal of Geophysical Research* **114**, B12203.

Waters, C.L., Sims, K.W.W., Perfit, M.R., Blichert-Toft, J. & Blusztajn, J. (2011). Perspective on the genesis of E-MORB from chemical and isotopic heterogeneity at 9–10°N East Pacific Rise. *Journal of Petrology* **52**, 565-602.

Wood, B.J. & Blundy, J.D. (1997). A predictive model for rare earth element partitioning between clinopyroxene and anhydrous silicate melt. *Contributions to Mineralogy and Petrology* **129**, 166-181.

Yaxley, G.M. & Green, D.H. (1998). Reactions between eclogite and peridotite: mantle refertilisation by subduction of oceanic crust. *Schweiz. Mineral. Petrogr. Mitt.* **78**, 243-255.

Yu, S., Xu, Y., Ma, J., Zheng, Y., Kuang, Y., Hong, L., Ge, W. & Tong, L. (2010). Remnants of oceanic lower crust in the subcontinental lithospheric mantle: trace element and Sr–Nd–O isotope evidence from aluminous garnet pyroxenite xenoliths from Jiaohe, Northeast China. *Earth and Planetary Science Letters* **297**, 413-422.

FIGURE CAPTIONS

Figure 1. (a) Tectonic sketch map of the Northern Apennines. Abbreviations for the tectonic units: IL, Internal Liguride Units; EL, External Liguride Units. Also reported are SV, crystalline massif of Savona, and GV, Voltri Group, belonging to the Ligurian Alps. Garnet pyroxenites investigated by Montanini et al. (2006, 2012) were sampled in outcrops located further north than the ultramafic bodies here studied, outside this map. (b) Simplified geological map showing ultramafic bodies hosting the investigated pyroxenites.

Figure 2. Centimeters-thick pyroxenite layers embedded in mantle peridotite from (a) M.te Castellaro and (b, c) Suvero ultramafic bodies (External Liguride Units, Northern Apennines, Italy). (d) A representative macroscopic sample of a pyroxenite layer, showing thin orthopyroxenite rims at the boundary with the host peridotite. White dotted lines delimit the pyroxenite layers in (b) and (d).

Figure 3. Photomicrographs of representative microstructures of EL spinel-plagioclase pyroxenites. Porphyroclasts of spinel and clinopyroxene partially replaced by fine-grained plagioclase-bearing assemblage, at parallel (a) and crossed (b) nichols. (c) Coarse orthopyroxene porphyroclast intensely substituted by the plagioclase-facies neoblastic assemblage in a spinel-bearing websterite. (d) Coarse mm-sized green spinel porphyroclast

surrounded by a rim of neoblastic assemblage mostly made by plagioclase, olivine and brownish amphibole. (e) Contact between a pyroxenite layer (on the right of the white dotted line) and orthopyroxene-rich rim (on the left); presence of large orthopyroxene porphyroclast (characterized by undulatory extinction) indicates that opx-rich rim was a mineralogical feature that predated the low-pressure metamorphic recrystallization. (f) Texture in pyroxenite lens GV12 showing a small clinopyroxene porphyroclast surrounded by a fined-grained band of clinopyroxene and dark-green spinel.

Figure 4. Variation diagrams of SiO_2, Al_2O_3, Na_2O, CaO (wt%) and Cr, Ni, Sc, V (ppm) vs Mg-number for the EL pyroxenite (circles). The compositional fields reported for comparison are: garnet pyroxenites (continue line) and spinel websterite (dashed line) in ultramafic orogenic massifs from Beni Boussera (Morocco, Pearson et al., 1993; Kumar et al., 1996; Gysi et al., 2011), Ronda (Spain, Suen & Frey, 1987; Garrido & Bodinier, 1999; Bodinier et al., 2008), Horoman (Japan, Takazawa et al., 1999; Morishita & Arai, 2001), Pyrenees (France, Bodinier et al., 1987a,b), and Balmuccia (Italy, Sinigoi et al., 1983; Voshage et al., 1988; Mukasa & Shervais, 1999). Grey field refers to the bulk compositions of garnet pyroxenite of the External Liguride Units investigated by Montanini et al. (2006). Dotted line defines the range of bulk solid compositions calculated using mineral phases in melting experiments on an hydrous arc melt (Müntener et al., 2001). Bulk compositions of pyroxenites adopted in mass balance calculations for estimating the garnet-bearing primary assemblages are also reported (see Suppl. Table 3): stars are samples from Beni Boussera (grey B7, black B9; white B15; Gysi et al., 2011), the square is sample 70379 selected from the Pyrenean garnet websterites (Bodinier et al., 1987a).

Figure 5. Chondrite-normalized rare earth element (REE) abundances in whole rock pyroxenites. Samples BG3, BG4, BG5 and BG14 are shown with the same symbol because they have very similar bulk REE compositions. Normalizing values are from Anders & Grevesse (1989). Also reported for comparison are the compositional fields of External Liguride garnet pyroxenites (Montanini et al., 2012), and Alpine-Apennine (A-A) gabbros (Borghini et al., 2007; Rampone et al., 1998; Rampone et al., 2014).

Figure 6. Variation of Mg# vs Al (a.p.f.u.) in clinopyroxene (a) and orthopyroxene (b) from pyroxenites. Filled symbols refer to spinel-facies porphyroclasts, open symbols refer to plagioclase-facies neoblasts (see the legend in figure).

Figure 7. Mg# vs Cr# (a), and Cr# vs Ti x 1000 (a.pf.u.) (b) in spinel from pyroxenites. Filled symbols refer to core of large spinel-facies porphyroclasts, open symbols refer to small relicts of plagioclase-facies spinel intensely replaced by the plagioclase-facies assemblage.

Figure 8. Chondrite-normalized REE patterns of clinopyroxene porphyroclasts from (a) HREE-enriched pyroxenites, (b) pyroxenites with rather flat MREE-HREE spectra, (c) samples GV8, GV12 and GV14 (details in text). (d) Representative chondrite-normalized REE patterns of clinopyroxene spinel-facies porphyroclast, and neoblasts of clinopyroxene, plagioclase and amphibole in pyroxenite BG13. Normalizing values are from Anders & Grevesse (1989).

Figure 9. Sc, Zr and REE abundance in clinopyroxene porphyroclasts along profile A-B analyzed in pyroxenite layer GV10, showing alternating px-rich and sp-rich zones (Suppl. Table 2). Data collected by in-situ laser ablation. Normalizing values for REE are from Anders & Grevesse (1989). Grey fields in the Sc diagram define the Sc content variations in garnet and its equilibrium clinopyroxene documented in garnet peridotites by Müntener et al. (2010).

Figure 10. Present-day $^{87}Sr/^{86}Sr$ versus $^{143}Nd/^{144}Nd$ measured on clinopyroxene separates from studied pyroxenites, compared to isotope data of pyroxenites from literature: Cr-Di websterites and Sp pyroxenites from Balmuccia (Ivrea Zone, Italy, Voshage et al., 1988; Mukasa & Shervais, 1999); pyroxenite, websterites and gnt-pyroxenites from Beni Boussera (BB, North Morocco, Pearson et al., 1993; Kumar et al., 1996); gnt-pyroxenites from (LA, Lowe Austria, Becker et al., 1996); websterites from Ronda (South Spain, Marchesi et al., 2012). The field of mid-ocean-ridge basalts (MORB) is from Class & Lehnert (2012); the field of ocean island basalts (OIB) is from GEOROC database (http://georoc.mpch-mainz.gwdg.de/georoc/).

Figure 11. (a) Present-day $^{143}Nd/^{144}Nd$ versus $^{147}Sm/^{144}Nd$ in clinopyroxenes from pyroxenites that define an errochron (dashed line) giving an age of 433 ± 51 Ma. Empty symbols refer to spatially controlled pyroxenite – wall-rock profiles, and relative isochrones (continuous lines), reported in Borghini et al. (2013). Data of EL garnet pyroxenites from Montanini et al. (2012) are reported for comparison. (b) Sm-Nd internal isochrons defined by whole rock (wr), plagioclase (plag) and clinopyroxene (cpx) from four pyroxenite samples (BG13, BG14, GV8 and BG5, this latter only based on clinopyroxene and plagioclase analyses). Ages and initial Nd isotopic ratios for the internal isochrons are: 178±11 Ma, initial $^{143}Nd/^{144}Nd$ = 0.512961 (±24), MSWD = 0.22 for BG13; 177±13 Ma, initial $^{143}Nd/^{144}Nd$ = 0.512837 (±20), MSWD = 0.69 for BG14; 174±25 Ma, initial $^{143}Nd/^{144}Nd$ = 0.512727 (±34), MSWD = 0.0024 for GV8; 183±14 Ma, initial $^{143}Nd/^{144}Nd$ = 0.512827 (±17) for BG5.

Figure 12. Whole-rock normative compositions of studied pyroxenites projected from Diopside within the (CMAS) triangle forsterite (Fo) - calcium tschermak (CaTs) - quartz (Qz)

(O'Hara, 1968). The compositional fields of EL garnet pyroxenites (EL gnt-pyrox, Montanini et al., 2012), Type-1 pyroxenites from Horoman (Takazawa et al., 1999), and Beni Boussera garnet pyroxenites (BB-gnt-pyrox, Gysi et al., 2011), are also shown for comparison. In the smaller CMAS triangle to the right, pyroxenite compositions are plotted together with the compositions of experimental partial melts from hybrid mafic-peridotite sources (Yaxley & Green, 1998; Kogiso et al., 1998; Takahashi & Nakajima, 2002), and the compositional field of melts in the eclogite-peridotite reaction experiments by Mallik & Dasgupta (2012)(tick-marks on the black arrow indicate the amount in wt% of eclogitic melt added to peridotite).

Figure 13. Bulk-rock Sm_N/Yb_N resulting from mass balance calculations compared to the Sm_N/Yb_N values measured in each pyroxenite sample (detailed explanation in the text). Open circles are the values calculated by using mineral compositions from Beni Boussera garnet pyroxenites (Gysi et al., 2011), open squares are obtained adopting in the calculation mineral compositions from Pyrenees garnet pyroxenites (Bodinier et al., 1987a).

Figure 14. Variation of bulk-rock Mg-number versus thickness (cm) of the studied pyroxenite layers and lens. Close to the symbols are also shown the Ni contents (ppm) of each pyroxenite sample.

Figure 15. (a) Chondrite-normalized REE patterns of clinopyroxene porphyroclasts in wall-rock peridotites from three profiles investigated by Borghini et al. (2013). (b) Computed melts in equilibrium with wall-rock clinopyroxenes shown in (a), using partition coefficients from Ionov et al. (2002). Also reported are the composition of average N-MORB (Hofmann, 1988), and average E-MORB from Mid-Atlantic Ridge 10-24°N (Hémond et al., 2006). The compositional fields refer to: 1) E-MORBs from South Atlantic Mid-Ocean-Ridge 5-11°S (A3 Seamount; Hoernle et al., 2011), 2) tholeiitic lavas (both olivine- and quartz-normative) from Iceland plume (Icelandic tholeiites; Hémond et al., 1993), 3) East Pacific Rise 9-10°N (Waters et al., 2011). Normalizing values are from Anders & Grevesse (1989).

Pyroxenite Layers in the Northern Apennines' Upper Mantle (Italy) – Generation by Pyroxenite Melting and Melt-infiltration

GIULIO BORGHINI[1,2,3], ELISABETTA RAMPONE[2], ALBERTO ZANETTI[4], CORNELIA CLASS[3], ANNA CIPRIANI[3,5], ALBRECHT W. HOFMANN[3,6], STEVEN L. GOLDSTEIN[3,7]

[1]DIPARTIMENTO DI SCIENZE DELLA TERRA, UNIVERSITÀ DI MILANO, VIA BOTTICELLI 23, 20133 MILANO, ITALY
[2]DIPARTIMENTO DI SCIENZE DELLA TERRA, DELL'AMBIENTE E DELLA VITA, UNIVERSITÀ DI GENOVA, CORSO EUROPA 26, 16132 GENOVA, ITALY
[3]LAMONT-DOHERTY EARTH OBSERVATORY OF COLUMBIA UNIVERSITY, 61 ROUTE 9W, PALISADES, NY 10964, USA
[4]CNR-ISTITUTO DI GEOSCIENZE E GEORISORSE, SEZIONE DI PAVIA, VIA FERRATA 1, I-27100 PAVIA, ITALY
[5]DIPARTIMENTO DI SCIENZE CHIMICHE E GEOLOGICHE, UNIVERSITÀ DEGLI STUDI DI MODENA E REGGIO EMILIA, LARGO S. EUFEMIA 19, 41100 MODENA, ITALY
[6]MAX PLANCK INSTITUTE FOR CHEMISTRY, P.O. BOX 3060, 55020 MAINZ, GERMANY
[7]DEPARTMENT OF EARTH AND ENVIRONMENTAL SCIENCES OF COLUMBIA UNIVERSITY, LAMONT-DOHERTY EARTH OBSERVATORY, 61 ROUTE 9W, PALISADES, NY 10964, USA

Corresponding Author:

Giulio Borghini
Dipartimento di Scienze della Terra "Ardito Desio"
Università degli Studi di Milano
Via Botticelli 23
20133 Milano (Italy)

Tel. 0039 02 50315600
Fax. 0039 02 50314597
Email: giulio.borghini@unimi.it

Keywords:

Pyroxenites, mantle heterogeneity, melt-rock reaction, mantle geochemistry, trace element, isotopes, External Ligurides ophiolites, mafic layers, ultramafic

Abstract

Pyroxenite layers embedded within peridotite represent wide-spread lithological mantle heterogeneities and are potential components in the mantle source of many oceanic basalts. Pyroxenites can be generated by several magmatic and metamorphic processes. However, in most natural samples (especially in ultramafic massifs), their primary characteristics are partially or completely erased by later petrologic evolution (e.g. metamorphism, metasomatism or partial melting). Here we investigate a suite of pyroxenites from the External Liguride Jurassic ophiolites (Northern Apennines, Italy). They are spinel-bearing websterites and clinopyroxenites, partially recrystallized under plagioclase-facies conditions, and occur as cm-scale layers parallel to the tectonite foliation of their host peridotites. Pyroxenites have bulk Mg-numbers from 74 to 88 and display rather constant LREE depletion over the MREE (La_N/Sm_N = 0.15-0.35), but variable MREE-HREE fractionation, with some of them having markedly positive HREE slopes (Sm_N/Yb_N=0.30-0.96). The HREE enrichment coupled with high Zr and Sc contents in clinopyroxene porphyroclasts from spinel-bearing domains provides strong evidence that garnet was present in the precursor mineral associations. Mass balance calculations suggest that the pyroxenites originally contained up to about 40 vol% of garnet, indicating they originated by segregation of melts at rather high pressure (P > 1.5 GPa). Parental melts of pyroxenites have reacted to some extent with the host peridotite during mantle infiltration. Lack of olivine in the primary mineral assemblage and orthopyroxene-rich rims along the contact with wall-rock peridotites indicate that pyroxenites have crystallized from silica-rich melts. These, likely, had REE patterns and Sr-Nd isotope compositions similar to enriched MORB. We propose that the pyroxenites originated from melts derived from a hybrid eclogite-bearing peridotite source, and then reacted with the host peridotite to form “secondary pyroxenites”. Their existence has been invoked in current models of basalts petrogenesis. During later decompression, they experienced an intermediate recrystallization at spinel-facies conditions, at 1.2-1.5 GPa and minimum temperature of 950-1000°C, and partial re-equilibration at low-pressure plagioclase-facies. The latter is dated by internal Sm-Nd isochrons at 178 (±8) Ma and is associated with Mesozoic exhumation, during extension of the Tethys lithosphere.

INTRODUCTION

Geochemical studies on oceanic basalts have documented that their upper mantle sources are chemically and isotopically heterogeneous (e.g. Hofmann, 2003). The nature, distribution and scale of such mantle heterogeneities are of fundamental importance for the understanding of the dynamics and long-term evolution of the upper mantle. Direct observations on mantle rocks, such as mantle xenoliths, abyssal peridotites and tectonically exhumed mantle sectors (Alpine-type peridotite massifs), have indicated that pyroxenite/mafic layers, commonly embedded within peridotite, represent wide-spread lithological mantle heterogeneities (e.g. Bodinier & Godard, 2003; Downes, 2007). Whether or not pyroxenite components occur in the upper mantle has been hotly debated during the last decades, mostly because of their potential involvement in mantle partial melting and generation of basalt (e.g. Hirschmann and Stolper 1996; Stracke et al., 1999; Salters & Dick, 2002; Kogiso et al., 2004a,b; Sobolev et al., 2005; Lambart et al., 2013).

Experimental studies (e.g. Yaxley & Green, 1998; Hirschmann et al., 2003; Pertermann & Hirschmann, 2003; Kogiso et al., 2004a; Sobolev et al., 2007; Lambart et al., 2009, 2012) have shown that the partial melting of mafic components, occurring at mantle depths as pyroxenites and eclogites, can produce highly variable melt compositions and, together with melts from depleted peridotite, reproduce the wide compositional range documented in oceanic basalts. On this basis, geochemical models have highlighted the role of a mixed pyroxenite-peridotite mantle source in the genesis of mid-ocean ridge (MORB) and ocean island (OIB) basalts (e.g. Allegre & Turcotte, 1986; Hirschmann & Stolper, 1996; Kogiso et al., 2004b; Sobolev et al., 2005; Stracke & Bourdon, 2009; Herzberg, 2011; Mallik & Dasgupta, 2012; Lambart et al., 2012).

The nature of mantle pyroxenites, however, remains a controversial subject, mostly because their origin has been related to a variety of magmatic and metamorphic processes, including: i) recycling of subducted oceanic crust stirred by mantle convection and incorporated into the lithosphere (e.g. Allègre & Turcotte, 1986; Kornprobst et al., 1990; Morishita & Arai, 2001; Morishita et al., 2003, Yu et al., 2010), ii) moderate- to high-pressure crystal segregation from magmas derived by melting of asthenospheric sources (Bodinier et al., 1987a,b; Vannucci et al., 1993; Rivalenti et al., 1995; Kempton et al., 1997; Takazawa et al., 1999; Mukasa & Shervais, 1999; Keshav et al., 2007; Dantas et al., 2007; Warren et al., 2009; Gysi et al., 2011) or subducted oceanic crust (Davies et al., 1993; Pearson et al., 1993; Becker, 1996; Pearson & Nowell, 2004), iii) refertilization of ‘infertile’ or ‘depleted’ upper mantle via melt-peridotite reactions (Garrido & Bodinier, 1999; Bodinier et al., 2008; Dantas

et al., 2009, van Acken et al., 2010). An additional difficulty in characterizing the role of pyroxenites in melting is associated with their reactivity within the mantle, causing them to be easily modified by magmatic and metamorphic processes subsequent to their emplacement at depth (e.g. Takazawa et al., 1999; Morishita & Arai, 2001; Morishita et al., 2003), interaction with transient melts (e.g. Garrido & Bodinier, 1999; Chazot et al., 2005; Kaeser et al., 2009), and decompressional partial melting (e.g. Pearson et al., 1993; Blichert-Toft et al., 1999; Montanini et al., 2012).

Orogenic and ophiolitic massifs offer the possibility to observe structural, spatial and geochemical relations between pyroxenites and host peridotites at different stages of their evolution (Bodinier & Godard, 2003). They are also important as the only locations with the possibility to gain insights on the distribution and extent of small-scale heterogeneities in the upper mantle through direct field observations. In this paper, we present petrographic, chemical and Sm-Nd isotope data on spinel pyroxenite samples from three, hundred-meter-sized ultramafic bodies from the western sector of the External Liguride Jurassic ophiolites (Northern Apennines, Italy; Fig. 1). Our microstructural and geochemical combined approach allows us to infer primary characteristics of pyroxenites, conditions and timing of their emplacement, geochemical affinities of their parental melts, and the later petrologic evolution. Our results impact the fundamental question of how pyroxenite components originate in the upper mantle, and provide further evidence of a "secondary-type" pyroxenite (also called "2stage" pyroxenite, Sobolev et al., 2005, 2007; Lambart et al., 2013) emplacement at rather deep mantle levels.

GEOLOGICAL BACKGROUND

Alpine-Apennine ophiolites represent lithospheric remnants of the Piemont-Ligurian ocean basin, a branch of the Mesozoic Tethys separating the European and Adriatic passive margins (Rampone & Hofmann, 2012, and references therein). The Middle Jurassic opening of the basin led to uplift and denudation of the subcontinental lithospheric mantle, the dominant lithotype exposed in Alpine-Apennine ophiolite sequences. Most of these mantle bodies have been affected by thermochemical erosion and refertilization processes, related to asthenospheric upwelling during rifting and oceanization (e.g. Rampone et al., 1997, 2004, 2008; Müntener et al., 2004; Piccardo et al., 2007). However, some of the mantle sequences from the Northern Apennines, namely the ultramafic massifs from the External Liguride Unit, have escaped these melt-rock interaction processes and preserved their old subcontinental signature (Beccaluva et al., 1984; Rampone et al., 1995; Montanini et al., 2006; Borghini et

al., 2011). The External Liguride (EL) ophiolites consist of large slide-blocks (up to km-scale) of ultramafic rocks, and minor MORB-type gabbros and basalts, within Cretaceous sedimentary melanges that were obducted during the closure of the Ligurian Tethys oceanic basin (Rampone et al., 1993, 1995; Tribuzio et al., 2004; Montanini et al., 2008). These mantle sequences consist mostly of fertile spinel-plagioclase lherzolites with disseminated Ti-rich amphibole and widespread spinel pyroxenite layers (Beccaluva et al., 1984). Lherzolites locally retain extremely "depleted" Nd-Sr isotopic compositions (Rampone et al., 1995) coupled with ancient Os model ages (1.6 Ga, Snow et al., 2000), which have been interpreted to reflect long residence times in the subcontinental mantle. The External Liguride ophiolitic mantle sequences have therefore been inferred to represent remnants of a fossil ocean-continent transition, where exhumed subcontinental mantle was associated with embryonic oceanic crust and rocks of continental origin (Marroni et al., 1998; Tribuzio et al., 2004; Montanini et al., 2008), an analogue to the modern Iberian passive margin (e.g. Whitmarsh et al., 2001).

Garnet pyroxenite layers from the northern sector of the External Liguride Unit have been recently investigated by Montanini et al. (2006, 2012) and consist of thin websterites and meter-scale thick garnet clinopyroxenites recording equilibration in the subcontinental lithosphere at T = 1100°C and P = 2.8 GPa. Sm-Nd and Lu-Hf geochronology on garnet-plagioclase pairs yielded 186±2 Ma and 220±13 Ma ages, interpreted as cooling ages that reflect the rifting-related exhumation of these mantle sectors (Montanini et al., 2006, 2012). Pyroxenites investigated in this study are from the southern sector of the Western External Liguride Unit (Suvero, La Spezia; Fig. 1). Borghini et al. (2011) recently showed that the peridotites from this mantle sector experienced a rather cold spinel- to plagioclase-facies decompressional tectonic evolution (T=870-930°C), thus confirming that this pyroxenite-peridotite association escaped melt-rock interaction and re-fertilization processes widely documented in most Alpine-Apennine ophiolitic peridotites (e.g. Müntener & Hermann, 1996; Rampone et al., 1997, 2004, 2008; Rampone & Borghini, 2008; Piccardo et al., 2004, 2007).

FIELD OCCURRENCE AND PETROGRAPHY

A summary of the location and description of samples is presented in Table 1. Pyroxenites occur as layers within the host mantle peridotites, mostly ranging in thickness from several millimetres to about 15 centimetres (Fig. 2). Samples GV12 and GV14 occur as lenses about 30 cm thick. Layers are parallel to the foliation plane of the host peridotites,

showing sharp contacts, and can be weakly boudinaged (Fig. 2d). In outcrop, pyroxenite layers are recognised by their pinkish or dark-grey colour (Fig. 2a,b,c) and by the occurrence of coarse black spinel grains. Pyroxenite abundance is variable, and in some outcrops can be as high as 50% (Fig. 2a,b). In some places, pyroxenite layers alternate with harzburgite portions within the peridotite, thus forming a compositional layering parallel to the tectonite foliation (Fig. 2a,d).

Most of the pyroxenites are characterized by a porphyroclastic texture defined by coarse-grained (up to 10-12 mm) porphyroclasts of pyroxenes and spinels, stretched along the tectonite foliation. Porphyroclastic minerals are partially substituted by a plagioclase-bearing granoblastic assemblage (Fig. 3a,b,c,d), indicating a retrograde evolution from spinel- to plagioclase-facies. The low-P metamorphic recrystallization is recorded by the development of i) millimeter and sub-millimeter bands of plagioclase and olivine (±amphibole) crystallized around coarse porphyroclasts of greenish spinels and pyroxenes (Fig. 3a,b), ii) orthopyroxene plus plagioclase exsolutions in large clinopyroxene porphyroclasts (Fig. 3b), iii) fine-grained (~200–300 μm) granoblastic aggregates made of plagioclase, olivine, newly formed pyroxenes and occasionally dark-brown spinel and brownish amphibole, partially replacing the spinel-facies pyroxene porphyroclasts (Fig. 3c,d). Amphibole is heterogeneously distributed in the pyroxenite samples and is always associated with the plagioclase-bearing neoblastic assemblage (Fig. 3d). In the most altered samples (GV14 and GV17), granoblastic olivine and plagioclase are almost completely substituted by low-T alteration products (chlorite and sausurrite, respectively).

Most of the pyroxenite samples are characterized by two alternating mineralogical domains: i) spinel-rich portions, where green spinel relics are rimmed by plagioclase and olivine (±amphibole), ii) pyroxene-bearing domains in which the large pyroxene porphyroclasts are partially substituted by neoblastic aggregates of new pyroxenes and plagioclase. The latter mineralogical feature is clearly observable in the thickest pyroxenite layers, whereas the two domains are usually stretched and boudinaged in the thinner bands (discussed further below). Most of the pyroxenite bands show irregular orthopyroxene-rich borders along the contact with the hosting peridotite (Fig. 3e). This is the result of interaction between the melt from which the pyroxenite crystallized and the host mantle peridotite during the pyroxenite emplacement (Borghini et al., 2013).

Olivine and amphibole are totally absent in pyroxenite GV12; this sample is texturally distinct and characterized by few small relics of clinopyroxene porphyroclasts that are strongly substituted by a fine-grained equigranular metamorphic texture consisting of

clinopyroxene, dark-green spinel and plagioclase (completely replaced by low-T alteration minerals, Fig. 3f). This granoblastic assemblage often forms clusters and seams stretched along the foliation (Fig. 3f).

ANALYTICAL METHODS

Whole-rock major and trace element analyses of pyroxenites were made by lithium metaborate/tetraborate fusion ICP-OES (for major elements) and ICP/MS (for trace elements) at the Actlabs Laboratories (Western Ontario, Canada; http://www.actlabs.com).

Mineral major element compositions were analyzed using: (1) a Philips SEM 515 equipped with an X-ray dispersive analyzer (accelerating potential 15 kV, beam current 20 nA), at the Dipartimento di Scienze della Terra, dell'Ambiente e della Vita, University of Genova, and (2) a JEOL JXA 8200 Superprobe equipped with five wavelength-dispersive (WDS) spectrometers, an energy dispersive (EDS) spectrometer, and a cathodoluminescence detector (accelerating potential 15 kV, beam current 15 nA), at the Dipartimento di Scienze della Terra "Ardito Desio", University of Milano. *In situ* trace element mineral analyses were carried out by laser ablation inductively coupled plasma mass spectrometry (LA-ICP-MS) at IGG-CNR in Pavia. A detailed description of analytical procedures is given in Miller et al. (2007).

Sm and Nd isotopic compositions were measured on clinopyroxene and plagioclase separates and on whole rock powders from pyroxenite samples. Clinopyroxenes and plagioclases (90-150 μm sized) were separated by grinding, sieving, electromagnetic separation and handpicking under a microscope. Weights of unleached mineral concentrates were 25-82 mg for clinopyroxenes and 54-132 mg for plagioclases. Minerals were leached in at least three steps using a solution of 5% HF + 6.2M HCl. Nd isotopic compositions, together with elemental abundances of Sm and Nd by isotope dilution, were measured by thermal ionization mass spectrometry (TIMS) on a VG Sector 54-30 at the Lamont-Doherty Earth Observatory of Columbia University (Palisades, NY, USA). The $^{143}Nd/^{144}Nd$ ratios were normalized to $^{146}Nd/^{144}Nd$ =0.7219, and reported relative to JNdi $^{143}Nd/^{144}Nd$ =0.512115 (Tanaka et al., 2000). Samples were analyzed during the course of 6 analytical sessions. Individual sample data were corrected to the standard values measured during the individual time intervals. Analyses of the JNdi-1 standard during the 6 sessions yielded $^{143}Nd/^{144}Nd$ ratios of 0.512080±9 (2σ, mean of n=7 analyses, 34 ppm external reproducibility), 0.512074±10 (n=10, 18 ppm), 0.512075±12 (n=13, 23 ppm), 0.512088±14 (n=5, 27 ppm),

0.512096±13 (n=26, 25 ppm), 0.512095±10 (n=5, 20 ppm). Total Sr and Nd blanks did not exceed 150 pg.

RESULTS

Bulk-rock chemistry

The bulk-rock major and trace element data of the pyroxenite samples (Table 2) display a large total range of Mg-numbers [molar $Mg/(Mg+Fe^{2+}_{tot})*100$] (74-88 mol%), although most values are concentrated between 83-85. Conversely, pyroxenites cover a large range of Al_2O_3 and CaO contents (10.6-16.5 wt% and 6.8-19.5 wt%, respectively; Fig. 4), mostly reflecting their modal variation between clinopyroxenite and websterite assemblages. In Figure 4, selected major and trace elements are plotted against Mg-number, together with the compositional fields of garnet pyroxenites and spinel-bearing websterites from orogenic and ophiolitic massifs (details and references in Fig. 4 caption).

Major element compositions of most samples lie in the fields of overlap between garnet-pyroxenites and spinel-bearing websterites from orogenic massifs at intermediate Mg-numbers (Fig. 4). However, they diverge from literature data by having generally higher CaO and lower Na_2O contents. Samples GV14 and GV17 have unusual, very low SiO_2 abundances (Table 2). Petrographic observations indicate that this is likely due to a high extent of low-temperature hydrothermal alteration, mostly dominated by chloritization of pyroxenes and olivine, as observed for many oceanic and ophiolitic mafic rocks (e.g. Alt et al., 1998). Pyroxenite lens GV12 plots within the compositional field of garnet pyroxenites, but with slightly higher CaO content (Fig. 4). Garnet-pyroxenites from other EL ultramafic massifs, recently studied by Montanini et al. (2012), show lower Mg-numbers and higher Na_2O, Al_2O_3 contents relative to our samples, but similar SiO_2 and CaO compositional variations (Fig. 4). In terms of Cr, Ni, V, Sc abundances, the pyroxenites also lie in the compositional field of overlap between garnet pyroxenites and websterites in the literature, except for samples GV12 and GV14, which plot within the compositional field of garnet-pyroxenites, at lower Mg values (Fig. 4). Our pyroxenites have low Cr, Ni (560-1530 ppm, 210-860 ppm, respectively) and moderate Sc, V (31-51 ppm, 163-280 ppm, respectively) concentrations. EL garnet-pyroxenites studied by Montanini et al. (2012) show similar values, at lower Mg-numbers (Fig. 4).

The CI-normalized REE and other refractory elements (Fig. 5) of most of the pyroxenites (BG3, BG4, BG5, BG13, BG14, BG22, GV10, GV17, MC3, MC5) display rather constant LREE depletion over the MREE (La_N/Sm_N = 0.15-0.35), but variable MREE-HREE

fractionation. In fact, the HREE slopes range from flat (GV17) to markedly positive (BG13) (Sm_N/Yb_N=0.30-0.96), with absolute concentrations varying from 3 to 20 x CI. In particular, samples BG13, GV10, MC3 and MC5 display HREE enriched patterns as observed in some garnet pyroxenites (e.g. Pearson et al., 1993; Gysi et al., 2011; Montanini et al., 2012). Spinel-rich clinopyroxenite GV12 has an overall lower REE content, showing a LREE-depleted pattern combined with slightly fractionated MREE to HREE (Sm_N/Yb_N=0.77). The pyroxenite GV14 shows a convex-upward pattern with HREE depletion over MREE (Sm_N/Yb_N=1.66). Finally, pyroxenite GV8 displays a nearly flat pattern at 3-4 x CI. Zr and Hf show a rather flat trend between Nd and Sm, with some small positive Zr anomalies. In contrast, Sr is highly enriched compared to the LREE. These "spikes" probably derived from later fluid-driven contamination as evidenced by very thin whitish veins orthogonal to the layer direction not completely eliminated from the samples during powder preparation for bulk-rock analysis. This is further supported by the absence of positive Sr anomalies in any of the porphyroclasts. Our samples have MREE-HREE abundances within the compositional field defined by the External Liguride garnet-pyroxenites studied by Montanini et al. (2012) (Fig. 5). However, they have higher LREE content, with the exception of sample GV12, which is consistent with literature data.

Mineral chemistry

Pyroxenes and spinel have Mg-numbers varying according to the Mg-number of their bulk-rock, and within each sample they show systematic major element variations according to the different mineral generations (porphyroblast vs. neoblast). Clinopyroxene porphyroclasts have Mg-numbers varying in agreement with their bulk-rock Mg-number, from 0.77 in the olivine-free clinopyroxenite GV12, to 0.88 in the high Mg-number websterites MC3 and MC5 (Table 3 and Fig. 6a). They also have rather high Al_2O_3 contents (6.21-10.12 wt%) and low Cr_2O_3 and Na_2O abundances (≤0.36 wt% and ≤1.0 wt% respectively; Table 3). A chemical profile on a representative pyroxenite layer shows that clinopyroxene porphyroclasts have Mg-numbers increasing from the center of the pyroxenite layer towards its margins (Suppl. Fig.1, and Suppl. Table 1), where Mg-numbers approach those of clinopyroxene of the host peridotite. As shown in Figure 6a, clinopyroxene neoblasts in each sample exhibit systematically lower Al_2O_3 concentrations (3.16-6.62 wt%) and higher Mg-numbers relative to corresponding clinopyroxene porphyroclasts. In the orthopyroxene porphyroclasts, the Mg-number varies from 0.82 to 0.88, and Al_2O_3 and CaO contents range between 4.33-7.56 wt% and 0.52-1.19 wt%, respectively (Table 4). Similar to clinopyroxenes,

orthopyroxene neoblasts display lower Al_2O_3 concentrations (1.17-3.43 wt%) and increased Mg-numbers (Fig. 6b); CaO abundance does not exceed 0.79 wt% (Table 4).

Coarse, millimeter-sized green spinels are characterized by very low Cr-numbers [molar Cr/(Cr+Al)] (average Cr-number between 0.01 and 0.03), Mg-numbers between 0.61-0.78, and TiO_2 lower than 0.24 wt% (Table 5). Small-sized, dark-brown spinels, associated with fine-grained plagioclase-bearing aggregates, show higher Cr-numbers (0.10-0.29) and TiO_2 contents (0.21-0.89 wt%), coupled to lower Mg-numbers (Fig. 7a,b).

Olivines have rather homogeneous compositions within each sample. Overall, olivine Mg-numbers vary between 0.80-0.87, in agreement with the bulk-rock Mg-number (Table 6). Plagioclase has anorthite contents [An = Ca/(Ca+Na)*100] of An_{55-68} in the cores of neoblasts; a few analyses on rims of plagioclase neoblasts gave significantly higher anorthite values (An_{74-83}; Table 7). Amphibole compositions range between kaersutite and Ti-rich pargasite (according to Leake classification 1997) with low K_2O (≤0.3 wt%) and Cr_2O_3 abundance not exceeding 1.37 wt% (Table 8).

In situ LA-ICP-MS trace element analyses have been performed mostly on clinopyroxene porphyroclasts and a few representative clinopyroxene, plagioclase and amphibole neoblasts (Table 9). Consistent with the bulk-rock REE variability described above, clinopyroxene porphyroclasts display heterogeneous trace element composition in the different samples (Fig. 8). LREE depletion (La_N/Sm_N=0.11-0.24) of clinopyroxene within a single sample is comparatively uniform, similar to the bulk-rock REE composition. However, the MREE to HREE are variably fractionated. Samples with the greatest bulk-rock MREE-HREE fractionation (BG13, GV10, MC3, MC5, Table 2) locally show marked HREE enrichment over the MREE in their clinopyroxenes (Sm_N/Yb_N=0.25-0.94; Yb_N=17.3-87.6) (Fig. 8a). Clinopyroxene porphyroclasts from pyroxenites with moderate bulk-rock HREE enrichment (BG4, BG5, BG14, BG22, GV17, Table 2) are similarly characterized by rather variable MREE-HREE fractionation, but with less pronounced HREE enrichment (Sm_N/Yb_N=0.60-1.20; Yb_N=10.2-42; Fig. 8b). Clinopyroxenes from the other pyroxenites show more homogeneous REE patterns (GV8, GV12, GV14, Fig. 8c), similar to their respective bulk-rock REE abundances (Fig. 5).

As described above, the thickest pyroxenite layer (sample GV10, Fig. 9) is characterized by two mineralogical domains, namely a spinel-rich and a pyroxene-rich domain. A trace element chemical profile within this single sample shows grain-to-grain (thin section scale, <5 cm) REE variability in clinopyroxene porphyroclasts, related to their microstructural location, i.e. in the spinel-rich versus pyroxene-rich domains (Suppl. Table 2).

We found that clinopyroxene porphyroclasts with the highest MREE-HREE fractionation are systematically located in the spinel-rich zone, and this HREE enrichment is coupled with higher Zr and Sc abundance relative to those in clinopyroxenes from the pyroxene-rich domains (Fig. 9). As discussed below, this peculiar chemical feature was likely inherited by metamorphic breakdown of precursor garnet in the primary assemblage.

Figure 8d shows the REE spectra of neoblasts from the plagioclase-bearing mineral assemblage of a representative sample (BG13). Compared to clinopyroxene porphyroclasts, clinopyroxene neoblasts always exhibit overall higher REE absolute concentrations and development of negative Eu anomalies. Amphiboles have REE patterns similar in shape to those of clinopyroxene neoblasts, but with higher absolute concentrations. Plagioclases have low REE abundances and LREE enrichment (La_N/Sm_N=3.55-5.41), as well as marked positive Eu anomalies.

Geothermometry

Conventional geothermometers, mostly based on Ca-Mg exchange between the two pyroxenes, have been applied to both spinel-facies porphyroclasts and plagioclase-bearing neoblasts (Table 10), in order to constrain the thermal evolution during the tectonic exhumation. For the spinel-facies pyroxenes, the two-pyroxene thermometers provide similar temperature ranges, between 830-940°C (Taylor, 1998) and 860-980°C ($T_{Opx-Cpx}$; Brey & Kohler, 1990), which are in good agreement with temperature estimated by the single-clinopyroxene thermometer of Nimis & Taylor (2000), between 820-960°C (Table 10). Systematically higher temperatures are obtained using the Ca-in-Opx thermometer of Brey & Kohler (1990), ranging between about 930 and 1100°C. As discussed by Nimis & Grutter (2010), the Ca-in-Opx thermometer is affected by a positive bias at temperatures lower than 1000°C; however, we observe (Table 10) that this overestimation of calculated T persists even after the empirical correction proposed by Nimis & Grutter (2010). Temperatures estimated for spinel-facies pyroxenes partially overlap the temperature range documented by Borghini et al. (2011) in the associated peridotites (940-1000°C), though extending to lower values. This is probably due to the higher extent of recrystallization shown by the pyroxenites relative to the host peridotites. The occurrence of thin (2-10 μm) exsolution in both clinopyroxene and orthopyroxene porphyroclasts of the pyroxenites suggests that the spinel-bearing porphyroclasts are likely affected by low-P re-equilibration. Accordingly, temperatures obtained for the spinel-facies stage must be considered as minimum T estimates.

Systematically lower temperature estimates have been calculated for the plagioclase-bearing neoblasts with four different thermometers: 830-890°C and 790-860°C with the Brey & Kohler (1990) thermometers (Ca-in Opx and Opx-Cpx, respectively), 770-860°C with the Taylor (1998) thermometer and 780-900°C with Nimis & Taylor (2000) thermometer. As observed for the spinel-facies minerals, Borghini et al. (2011) found temperatures up to 950°C in the plagioclase-facies recrystallization in the associated peridotites, about 50°C higher than those of the pyroxenites (Table 10).

Sr-Nd isotope compositions and Sm-Nd geochronology

Sr and Nd isotopic compositions of clinopyroxenes from pyroxenites investigated in this work have been reported by Borghini et al. (2013), together with spatially associated host rocks and distal peridotites, i.e. peridotite sampled in pyroxenite-free outcrops. In Figure 10a, the present-day Sr and Nd isotope ratios of pyroxenites are plotted along with isotopic data previously documented in orogenic and ophiolitic massifs (references reported in caption of Fig. 10), and the compositional field of global MORB (Class & Lehnert, 2012: PetDB Expert MORB, Mid-Ocean Ridge Basalt, Compilation. EarthChem Library. http://dx.doi.org/10.1594/IEDA/100060) and OIB (GEOROC database: http://georoc.mpch-mainz.gwdg.de/georoc/).

Our pyroxenites have MORB-type Sr and Nd isotopic compositions, and when compared to the data of pyroxenites from orogenic and ophiolitic massifs, they plot among the samples with the lowest $^{87}Sr/^{86}Sr$ and highest $^{143}Nd/^{144}Nd$ ratios (Fig. 10a). Initial εNd values computed at the inferred age of pyroxenite emplacement (433 ±51 Ma; Borghini et al., 2013) range between +3 and +8, consistent with enriched MORB compositions.

Here, we present new Sm-Nd isotopic data on plagioclase separates and whole-rock powders of selected pyroxenite samples that, together with clinopyroxene data from Borghini et al. (2013), are used to construct internal isochrons. The Sm-Nd isotopic compositions of whole-rocks and leached clinopyroxene and plagioclase mineral separates of selected pyroxenites are listed in Table 11, together with elemental abundances of Nd and Sm determined by isotope dilution. The latter are largely within 10% of the bulk-rock analyses (Table 2), and most of Sm and Nd concentrations in clinopyroxenes and plagioclases obtained by ID are within the variability shown by corresponding *in situ* LA-ICP-MS data (Table 9).

Sm-Nd internal isochrons have been defined by whole rock, plagioclase and clinopyroxene for pyroxenites BG13, BG14 and GV8, and by plagioclase and clinopyroxene for sample BG5 (Fig. 11). Age calculations have been performed using Isoplot (Ludwig,

2003). The strong Sm-Nd fractionation between plagioclase and clinopyroxene in the four pyroxenite samples provides for well-constrained ages of 177±13, 178±11, 174±25 and 183±14 Ma. According to petrographic features, these ages date the event of partial metamorphic recrystallization at low-pressure plagioclase-facies conditions, as temperature estimates for plagioclase-facies neoblasts (Table 10) are largely higher than the closure temperature for the Sm-Nd system (Mezger et al., 1992). Considering that the ages are indistinguishable within uncertainty, and given the field and geochemical evidence of the decompressional evolution, documented also in the associated host peridotites (Borghini et al., 2011), we conclude that the EL pyroxenite-peridotite mantle experienced subsolidus recrystallization in a single event. The age of this event is given by the weighted average of the individual internal isochrons, at 178±8 Ma.

DISCUSSION

Reconstruction of the precursor mineral assemblage

The pyroxenites investigated in this study contain an older spinel-bearing mineral assemblage partially replaced by subsequent plagioclase-bearing neoblastic aggregates (Fig. 3). However, some microstructural and chemical features shown by several pyroxenite samples suggest that variable modal amounts of garnet were present in the precursor mineral associations. The most important evidence is that clinopyroxene porphyroclasts from spinel-rich domains systematically show HREE enrichment coupled to high Zr and Sc contents (Fig. 9). These compositional features can be explained by the replacement of previously existing garnet, which preferentially partitions HREE over the MREE. Moreover, the Zr and Sc Kd values of garnet/melt are much higher than those of clinopyroxene/melt (e.g. Hauri et al., 1994; Johnson, 1998, Ionov et al., 2002). Conversely, experimentally determined Kds (spinel/melt) for HFSE are about an order of magnitude lower than those of both garnet and clinopyroxene (Horn et al., 1994). Similar trace element characteristics of precursor garnets have been previously documented by Vannucci et al. (1993) in pyroxenes of spinel+plagioclase-bearing pyroxenites from Zabargad (Red Sea). They also observed that this garnet imprint has been partially erased by subsequent metamorphic recrystallization at lower pressure and is only evident in a few relicts. Low pressure overprinting could also explain the variability of HREE-MREE fractionation of clinopyroxene porphyroclasts in spinel-rich domains of our pyroxenites (Fig. 9). Zr and Sc enrichments seem to be better preserved, as shown by the kink in the chemical profile of Figure 9, even though Zr and Sc contents could have been higher in the early garnet and later partially smoothed by chemical

diffusion during subsequent spinel- and plagioclase-facies partial re-equilibration. It is remarkable that Sc contents observed in clinopyroxene porphyroclasts from spinel-rich and pyroxene-rich domains match very well with the range of Sc variations in garnet and its equilibrium clinopyroxene, respectively, documented by Müntener et al. (2010) in garnet pyroxenite from Totalp and Malenco (Fig. 9).

The CMAS projection in the garnet-pyroxene plane of pyroxenite bulk-rock compositions is usually considered as evidence of primary crystallization of a mineral assemblage dominated by garnet and pyroxene (e.g. Garrido & Bodinier, 1999; Takazawa et al., 1999). Accordingly, in the CaTs-Fo-Qz triangle of Figure 12, most pyroxenites plot close to the enstatite-garnet-CaTs line.

HREE enrichment over the MREE shown by some pyroxenite bulk-rock REE spectra (samples BG13, GV10, MC3, MC5; Fig. 5) is comparable to that observed in garnet-bearing pyroxenites from orogenic ultramafic massifs (e.g. Beni Bousera, Pearson et al., 1991, 1993; Kumar et al., 1996; Gysi et al., 2011; Ronda, Garrido & Bodinier, 1999; Pyrenees, Bodinier et al., 1987a), and has been interpreted as indicative of high-pressure magmatic segregation of garnet (e.g. Kornprobst et al., 1969, 1970; Loubet & Allegre 1982). Similar bulk HREE-MREE fractionation indicating precursor garnet has been documented in low-pressure recrystallized pyroxenites from Zabargad and Horoman (Vannucci et al., 1995; Takazawa et al., 1999).

In order to test the hypothesis of a precursor garnet-bearing assemblage in some of our pyroxenites, we performed a mass balance calculation to derive an estimate of the original modal compositions, in two separate steps. First, we calculated the modal abundances of a potential garnet-bearing assemblage by using whole-rock major element data of the studied pyroxenites (Table 2) and mineral compositions of garnet pyroxenites having similar bulk-rock chemistry from the literature (see details below). Mass balance calculations, performed by weighted least-squares minimization, included seven major element oxides (SiO_2, TiO_2, Al_2O_3, Cr_2O_3, FeO, MgO, CaO and Na_2O), and were computed by using the software Wolfram Mathematica 8. The quality of the fit was evaluated based on the sum of the squares of the residuals (R2 in Table 12); we considered as realistic only the computed garnet-bearing assemblages with errors well below 1.

In the second step, we derived the hypothetical Sm_N/Yb_N ratios of bulk-rocks from the Sm_N/Yb_N ratios of minerals used to calculate the primary garnet-bearing assemblage.

Results of the first step of the mass balance calculation are reported in Table 12, together with the spinel-facies modes computed using the whole rock major element

abundances and the compositions of spinel-facies porphyroclasts in each pyroxenite. We estimated garnet-bearing modes by adopting the mineral compositions of selected garnet pyroxenite samples from the Beni Bousera (Gysi et al., 2011) and Pyrenees (Bodinier et al., 1987a) ultramafic massifs, with bulk-rock compositions similar to our pyroxenites (sample B7, B9 and B15 with Mg-numbers ranging from 78-85, Gysi et al., 2011; sample 70-379 Mg-number = 86, Bodinier et al., 1987a; Figure 4, Suppl. Table 3 and Suppl. Fig. 2). Beni Boussera pyroxenites cover a broader range in both whole-rock and mineral chemistry, thus providing a larger choice of compositions that can better simulate our samples, particularly in terms of major element contents of garnet and pyroxenes (Gysi et al., 2011). Garnet websterites from the Pyrenees have minerals with Mg-numbers comparable with our samples MC3 and MC5 (Fig. 4 and Suppl. Table 3).

In addition to pyroxene, garnet and spinel compositions from literature garnet pyroxenites, we used, in the mass balance calculation, the average composition of olivine measured in each sample, as it strongly depends on bulk-rock Mg-number and it is not expected to change composition in the different mineral assemblages within a single sample.

The mass balance shows that all the bulk pyroxenite compositions characterized by HREE enrichment over the MREE are consistent with primary garnet-bearing assemblages, with modal garnet varying between 20-40 vol% (samples BG13, GV8, GV10, GV12, MC3, MC5, Table 12). Moreover, our calculations show that lower garnet modal abundances (generally_<17 vol%) could have been present in the precursor assemblage also for other pyroxenites with nearly flat MREE-HREE spectra (samples BG4, BG5, BG14, Table 12). This is, for example, documented in some garnet pyroxenites from Beni Bousera, characterized by bulk-rock REE patterns lacking MREE-HREE fractionation (Gysi et al., 2011).

The reliability of the computed garnet-bearing mineral modes has then been checked by comparing calculated bulk $(Sm/Yb)_N$ ratios with measured values (Fig. 13). Except for sample BG14, good agreement is generally observed between the two values. Pyroxenites with Mg-numbers between 74 and 84 are well modelled by major and trace element data of minerals from Beni Bousera garnet pyroxenites (sample B7, B9 and B15; Gysi et al., 2011), whereas pyroxenites MC3 and MC5, with slightly higher Mg-numbers (86-87), yield a better fit using data from Pyrenean garnet websterites (Bodinier et al., 1987a). For samples GV14 and GV17 with very low SiO_2 bulk-rock abundances, we could not compute realistic garnet-bearing assemblages, and their spinel-bearing modal compositions have also the highest errors (R2, Table 12). In terms of the estimated REE patterns (Suppl. Fig. 2), our mass balance

modelling is able to simulate the overall MREE-HREE fractionation, but does not reproduce the kink between Sm and Gd. It must be noted that modelling is very sensitive to the MREE-to-HREE compositions of garnet and pyroxenes used in the calculation. However, selective Gd_N-Yb_N enrichment in whole-rock chemistry has been documented also in garnet pyroxenite from the literature (e.g. Gysi et al., 2011; Marchesi et al., 2013).

We are well aware that the above mass balance calculations do not constitute absolute proof of the occurrence of garnet in the precursor assemblage. They do, however, demonstrate that this is a highly plausible explanation for the otherwise rather difficult-to-explain abundance patterns of the HREE. Garnet has important implications for the chemistry of melts formed in its presence, and for the depth of melting, and we will explore some of the consequences of this in the remainder of this paper.

Origin of pyroxenites by deep melt infiltration

Garnet pyroxenites have been described in orogenic and ophiolitic ultramafic massifs (Downes, 2007, and references therein; Montanini et al., 2006, 2012; Gysi et al., 2011, Marchesi et al., 2013), and in mantle xenoliths (e.g. Jacob, 2004; Bizimis et al., 2005; Gonzaga et al., 2009), and their origin has been related to a range of processes. Garnet is the typical high-pressure metamorphic Al-rich mineral in both mantle peridotites and pyroxenites (Herzberg, 1978; Gasparik, 1984). In addition, a garnet-bearing assemblage can result from high-pressure crystallization of a mafic magma or by complete high-pressure metamorphic recrystallization of mafic rocks with primary low-pressure mineral assemblages (i.e., "eclogites").

Garnet pyroxenites of both origins can be present in a single ultramafic massif, as documented in Lherz (Bodinier et al., 1987a,b), Ronda (Garrido & Bodinier, 1999) and Beni Boussera (Kornpbrost et al., 1990). In some garnet pyroxenites, whole-rock trace element compositions with positive Eu and Sr anomalies, relatively low HREE and MREE, and high LREE/HREE, reflect high modal abundances of primary plagioclase, and thus they have been considered of crustal origin (e.g. Kornpbrost et al., 1990; Garrido & Bodinier, 1999; Morishita et al., 2003, Marchesi et al., 2013). In some garnet pyroxenites from Beni Boussera, a low-P crustal imprinting is also supported by peculiar Nd-Hf-O isotopic compositions (Pearson et al., 1993; Pearson & Nowell, 2004). Based on geochemical and isotopic data, a similar conclusion has also been inferred for a few garnet pyroxenites from other sectors of the External Liguride ophiolites by Montanini et al. (2006, 2012). When compared to our pyroxenites, the latter have significantly lower bulk Mg-numbers and higher Al_2O_3 and Na_2O

contents (Fig. 4). Montanini et al. (2012) inferred that these garnet pyroxenites represent either melt residues of precursor eclogites, or high-pressure segregation products of eclogite-derived melts. Pyroxenites investigated in our study are not consistent with these origins. First, they lack the trace element bulk-rock compositions indicative of plagioclase-rich gabbros characterized by positive Sr and Eu anomalies, rather high LREE and very low HREE, thus, ruling out an origin as recrystallization products from low-pressure magmatic protoliths (Fig. 5). Second, almost flat or weakly LREE-depleted bulk REE spectra (La_N/Sm_N= 0.15-0.66; Table 2) do not support an origin as melting residues of precursor mafic rocks (Fig. 5).

Instead, the inferred occurrence of primary garnet in most samples (Table 12) indicates that the pyroxenites likely originated by segregation of melts at rather high pressure, as garnet is stable at P >1.5 GPa in pyroxenitic assemblages (e.g. Kogiso et al., 2004, Downes 2007). Garnet-bearing assemblages have been obtained by crystallization of a hydrous primitive magma in experiments at 1.2 GPa and variable T (Müntener et al., 2001). However, the bulk compositions of these experimental magmatic products do not match the compositions of our pyroxenites (Fig. 4), and the lack of evidence of primary amphibole in the pyroxenites does not support the origin from a hydrous melt.

Geochemical affinity of the parental melts

In this section we discuss the nature of the parental melts to the pyroxenites, but note two major limitations: i) the primary garnet-facies mineral assemblage has been completely obliterated by metamorphic recrystallization events, most likely related to the tectonic exhumation of the pyroxenite-peridotite mantle sequence (Borghini et al., 2011), ii) magmatic interaction and/or subsolidus diffusion between pyroxenite and host peridotite have likely partially modified the original chemical signatures of the melts (e.g. the Mg-number). This precludes the possibility to compute equilibrium melts by using the present trace element mineral composition. Therefore, the nature of pyroxenite parental melts can only be inferred by combining available microstructural and chemical observations.

The bulk-rock Mg-numbers vary from 74-88, and are inversely correlated with the thickness of layers and lenses, and positively correlated with the bulk Ni contents (Fig. 14). An inverse relationship between dyke thickness and bulk Mg-number has been documented in pyroxenitic layers from the Lherz ultramafic massif and explained as the result of local chemical re-equilibration with the adjacent peridotite (Bodinier et al., 1987b; Fabries et al., 2001). Bodinier et al. (2008) have investigated in detail this process by studying some

pyroxenites from Ronda (Spain). These authors performed numerical modeling demonstrating that interaction between the host peridotite and variably evolved melts can generate pyroxenites with Mg-numbers intermediate between those of the peridotite and melts.

The chemical profile along the GV10 pyroxenite (9 cm-long, Fig. 9 and Suppl. Fig. 1), where data were acquired only in cores of large clinopyroxene porphyroclasts, shows a significant zonation across the pyroxenite layer, with Mg-numbers of clinopyroxenes at the margins of the layer close to those of clinopyroxenes in the surrounding peridotite (a complete data set of this profile is provided in Suppl. Tables 1 and 2). Similar chemical gradients have been described across mafic-peridotite associations from orogenic massifs (e.g. Pearson et al., 1993; Takazawa et al., 1999; Mazzucchelli et al., 2010). They indicate that most of these pyroxenites, having a thickness of only a few centimetres, do not reflect equilibrium with the infiltrating parental melts but rather show a modified Mg-number due to the interaction with the surrounding peridotite. Accordingly, the composition of clinopyroxene porphyroclasts from the core of our thickest pyroxenite layer, GV10 and lens GV12, are likely to be the least affected by interaction with the peridotite. We thus used their compositions to calculate the Mg-number of the equilibrium parental melt, with the equation $Mg\#_{melt} = (K^{cpx}_{Fe\text{-}Mg} * Mg\#_{cpx})/(1\text{-}Mg\#_{cpx} + Mg\#_{cpx} * K^{cpx}_{Fe\text{-}Mg})$ proposed by Wood and Blundy (1997).

We assume that primary garnet-bearing clinopyroxenes had Mg-numbers similar to those of spinel-facies clinopyroxenes, because Mg-number is not expected to be significantly modified by subsequent lower-pressure recrystallization (e.g. Robinson & Wood, 1998). Computed Mg-numbers of the melt vary between 52-56 for layer GV10 and 44-50 for lens GV12. Melts with such values, significantly lower than the Mg-number of melts in equilibrium with mantle minerals, must have been very reactive with the surrounding peridotite. This is consistent with the occurrence of orthopyroxene-rich rims at the pyroxenite-peridotite boundary, as well as the orthopyroxene blebs and orthopyroxene modal enrichment in the wall rocks documented by Borghini et al. (2013).

Orthopyroxene enrichment at the pyroxenite-peridotite boundaries has been documented in other ultramafic massifs (e.g. Bodinier et al., 1987a; Varfalvy et al., 1996; Takazawa et al., 1999), and interpreted as the result of either solid-state reaction (e.g. Kogiso et al., 2004b; Herzberg et al., 2011) or reaction between high-silica activity melts, coming from the pyroxenites, and the surrounding peridotite (e.g. Varfalvy et al., 1996; Yaxley & Green, 1998; Sobolev et al., 2005; Lambart et al., 2012). In the studied pyroxenites, Borghini et al. (2013) have documented that clinopyroxenes in the first few (<5) centimetres of the host peridotite, at the contact with the pyroxenite layer (i.e. our so-called “wall-rock” peridotite),

have been chemically modified. In particular, the cm-scale progressive REE enrichment observed in clinopyroxene porphyroclasts of wall-rock peridotite points to reactive percolation of the pyroxenite-derived melt into the adjacent mantle. This is also consistent with the complete isotopic resetting observed in the first centimeters of the wall-rock peridotite (Borghini et al., 2013).

Lack of evidence for precursor garnet in the host peridotites suggests that this melt-rock reaction process occurred under spinel-facies mantle conditions, at pressures below garnet-lherzolite stability (P <2.8 GPa, e.g. O'Neill et al., 1981; Robinson & Wood, 1998), but likely above 1.5 GPa, to account for the garnet-bearing primary modes reconstructed for the pyroxenites. Spinel-facies clinopyroxene porphyroclasts in the wall-rock peridotites, thus, retain a trace element signature acquired by the interaction with the pyroxenite-derived melts (Borghini et al., 2013), and their REE composition can be used to obtain information on the geochemical signature of the pyroxenite parental melts.

Computed melts in equilibrium with wall-rock clinopyroxene porphyroclasts in the three profiles investigated by Borghini et al. (2013) are shown in Figure 15. We note here that a large set of trace element data has been filtered in order to select only the clinopyroxene porphyroclasts not affected by the subsequent plagioclase-bearing recrystallization, for example by checking Sr-Zr elemental variations (Rampone et al., 1993). However, the effect of a partial subsolidus plagioclase-facies re-equilibration would tend to slightly increase the REE absolute contents in clinopyroxene, without causing significant change of the LREE/HREE fractionation (Rampone et al., 1993; Hellebrand et al., 2005). Equilibrium melts are characterized by enrichment of LREE over HREE (La_N/Yb_N = 4-7.6) and moderate MREE-HREE fractionation (Dy_N/Yb_N = 1.2-1.4). The resulting melts have LREE significantly higher than a normal MORB and, rather, they resemble the REE compositions of enriched MORBs (E-type MORB) sampled in oceanic settings (Hemond et al., 1993, 2006; Hoernle et al., 2011; Waters et al., 2011). This is consistent with the initial epsilonNd values of clinopyroxenes in the pyroxenites, ranging from +3.29 to +8.25 (Borghini et al., 2013).

In summary, based on our microstructural and chemical observations, we conclude that the studied pyroxenites have originated from the segregation of low-Mg-number E-MORB melts. Moreover, very low alkali abundances of the bulk-rock pyroxenite compositions (Fig. 4 and Table 2), suggest a tholeiitic affinity of the parental melts.

Borghini et al. (2013) showed that interaction of EL pyroxenites with wall-rock peridotites reset the Nd isotopic compositions of the wall-rocks. They demonstrated that Sm-Nd isotopic investigations on clinopyroxene from pyroxenite-wall rock peridotite pairs

provide linear correlations yielding ages of 424-452 Ma, which are in good agreement with the age resulting from the errorchron defined by all pyroxenites (433±51 Ma), thus indicating the most likely timing of melt infiltration and pyroxenite emplacement. The ages indicate that this event significantly predated the Mesozoic evolution of this mantle sector (discussed below), and may have been related to Late Ordovician-Silurian lithosphere extension that led to the opening of the PaleoTethys oceanic basin (e.g. Stampfli & Borel 2002; von Raumer & Stampfli, 2008; Murphy et al., 2008).

Inferences on the nature of mantle source

The computed Mg-numbers of the parental melt (44-56) of the pyroxenites are too low to represent a primitive basaltic melt from a peridotitic mantle source (e.g. Walter, 1998). This indicates that pyroxenites originated either from i) a peridotite-derived melt that experienced significant chemical evolution, or ii) a melt derived by melting of a low-Mg-number hybrid source. The first hypothesis has been inferred for garnet pyroxenites from xenoliths (e.g. Frey et al., 1980; Keshav et al., 2007) and orogenic massifs (e.g. Bodinier et al., 1987a,b), and requires processes of liquid-crystal separation. A commonly invoked mechanism of high-pressure crystal segregation and melt differentiation is the dynamic flow crystallization in conduits described by Irving (1980). This model provides a possible alternative to the cumulus processes requiring the settling of crystals by gravity in magma chambers, a process difficult to be envisaged at pressures above 1.5 GPa within a plastically-deforming peridotite. However, how hydraulic fractures can form at such depth is unknown, because the deep mantle is not expected to be brittle enough to fracture (e.g. Kelemen et al., 1995, 1997). Moreover, it is noteworthy that the lowest Mg-number computed for our pyroxenite parental melts (around 44-50) would require more than 60% of fractional crystallization of a primitive melt with a Mg-number of 70 (Villiger et al., 2004). This would imply that a large amount of magmatic products should have been created in the mantle, before generating the evolved melt parental to the observed pyroxenites. Although there is no evidence of such large fractionation processes, we cannot exclude that this process played a role in the origin of our pyroxenites.

An alternative hypothesis calls for the involvement of a low-MgO mafic source component, as proposed for some pyroxenites from orogenic and ophiolitic massifs (e.g. Garrido & Bodinier, 1999; van Acken et al., 2010; Montanini et al., 2012; Marchesi et al., 2013; Montanini & Tribuzio, 2015). This means that low-Mg-number melts parental to pyroxenites can be the result of partial melting of a precursor mafic/pyroxenitic component or

a mixed pyroxenite-peridotite source. Several experimental studies have been dedicated to the melting behaviour of mafic lithologies at variably high pressure, and they have shown that a wide range of melt compositions can be produced, depending on the choice of starting bulk composition (e.g. Kogiso et al., 2004; Lambart et al., 2013).

In a review study on the composition of melts produced by pyroxenite melting at high pressure (>2 GPa), Kogiso et al. (2004) suggested that silica-deficient (SD) pyroxenites can be involved in the genesis of alkalic OIB lavas, whereas mixing of silica-excess (SE) pyroxenite melts with MgO-rich peridotitic melts would account for the genesis of tholeiitic OIB. Lack of olivine in the primary garnet-bearing assemblage of our pyroxenites (Table 12), together with the occurrence of orthopyroxene-rich rims along the contact with wall-rock peridotites, indicate that the observed pyroxenites have crystallized from melts with high silica activity, suggesting the involvement of a silica-excess pyroxenite component (e.g. Sobolev et al., 2005, 2007). Conversely, olivine-rich websterite and wehrlite are expected to form by reaction between melts produced by melting of SD pyroxenites and a peridotite (Lambart et al., 2012). Furthermore, the compositions of the pyroxenites in the proximity of the thermal divide in the pseudo-ternary CaTs-Fo-Qz diagram (see Fig. 12), suggest that they could have formed by partial melting of mantle sources with mixed eclogite-peridotite lithologies (Yaxley and Green, 1998; Kogiso et al., 1998; Takahashi & Nakajima, 2002; Mallik and Dasgupta, 2012; Fig. 12). Mallik and Dasgupta (2012) have recently demonstrated that saturated tholeiitic melts, with Mg-numbers as low as about 56, can form through reaction between eclogite-derived partial melts and a fertile peridotite. Remarkably, the compositions of such melts cover the range defined by our pyroxenites in the CMAS system (Fig. 12).

We propose that the EL pyroxenites originated from melts produced by a hybrid eclogite-peridotite mantle source, further modified through reaction with the host peridotite after their infiltration. The E-MORB signature inferred for the parental melts is consistent with this origin, given that similar E-MORB melts from modern mid-ocean-ridge settings are often interpreted to be the products of partial melting of a mantle peridotite source enriched by a pyroxenitic/mafic component (e.g. Hémond et al., 2006; Waters et al., 2011; Hoernle et al., 2011).

The major limitation of this hypothesis is that these low-Mg-number melts are highly reactive in the mantle; indeed, if their migration occurs by pervasive porous flow, then the compositions of these melts are expected to be rapidly buffered by reaction with the host peridotite (e.g. Daines & Kohlstedt, 1994). However, the occurrence of residues of precursor

eclogites within the EL mantle sector, in the form of garnet pyroxenites (Montanini et al., 2012), may support the scenario of a pristine eclogite-bearing mantle affected by partial melting. This could also indicate that such melts, after their production, migrated only over short distances, thus, preventing significant re-equilibration with the surrounding peridotite. The migration of these melts could have been enhanced by stress-driven melt segregation along shear zones, a mechanism able to produce high-permeability pathways within partially molten ductile rocks (e.g. Holtzman et al., 2003; Havlin et al., 2013). This is consistent with some field and geochemical evidence (Borghini unpublished), suggesting that the pyroxenite emplacement occurred within an already plastically deformed mantle. Part of the evolved signature of parental melts to the pyroxenites, such as the low Mg-numbers, could have been acquired by crystal segregation and melt evolution along these high-porosity magma conduits.

In summary, a possible scenario is that low-Mg-number melts produced by moderate degrees of SE pyroxenite/eclogite melting were mixed with low-degree peridotitic melts, which infiltrated and reacted with the overlying mantle to form the Suvero suite of pyroxenites layers.

This scenario is in agreement with recent models of basalt petrogenesis that invoke the generation of secondary pyroxenites in the upper mantle by interaction between peridotites and silica-rich melts derived by deeper melting of mafic components prior to major basalt production with larger degrees of melting (Sobolev et al., 2005, 2007; Lambart et al., 2012). According to our petrological reconstruction, the EL pyroxenites represent an excellent natural example of such secondary pyroxenites. We argue that partial melting of mafic components within a rising heterogeneous mantle, and the infiltration of the resulting melts, reacting with the host mantle peridotites, are efficient processes to generate additional heterogeneities in the upper mantle (Garrido & Bodinier, 1999; Borghini et al., 2013; Marchesi et al., 2013; Montanini & Tribuzio, 2015).

Metamorphic evolution and timing of exhumation

The mass balance modelling in this work accounts for the fractionation of HREE over the MREE shown by the bulk composition of many of the pyroxenites, thus supporting the hypothesis that they originally contained a primary garnet-bearing mineral assemblage, which is not preserved. The oldest mineral assemblage observed in the pyroxenites consists of coarse porphyroclasts of green spinel, clinopyroxene ± orthopyroxene, partially replaced by plagioclase-bearing neoblasts. The occurrence of plagioclase+olivine coronas around spinel porphyroclasts suggests that plagioclase did not originate directly from the breakdown of the

garnet-bearing assemblage. Rather, textural observations indicate that the plagioclase-bearing neoblastic assemblage replaced a previous spinel-bearing association, thus suggesting that plagioclase appeared at lower pressure than the spinel+pyroxenes assemblage. This is in agreement with experimental results on a low-Na garnet-spinel websterite (pyroxenite R394 from Irving, 1974) and computed subsolidus phase relations for a low-Na, high-Mg websterite from Ronda ultramafic massif (southern Spain, Hidas et al., 2013). A similar mineralogical evolution has been documented in Mg-rich clinopyroxenites and websterites from other External Liguride Units, and related to progressive mantle exhumation, from garnet- to spinel- to plagioclase-facies conditions (Montanini et al., 2006).

Thermometric estimates on cores of coarse spinel-facies pyroxenes indicate temperatures around 950-1000°C, which must be considered as minimum temperatures, given the occurrence of exsolution textures in both pyroxenes. According to experimental results on a garnet-spinel websterite, the spinel-bearing assemblage observed in the pyroxenites should record a recrystallization stage within the P-T range of 1.2-1.5 GPa and T <1200°C, as this is expected to be the solidus temperature at 1.5 GPa (Irving 1974).

Continued pressure decrease led to crystallization of a plagioclase-bearing neoblastic assemblage at the expense of spinel-facies porphyroclasts. This process is accompanied by systematic changes in mineral compositions, including lower Al content in pyroxenes (Fig. 6) and higher Cr-number and TiO_2 content at lower Mg-number in the small relicts of spinel (Fig. 7), similar to what is observed in plagioclase peridotites of metamorphic origin (e.g. Gasparik, 1984; Rampone et al., 1993; Montanini et al., 2006; Borghini et al., 2010, 2011). Borghini et al. (2011) previously traced the exhumation of mantle peridotite hosting the pyroxenites from 0.7 to 0.3 GPa by applying thermometric estimates on neoblastic pyroxenes and experimentally-derived An-isopleths of plagioclase. Therefore, we infer that associated pyroxenites reasonably followed the same P-T path as the host peridotites. Average compositions of plagioclase in pyroxenites (core: An = 0.58-0.64; rim: An = 0.76-0.82; Table 6) are very close to those documented in the associated peridotites (core: An = 0.56-0.59; rim: An = 0.74-0.79; Borghini et al., 2011). This may indicate that the plagioclase composition does not depend on the bulk-rock chemistry even in pyroxenite bulks, which are significantly different from peridotite lithologies (Borghini et al., 2010), however, this needs to be confirmed by further experimental data. As a consequence, according to the An in plagioclase geobarometer proposed by Borghini et al. (2011), the similarity of An contents would constitute robust evidence that plagioclase crystallized contemporaneously in both pyroxenites and peridotites during their decompressional evolution.

Internal Sm-Nd isochrons, based on clinopyroxene-plagioclase-whole rocks analyses performed on four samples, give an average age of 178 (±8) Ma (Fig. 11) for the plagioclase-facies recrystallization event, which dates the exhumation of this mantle sector at relatively shallow depth. This age is slightly younger than the ages obtained by internal Sm-Nd isochrons documented in garnet pyroxenites investigated by Montanini et al. (2006). They proposed a Middle to Late Triassic age for the near-isothermal spinel- to plagioclase-facies decompression recorded by the External Liguride mantle section. Sm-Nd ages provided by this study indicate that exhumation of this EL mantle sector occurred in the Early Jurassic, which is coeval with the first syn-rift MOR-type intrusions in the subcontinental mantle of the Piedmont-Ligurian oceanic basin (Tribuzio et al., 2004, Rampone et al., 2014).

CONCLUDING REMARKS

Pyroxenites form centimetre-thick layers and lenses in peridotite from the External Liguride ultramafic massif (Northern Apennines, Italy); they range from websterites to clinopyroxenites, and are characterized by a porphyroclastic spinel-facies assemblage partially replaced by a low-pressure plagioclase-bearing neoblastic association.

Microstructural and chemical features shown by several pyroxenite samples suggest that variable modal amounts of garnet were present in the primary mineral association, thus indicating that pyroxenites likely originated by segregation of melts at rather high pressure (above 1.5 GPa).

Chemical and Sr-Nd isotopic compositions indicate that pyroxenites crystallized from a E-MORB-type melt, similar to those documented in modern mid-ocean-ridge settings. Low Mg-numbers together with the lack of olivine in most of the primary mineral assemblages suggest that their parental melts were produced by partial melting of a hybrid pyroxenite-bearing mantle, which then reacted with the host peridotite during high-pressure infiltration. The EL pyroxenites studied in this work are an example of a "secondary pyroxenite" component in the upper mantle, which has been proposed in recent models of basalt petrogenesis at oceanic intra-plate and mid-ocean ridge settings.

Finally, later decompressional metamorphic evolution from spinel- to plagioclase-facies followed the same P-T path defined for the host peridotites (Borghini et al., 2011). Low-P plagioclase-facies re-equilibration is dated by internal (clinopyroxene-plagioclase-whole rocks) Sm-Nd isochrons at 178±8 Ma, indicating that the exhumation of this mantle sector can be attributed to the Mesozoic continental rifting that led to the opening of the Jurassic Tethys.

ACKNOWLEDGEMENTS

This study was supported by the University of Genova (grant PRA2011 and PRA2013), the U.S. National Science Foundation grant ANT10-43540 (to Class and Goldstein), and the Storke Endowment of the Department of Earth and Environmental Sciences of Columbia University. L. Negretti and A. Risplendente are greatly thanked for assistance with the EDS and WDS analyses. L. Bolge, Y. Cai, P. Montagna and N. Rollins are acknowledged for their laboratory and analytical help. Reviews by J.-L. Bodinier, O. Müntener and an anonymous referee are gratefully acknowledged for constructive criticisms and suggestions, which improved an early version of the paper. We thank M. Wilson for the editorial handling. This is Lamont-Doherty Earth Observatory (LDEO) Contribution # XXXX (number to be filled in if accepter for publication).

REFERENCES

Adam, J., Green, T. H. & Day, R.A. (1992). An experimental study of two garnet pyroxenite xenoliths from the Bullenmerri and Gnotuk Maars of western Victoria, Australia. *Contributions to Mineralogy and Petrology* **111**, 505–514.

Allègre, C.J. & Turcotte, D.L. (1986). Implications of a two-component marble-cake mantle: *Nature* **323**, 123–127.

Alt, J.C., Teagle, D.A.H., Brewer, T., Shanks, W.C. & Halliday, A. (1998). Alteration and mineralization of an oceanic forearc and ophiolite-oceanic crust analogy. *Journal of Geophysical Research* **103**, 12365-12380.

Anders, E. & Grevesse, N. (1989). Abundances of the elements: meteoric and solar: *Geochimica et Cosmochimica Acta* **53**, 197–214.

Beccaluva, L., Macciotta, G., Piccardo, G. B. & Zeda, O. (1984). Petrology of lherzolitic rocks from the Northern Apennine ophiolites. *Lithos* **17**, 299–316.

Becker, H. (1996). Crustal trace element and isotopic signatures in garnet pyroxenites from garnet peridotite massifs from Lower Austria. *Journal of Petrology* **37**, 785-810.

Bizimis, M., Sen, G., Salters, V.J.M. & Keshav, S. (2005). Hf–Nd–Sr isotope systematics of garnet pyroxenites from Salt Lake Crater, Oahu, Hawaii: evidence for a depleted component in Hawaiian volcanism. *Geochimica et Cosmochimica Acta* **69**, 2629-2646.

Blichert-Toft, J., Albare`de, F. & Kornprobst, J. (1999). Lu–Hf isotope systematics of garnet pyroxenites from Beni Bousera, Morocco: implications for basalt origin. *Science* **283**, 1303–1306.

Bodinier, J.-L., Guiraud, M., Fabries, J., Dostal, J. & Dupuy, C. (1987a). Petrogenesis of layered pyroxenites from the Lherz, Freychinede and Prades ultramafic bodies (Ariege, French Pyrenees). *Geochimica et Cosmochimica Acta* **51**, 279-290.

Bodinier, J.-L., Fabries, J., Lorand, J.-P., Dostal, J. & Dupuy, C. (1987b). Geochemistry of amphibole pyroxenite veins from the Lherz and Freychinede ultramafic bodies (Ariege, French Pyrenees). *Bull. Mineral.* **110**, 345-358.

Bodinier, J.-L. & Godard, M. (2003). Orogenic, ophiolitic and abyssal peridotites: Treatise on Geochemistry, v. 2, H.D. Holland and K.K. Turkian (eds). Oxford, UK, Elsevier Science.

Bodinier, J.-L., Garrido, C.J., Chanefo, I., Bruguier, O. & Gervilla, F. (2008). Origin of pyroxenite-peridotite veined mantle by refertilization reactions: Evidence from the Ronda peridotite (Southern Spain). *Journal of Petrology* **49**, 999-1025.

Borghini, G., Fumagalli, P. & Rampone, E. (2010). The stability of plagioclase in the upper mantle: subsolidus experiments on fertile and depleted lherzolite. *Journal of Petrology* **51**, 229-254.

Borghini, G., Fumagalli, P. & Rampone, E. (2011). The geobarometric significance of plagioclase in mantle peridotites: A link between nature and experiments: *Lithos* **126**, 42–53.

Borghini, G., Rampone, E., Zanetti, A., Class, C., Cipriani, A., Hofmann, A.W. & Goldstein, S. (2013). Meter-scale Nd isotopic heterogeneity in pyroxenite-bearing Ligurian peridotites encompasses global-scale upper mantle variability. *Geology* **41**, 1055-1058.

Brey, G.P. & Köhler, T. (1990). Geothermobarometry in four-phase lherzolites II. New thermobarometers, and practical assessment of existing thermobarometers. *Journal of Petrology* **31**, 1353-1378.

Chazot, G., Charpentier, S., Kornprobst, J., Vannucci, R. & Luais, B. (2005). Lithospheric mantle evolution during continental break-up: the West Iberia non-volcanic passive margin. *Journal of Petrology* **46**, 2527-2568.

Class, C. & Lehnert, K. (2012). PetDB Expert MORB, Mid-Ocean Ridge Basalt, Compilation. EarthChem Library. http://dx.doi.org/10.1594/IEDA/100060.

Daines, M.J. & Kohlstedt, D.L. (1994). The transition from porous to channelized flow due to melt/rock reaction during melt migration. *Geophys. Res. Lett.* **21**, 145-148.

Dantas, C., Ceuleneer, G., Gregoire, M., Python, M., Freydier, R., Warren, J. & Dick, H.J.B. (2007). Pyroxenites from the Southwest Indian Ridge, 9–16°E: cumulates from incremental melt fraction produced at the top of a cold melting regime. *Journal of Petrology* **48**, 647-660.

Dantas, C., Gregoire, M., Koester, E., Conceicao, R.D. & Rieck Jr., N. (2009). The lherzolite-websterite xenolith suite from Northern Patagonia (Argentina): evidence of mantle-melt reaction processes. *Lithos* **107**, 107-120.

Davies, G. R., Nixon, P. H., Pearson, D. G. & Obata, M. (1993). Tectonic implications of graphitized diamonds from the Ronda peridotite massif, southern Spain. *Geology* **21**, 471–474.

Downes, H. (2007). Origin and significance of spinel and garnet pyroxenites in the shallow lithospheric mantle: Ultramafic massifs in orogenic belts in Western Europe and NW Africa. *Lithos* **99**, 1-24.

Fabries, J., Lorand, J.-P. & Guiraud, M. (2001). Petrogenesis of the amphibole-rich veins from Lherz orogenic lherzolite massif (Easter Pyrenees, France): a case study for the origin of orthopyroxene-bearing amphibole pyroxenites in the lithospheric mantle. *Contribution to Mineralogy and Petrology* **140**, 383-403.

Frey, F.A. (1980). The origin of pyroxenites and garnet pyroxenites from Salt Lake Crater, OAHU, Hawaii: trace element evidence. *American Journal of Science* **280**, 427-449.

Garrido, C.J. & Bodinier, J.L. (1999). Diversity of mafic rocks in the Ronda peridotite: evidence for pervasive melt–rock reaction during heating of subcontinental lithosphere by upwelling asthenosphere. *Journal of Petrology* **40**, 729-754.

Gasparik, T. (1984). Two-pyroxene thermobarometry with new experimental data in the system CaO-MgO-Al_2O_3-SiO_2. *Contribution to Mineralogy and Petrology* **87**, 87-97.

Green, D.H. & Falloon, T.J. (1998). Pyrolite: A Ringwood concept and its current expression. In: The Earth's Mantle, edited by I. Jackson, 311-378, Cambridge University Press, Cambridge.

Gonzaga, R.G., Lowry, D., Jacob, D.E., LeRoex, A., Schulze, D. & Menzies, M.A. (2009). Eclogites and garnet pyroxenites: similarities and differences. *J. Volcanol. Geotherm. Res.* **190**, 235-247.

Gysi, A.P., Jagoutz, O., Schmidt, M.W. & Targuisti, K. (2011). Petrogenesis of pyroxenites and melt infiltrations in the ultramafic complex of Beni Boussera, Northern Morocco. *Journal of Petrology* **52**, 1676-1735.

Hauri, E.H., Wagner, T.P. & Grove, T.L. (1994). Experimental and natural partitioning of Th, U, Pb and other trace elements between garnet, clinopyroxene and basaltic melts. *Chemical Geology* **117**, 149-166.

Havlin, C., Parmentier, E.M. & Hirth, G. (2013). Dike propagation driven by melt accumulation at the lithosphere-asthenosphere boundary. *Earth and Planetary Sciences Letters* **376**, 20-28.

Hellebrand, E., Snow, J.E., Mostefaoui, S. & Hoppe P. (2005). Trace element distribution between orthopyroxene and clinopyroxene in peridotites from Gakkel Ridge: a SIMS and NanoSIMS study. *Contribution to Mineralogy and Petrology* **150**, 486-504.

Hémond, C., Arndt, N.T., Lichtenstein, U. & Hofmann, A.W. (1993). The heterogeous Iceland plume: Nd-Sr-O isotopes and trace element constraints. *Journal of Geophysical Research* **98**, 15833-15850.

Hémond, C., Hofmann, A.W., Vlastelic, I. & Nauret, F. (2006). Origin of MORB enrichment and relative trace element compatibilities along the Mid-Atlantic Ridge between 10° and 24°N. *Geochemistry Geophysics Geosystems* **7**, Q12010.

Herzberg, C.T. (1978). Pyroxene geothermometry and geobarometry: experimental and thermodynamic evaluation of some subsolidus phase relations involving pyroxenes in the system CaO-MgO-Al_2O_3-SiO_2. *Geochimica et Cosmochimica Acta* **42**, 945-957.

Herzberg, C. (2011). Identification of source lithology in the Hawaiian and Canary Island: implications for origins. *Journal of Petrology* **52**, 113-146.

Hidas, K., Garrido, C., Tommasi, A., Padron-Navarta, J.A., Thielmann, M., Konc, Z., Frets, E. & Marchesi, C. (2013). Strain localization in pyroxenite by reaction-enhanced softening in the shallow subcontinental lithospheric mantle. *Journal of Petrology* **54**, 1997-2031.

Hirschmann, M.M. & Stolper, E.M. (1996). A possible role for garnet pyroxenite in the origin of the 'garnet signature' in MORB. *Contributions to Mineralogy and Petrology* **124**, 185-208.

Hirschmann, M. M., Kogiso, T., Baker, M. B. & Stolper, E. M. (2003). Alkalic magmas generated by partial melting of garnet pyroxenite. *Geology* **31**, 481-484.

Hoernle, K., Hauff, F., Kokfelt, T.F., Haase, K., Garbe-Shonberg, D. & Werner, R. (2011). On- and off-axis chemical heterogeneities along the South Atlantic Mid-Ocean-Ridge (5–11°S): shallow or deep recycling of ocean crust and/or intraplate volcanism? *Earth and Planetary Science Letters* **306**, 86-97.

Hofmann, A.W. (1988). Chemical differentiation of the earth: the relationships between mantle, continental crust and oceanic crust. *Earth and Planetary Science Letters* **90**, 297-314.

Hofmann, A.W. (2003). Sampling mantle heterogeneity through oceanic basalts: Isotopes and trace elements, in Carlson, R.W., ed., The Mantle and Core: Treatise on Geochemistry, v. 2, 61-101.

Holtzman, B., Groebner, N., Zimmerman, M., Ginsberg, S. & Kohlstedt, D. (2003). Stress-driven melt segregation in partially molten rocks. *Geochem. Geophys. Geosyst.* **4**, 8607.

Horn, I., Foley, S.F., Jackson, S.E. & Jenner, G.A. (1994). Experimentally determined partitioning of high field strength- and selected transition elements between spinel and basaltic melt. *Chemical Geology* **117**, 193-218.

Ionov, D. A., Bodinier, J. L., Mukasa, S. B. & Zanetti, A. (2002). Mechanisms and sources of mantle metasomatism: major and trace element conditions of peridotite xenoliths from Spitzbergen in the context of numerical modelling. *Journal of Petrology* **43**, 2219-2259.

Irving, A.J. (1974). Geochemical and high pressure experimental studies on garnet pyroxenite and pyroxene granulite xenoliths from the Delegate basaltic pipes. Australia. *Journal of Petrology* **15**, 1-40.

Jacob, D.E. (2004). Nature and origin of eclogite xenoliths from kimberlites. *Lithos* **77**, 295-316.

Jacobsen, S.B. & Wasserburg, G.J. (1980). Sm-Nd isotopic evolution of chondrites. *Earth and Planetary Science Letters* **50**, 139-155.

Johnson, K.T.M. (1998). Experimental determination of partition coefficient for rare earth and high-field-strenght elements between clinopyroxene, garnet, and basaltic melt at high pressures. *Contributions to Mineralogy and Petrology* **133**, 60-68.

Kelemen, P.B., Whitehead, J.A., Aharonov, E. & Jordahl, K.A. (1995). Experiments on flow focusing in soluble porous-media, with applications to melt extraction from the mantle. *Journal of Geophysical Research* **100**, 475-496.

Kelemen, P.B., Hirth, G., Shimizu, N., Spiegelman, M. & Dick, H.J.B. (1997). A riview of melt migration processes in the adiabatically upwelling mantle beneath oceanic spreading ridges. *Philosophical Transactions: Mathematical, Physical and Engineering Sciences* **355**, 283-318.

Kempton, P.D. & Stephens, C.J. (1997). Petrology and geochemistry of nodular websterites inclusions in harzburgite, Hole 920D, in Karson, J.A., et al., eds., Proceedings of the Ocean Drilling Program, Scientific results **153**: College Station, Texas, Ocean Drilling Program, p. 321-331.

Kaeser, B., Olker, B., Kalt, A., Altherr, R. & Pettke, T. (2009). Pyroxenite xenoliths from Marsabit (Northern Kenya): evidence for different magmatic events in the lithospheric mantle and interaction between peridotite and pyroxenite. *Contributions to Mineralogy and Petroogy* **157**, 453-472.

Keshav, S., Sen, G. & Presnall, D.C. (2007). Garnet-bearing xenoliths from Salt Lake Crater,

Oahu, Hawaii: high-pressure fractional crystallisation in the oceanic mantle. *Journal of Petrology* **48**, 1681-1724.

Kogiso, T., Hirose, K. & Takahashi, E. (1998). Melting experiments on homogeneous mixtures of peridotite and basalt: application to the genesis of ocean island basalts. *Earth and Planetary Science Letters* **162**, 45-61.

Kogiso, T., Hirschmann, M. M. & Frost, D. J. (2003). High-pressure partial melting of garnet pyroxenite: possible mafic lithologies in the source of ocean island basalts. *Earth and Planetary Science Letters* **216**, 603-617.

Kogiso, T., Hirschmann, M.M. & Pertermann, M. (2004a). High-pressure partial melting of mafic lithologies in the mantle. *Journal of Petrology* **45**, 2407-2422.

Kogiso, T., Hirschmann, M.M. & Reiners, W. (2004b). Length scales of mantle heterogeneities and their relationship to ocean island basalt geochemistry. *Geochimica et Cosmochimica Acta* **68**, 345-360.

Kornprobst, J., Piboule, M., Roden, M. & Tabit, A. (1990). Corundum-bearing garnet clinopyroxenites at Beni Bousera (Morocco): original plagioclase-rich gabbros recrystallized at depth within the mantle? *Journal of Petrology* **31**, 717-745.

Kumar, N., Reisberg, L. & Zindler, A. (1996). A major and trace element and strontium, neodymium, and osmium isotopic study of a thick pyroxenite layer from the Beni Bousera ultramafic complex of northern Morocco. *Geochimica et Cosmochimica Acta* **60**, 1429-1444.

Lambart, S., Laporte, D. & Schiano, P. (2009). An experimental study of pyroxenite partial melts at 1 and 1·5 GPa: implications for the major-element composition of mid-ocean ridge basalts. *Earth and Planetary Science Letters* **288**, 335-347.

Lambart, S., Laporte, D., Provost, A. & Schiano, P. (2012). Fate of pyroxenite-derived melts in the peridotitic mantle: thermodynamic and experimental constraints. *Journal of Petrology* **53**, 451-476.

Lambart, S., Laporte, D., and Schiano, P. (2013). Markers of the pyroxenite contribution in the major-element compositions of oceanic basalts: Review of the experimental constraints. *Lithos* **160-161**, 14-36.

Leake, B.E. (1997). Nomenclature of amphiboles: report of the subcommittee on amphiboles of the international mineralogical association, commission on new minerals and mineral names. *American Mineralogists* **82**, 1019-1037.

Lehnert, K., Su, Y., Langmuir, C., Sarbas, B. & Nohl, U. (2000). A global geochemical database structure for rocks. *Geochemistry Geophysics Geosystems* **1**, 1012-1025.

Loubet, M. & Allègre, C.J. (1982). Trace elements in orogenic lherzolites reveal the complex history of the upper mantle. *Nature* **298**, 809.

Mallik, A. & Dasgupta, R. (2012). Reaction between MORB-eclogite derived melts and fertile peridotite and generation of ocean island basalts. *Earth and Planetary Science Letters* **329-330**, 97-108.

Marchesi, C., Garrido, C.J., Bosch, D., Bodinier, J-L., Hidas, K., Padron-Navarta, A. & Gervilla, F. (2012). A late Oligocene suprasubduction setting in the Westernmost Mediterranean revealed by intrusive pyroxenite dikes in th Ronda peridotite (Southern Spain). *Journal of Geology* **120**, 237-247.

Marchesi, C., Garrido, C.J., Bosch, D., Bodinier, J-L., Gervilla, F. & Hidas, K. (2013). Mantle refertilization by melts of crustal-derived garnet pyroxenite: Evidence from the Ronda peridotite massif, southern Spain. *Earth and Planetary Science Letters* **362**, 66-75.

Marroni, M., Molli, G., Montanini, A. & Tribuzio, R. (1998). The association of continental crust rocks with ophiolites in the Northern Apennines (Italy): implications for the continent-ocean transition in the Western Tethys: *Tectonophysics* **292**, 43-66.

Mazzucchelli, M., Zanetti, A., Rivalenti, G., Vannucci, R., Correia, C.T. & Tassinari, C.C.G. (2010). Age and geochemistry of mantle peridotites and diorite dykes from the Baldissero body: Insights into the Paleozoic-Mesozoic evolution of the Southern Alps. *Lithos* **119**, 485-500.

Mezger, K., Essene, E.J. & Halliday, A.N. (1992). Closure temperature of the Sm-Nd system in metamorphic garnets. *Earth Planetary Sciences Letters* **113**, 397-409.

Miller, C., Zanetti, A., Thoni, C. & Konzett, J. (2007). Eclogitisation of gabbroic rocks: redistribution of trace elements and Zr in rutile thermometry in an Eo-Alpine subduction zone (Eastern Alps). *Chemical Geology* **239**, 96-123.

Montanini, A., Tribuzio, R. & Anczkiewicz, R. (2006). Exhumation history of a garnet pyroxenite-bearing mantle section from a continent-ocean transition (Northern Apennine ophiolites, Italy). *Journal of Petrology* **47**, 1943-1971.

Montanini, A., Tribuzio, R. & Thirlwall, M. (2012). Garnet clinopyroxenite layers from the mantle sequences of the Northern Apennine ophiolites (Italy): Evidence for recycling of crustal material. *Earth and Planetary Science Letters* **351-352**, 171-181.

Montanini, A. & Tribuzio, R. (2015). Evolution of recycled crust within the mantle: constraints from the garnet pyroxenites of the External Ligurian ophiolites (northern Apennines, Italy). *Geology* **43**, 911-914.

Morishita, T. & Arai, S. (2001). Petrogenesis of corundum-bearing mafic rock in the

Horoman Peridotite Complex, Japan. *Journal of Petrology* **42**, 1279-1299.

Morishita, T., Arai, S., Gervilla, F. & Green, D. H. (2003). Closed-system geochemical recycling of crustal materials in the upper mantle. *Geochimica et Cosmochimica Acta* **67**, 303-310.

Mukasa, S.B. & Shervais, J.W. (1999). Growth of sub-continental lithosphere: Evidence from repeated injections in the Balmuccia lherzolite massif, Italian Alps. *Lithos* **48**, 287-316.

Müntener, O., Hermann, J. (1996). The Val Malenco lower crust – Upper mantle complex and its field relations (Italian Alps). *Schweizerische Mineralogishe und Petrographische Mitteilungen* **76**, 475-500.

Müntener, O., Kelemen, P.B. & Grove, T.L. (2001). The role of H2O during crystallization of primitive arc magmas under uppermost mantle conditions and genesis of igneous pyroxenites: an experimental study. *Contributions to Mineralogy and Petrology* **141**, 643-658.

Müntener, O., Pettke, T., Desmurs, L., Meier, M. & Schaltegger. U. (2004). Refertilization of mantle peridotite in embryonic ocean basins: trace element and Nd-isotopic evidence and implications for crust-mantle relationships. *Earth and Planetary Science Letters* **221**, 293-308.

Müntener, O., Manatschal, G., Desmurs, L. & Pettke, T. (2010). Plagioclase peridotites in Oceanic-Continent transitions: refertilized mantle domains generated by melt stagnation in the shallow mantle lithosphere. *Journal of Petrology* **51**, 255-294.

Murphy, B.J., Gutierrez-Alonso, G., Fernandez-Suarez, J. & Braid, J.A. (2008). Probing crustal and mantle lithosphere origin through Ordovician volcanic rocks along the Iberian passive margin of Gondwana. *Tectonophysics* **461**, 166-180.

Nimis, P., Taylor, W.R. (2000). Single-clinopyroxene thermobarometry for garnet peridotites. Part I. Calibration and testing of a Cr-in- Cpx barometer and an enstatite-in-Cpx thermometer. *Contributions to Mineralogy and Petrology* **139**, 541-554.

Nimis, P. & Grutter, H. (2010). Internally consistent geothermometers for garnet peridotites and pyroxenites. *Contributions to Mineralogy and Petrology* **159**, 411-427.

O'Hara, M.J. (1968). The bearing of phase equilibria studies in synthetic and natural systems on the origin and evolution of basic and ultrabasic rocks. *Earth-Science Reviews* **4**, 69-133.

O'Neill, H. St. C. (1981). The transition between spinel lherzolite and garnet lherzolite, and its use as a geobarometer. *Contributions to Mineralogy and Petrology* **77**, 185-194.

Pearson, D.G., Davies, G.R. & Nixon, P.H. (1993). Geochemical constraints on the petrogenesis of diamond facies pyroxenites from the Beni Bousera peridotite massif, North Morocco. *Journal of Petrology* **34**, 125-172.

Pearson, D.G. & Nowell, G.M. (2004). Re-Os and Lu-Hf isotope constraints on the origin and age of pyroxenites from the Beni Bousera peridotite massif: implications for mixed peridotite-pyroxenite mantle source. *Journal of Petrology* **45**, 439-455.

Pertermann, M. & Hirschmann, M. M. (2003). Anhydrous partial melting experiments on MORB-like eclogite: phase relations, phase compositions and mineral–melt partitioning of major elements at 2– 3 GPa. *Journal of Petrology* **44**, 2173–2201.

Piccardo, G.B., Zanetti, A., Poggi, E., Spagnolo, G. & Müntener, O. (2007). Melt/peridotite interaction in the Lanzo South peridotite: field, textural and geochemical evidence. *Lithos* **94**, 181-209.

Rampone, E., Piccardo, G.B., Vannucci, R., Bottazzi, P. & Ottolini, L. (1993). Subsolidus reactions monitored by trace element partitioning: the spinel- to plagioclasi-facies transition in mantle peridotites. *Contribution to Mineralogy and Petrology* **115**, 1-17.

Rampone, E., Hofmann, A.W., Piccardo, G.B., Vannucci, R., Bottazzi, P. & Ottolini, L. (1995). Petrology, mineral and isotope geochemistry of the External Liguride peridotites (Northern Appennine, Italy). *Journal of Petrology* **123**, 61-76.

Rampone, E., Piccardo, G.B., Vannucci, R. & Bottazzi, P. (1997). Chemistry and origin of ted melts in ophiolitic peridotites. *Geochimica et Cosmochimica Acta* **61**, 4557-4569.

Rampone, E., Hofmann, A.W. & Raczek, I. (1998). Isotopic contrasts within the Internal Liguride ophiolite (N. Italy): the lack of a genetic mantle-crust link. *Earth and Planetary Science Letters* **163**, 175-189.

Rampone, E., Romairone, A. & Hofmann, A.W. (2004). Contrasting bulk and mineral chemistry in depleted peridotites: evidence for reactive porous flow. *Earth and Planetary Science Letters* **218**, 491-506.

Rampone, E., Piccardo, G.B. & Hofmann, A.W. (2008). Multi-stage melt-rock interaction in the Mt. Maggiore (Corsica, France) ophiolitic peridotites: microstructural and geochemical records. *Contribution to Mineralogy and Petrology* **156**, 453-475.

Rampone, E. & Hofmann, A.W. (2012). A global overview of isotopic heterogeneities in the oceanic mantle. *Lithos* **148**, 247-261.

Rampone, E., Borghini, G., Romairone, A., Abouchami, W., Class, C. & Goldstein, S.L. (2014). Sm-Nd geochronology of the Erro-Tobbio gabbros (Ligurian Alps, Italy): insights on the evolution of the Alpine Tethys. *Lithos* **205**, 236-246.

Rivalenti, G., Mazzucchelli, M., Vannucci, R., Hofmann, A.W., Ottolini, L. & Obermiller, W. (1995). The relationship between websterite and peridotite in the Balmuccia peridotite massif (NW Italy) as revealed by trace element variations in clinopyroxene. *Contributions to Mineralogy and Petrology* **121**, 275-288.

Robinson, J.A.C. & Wood, B.J. (1998). The depth of the spinel to garnet transition at the peridotite solidus. *Earth and Planetary Science Letters* **164**, 277-284.

Salters, V.J.M. & Dick, H.J.B. (2002). Mineralogy of the mid-ocean-ridge basalt source from neodymium isotopic composition of abyssal peridotites. *Nature* **418**, 68-72.

Sinigoi, S., Comin-Chiaramonti, P., Demarchi, G. & Siena, F. (1983). Differentiation of partial melts in the mantle: evidence from the Balmuccia peridotite, Italy. *Contributions to Mineralogy and Petrology* **82**, 351-359.

Snow, J. E., Schmidt, G. & Rampone, E. (2000). Os isotopes and highly siderophile elements (HSE) in the Ligurian ophiolites, Italy. *Earth and Planetary Science Letters* **175**, 119-132.

Sobolev, A.V., Hofmann, A.W., Sobolev, S.V. & Nikogosian, I.K. (2005). An olivine-free mantle source of Hawaiian shield basalts. *Nature* **434**, 590-597.

Sobolev, A.V., Hofmann, A.W. & Kuzmin, D.W. (2007). The amount of recycled crust in sources of mantle-derived melts. *Science* **316**, 412-417.

Stampfli, G.M. & Borel, G.D. (2002). A plate tectonic model for the Paleozoic and Mesozoic constrained by dynamic plate boundaries and restored synthetic oceanic isochrons. *Earth and Planetary Science Letters* **196**, 17-33.

Stracke, A., Salters, V.J.M. & Sims, K.W.W. (1999). Assessing the presence of garnet–pyroxenite in the mantle sources of basalts through combined hafnium–neodymium–thorium isotope systematics. *Geochemistry Geophysics Geosystems* **1**.

Stracke, A. & Bourdon, B. (2009). The importance of melt extraction for tracing mantle heterogeneity. *Geochimica et Cosmochimica Acta* **73**, 218-238.

Suen, C.J. & Frey F.A. (1987). Origin of the mafic and ultramafic rocksin the Ronda peridotite. *Earth and Planetary Science Letters* **85**, 183-202.

Takahashi, E., Nakajima, K. & Wright, T. L. (1998). Origin of the Columbia River basalts: melting model of a heterogeneous plume head. *Earth and Planetary Science Letters* **162**, 63-80.

Takahashi, E. & Nakajima, K. (2002). Melting process in the Hawaiian plume: an experimental study. In: Takahashi, E., Lipman, P. W., Garcia, M. O., Naka, J. & Aramake, S. (eds) Hawaiian Volcanoes: Deep Underwater Perspectives. Geophysical

Mono-graph, American Geophysical Union **128**, 403-418.

Takazawa, E., Frey, F.A., Shimizu, N., Saal, N. & Obata, M. (1999). Polybaric petrogenesis of mafic layers in the Horoman peridotite complex, Japan. *Journal of Petrology* **40**, 1827-1831.

Tanaka, T., Togashi, S., Kamioka, H. et al. (2000). JNdi-1: a neodymium isotopic reference in consistency with LaJolla neodymium. *Chemical Geology* **168**, 279-281.

Taylor, W.R. (1998). An experimental test of some geothermometer an geobarometer formulation for upper mantle peridotites with application to the thermobarometry of fertile lherzolite and garnet websterite. *N. Jb. Min. Abh.* **172**, 381-408.

Thirlwall, M.F. (1991). Long-term reproducibility of multicollector Sr and Nd isotope ratio analysis. *Chemical Geology* **94**, 85-104.

Tribuzio, R., Thirwall, M.F. & Vannucci, R. (2004). Origin of the gabbro-peridotite association from the Northern Apennine ophiolites (Italy). *Journal of Petrology* **45**, 1109-1124.

Tsuruta, K. & Takahashi, E. (1998). Melting study of an alkali basalt JB-1 up to 12.5GPa: behavior of potassium in the deep mantle. *Physics of the Earth and Planetary Interiors* **107**, 119-130.

Van Acken, D., Becker, H., Walker, R.J., McDonough, W.F., Wombacher, F., Ash, R.D. & Piccoli, P.M. (2010). Formation of pyroxenite layers in the Totalp ultramafic massif (Swiss Alps) – Insights from highly siderophile elements and Os isotopes. *Geochimica et Cosmochimica Acta* **74**, 661-683.

Vannucci, R., Shimizu, N., Piccardo, G.B., Ottolini, L. & Bottazzi, P. (1995). Distribution of trace-elements during breakdown of mantle garnet: an example from Zabargad. *Contributions to Mineralogy and Petrology* **113**, 437-449.

Villiger, S., Ulmer, P., Müntener, O. & Thompson, A.B. (2004). The liquid line of descent of anhydrous, mantle-derived, tholeiitic liquids by fractional and equilibrium crystallization – an experimental study at 1.0 GPa. *Journal of Petrology* **45** 2369-2388.

von Raumer, J. & Stampfli, G.M. (2008). The birth of the Rheic Ocean-Early Paleozoic subsidence patters and tectonic plate scenario. *Tectonophysics* **461**, 9-20.

Voshage, H., Sinigoi, S., Mazzucchelli, M., Demarchi, G., Rivalenti, G. & Hofmann, A.W. (1988). Isotopic constraints on the origino f ultramafic and mafic dikes in the Balmuccia peridotite (Ivrea Zone). *Contributions to Mineralogy and Petrology* **100**, 261-267.

Walter, M.J. (1998). Melting of garnet peridotite and the origin of komatiite and depleted lithosphere. *Journal of Petrology* **39**, 29-60.

Warren, J.M., Shimizu, N., Sakaguchi, C., Dick, H.J.B. & Nakamura, E. (2009). An assessment of upper mantle heterogeneity based on abyssal peridotite isotopic compositions. *Journal of Geophysical Research* **114**, B12203.

Waters, C.L., Sims, K.W.W., Perfit, M.R., Blichert-Toft, J. & Blusztajn, J. (2011). Perspective on the genesis of E-MORB from chemical and isotopic heterogeneity at 9–10°N East Pacific Rise. *Journal of Petrology* **52**, 565-602.

Wood, B.J. & Blundy, J.D. (1997). A predictive model for rare earth element partitioning between clinopyroxene and anhydrous silicate melt. *Contributions to Mineralogy and Petrology* **129**, 166-181.

Yaxley, G.M. & Green, D.H. (1998). Reactions between eclogite and peridotite: mantle refertilisation by subduction of oceanic crust. *Schweiz. Mineral. Petrogr. Mitt.* **78**, 243-255.

Yu, S., Xu, Y., Ma, J., Zheng, Y., Kuang, Y., Hong, L., Ge, W. & Tong, L. (2010). Remnants of oceanic lower crust in the subcontinental lithospheric mantle: trace element and Sr–Nd–O isotope evidence from aluminous garnet pyroxenite xenoliths from Jiaohe, Northeast China. *Earth and Planetary Science Letters* **297**, 413-422.

FIGURE CAPTIONS

Figure 1. (a) Tectonic sketch map of the Northern Apennines. Abbreviations for the tectonic units: IL, Internal Liguride Units; EL, External Liguride Units. Also reported are SV, crystalline massif of Savona, and GV, Voltri Group, belonging to the Ligurian Alps. Garnet pyroxenites investigated by Montanini et al. (2006, 2012) were sampled in outcrops located further north than the ultramafic bodies here studied, outside this map. (b) Simplified geological map showing ultramafic bodies hosting the investigated pyroxenites.

Figure 2. Centimeters-thick pyroxenite layers embedded in mantle peridotite from (a) M.te Castellaro and (b, c) Suvero ultramafic bodies (External Liguride Units, Northern Apennines, Italy). (d) A representative macroscopic sample of a pyroxenite layer, showing thin orthopyroxenite rims at the boundary with the host peridotite. White dotted lines delimit the pyroxenite layers in (b) and (d).

Figure 3. Photomicrographs of representative microstructures of EL spinel-plagioclase pyroxenites. Porphyroclasts of spinel and clinopyroxene partially replaced by fine-grained plagioclase-bearing assemblage, at parallel (a) and crossed (b) nichols. (c) Coarse orthopyroxene porphyroclast intensely substituted by the plagioclase-facies neoblastic assemblage in a spinel-bearing websterite. (d) Coarse mm-sized green spinel porphyroclast

surrounded by a rim of neoblastic assemblage mostly made by plagioclase, olivine and brownish amphibole. (e) Contact between a pyroxenite layer (on the right of the white dotted line) and orthopyroxene-rich rim (on the left); presence of large orthopyroxene porphyroclast (characterized by undulatory extinction) indicates that opx-rich rim was a mineralogical feature that predated the low-pressure metamorphic recrystallization. (f) Texture in pyroxenite lens GV12 showing a small clinopyroxene porphyroclast surrounded by a fined-grained band of clinopyroxene and dark-green spinel.

Figure 4. Variation diagrams of SiO_2, Al_2O_3, Na_2O, CaO (wt%) and Cr, Ni, Sc, V (ppm) vs Mg-number for the EL pyroxenite (circles). The compositional fields reported for comparison are: garnet pyroxenites (continue line) and spinel websterite (dashed line) in ultramafic orogenic massifs from Beni Boussera (Morocco, Pearson et al., 1993; Kumar et al., 1996; Gysi et al., 2011), Ronda (Spain, Suen & Frey, 1987; Garrido & Bodinier, 1999; Bodinier et al., 2008), Horoman (Japan, Takazawa et al., 1999; Morishita & Arai, 2001), Pyrenees (France, Bodinier et al., 1987a,b), and Balmuccia (Italy, Sinigoi et al., 1983; Voshage et al., 1988; Mukasa & Shervais, 1999). Grey field refers to the bulk compositions of garnet pyroxenite of the External Liguride Units investigated by Montanini et al. (2006). Dotted line defines the range of bulk solid compositions calculated using mineral phases in melting experiments on an hydrous arc melt (Müntener et al., 2001). Bulk compositions of pyroxenites adopted in mass balance calculations for estimating the garnet-bearing primary assemblages are also reported (see Suppl. Table 3): stars are samples from Beni Boussera (grey B7, black B9; white B15; Gysi et al., 2011), the square is sample 70379 selected from the Pyrenean garnet websterites (Bodinier et al., 1987a).

Figure 5. Chondrite-normalized rare earth element (REE) abundances in whole rock pyroxenites. Samples BG3, BG4, BG5 and BG14 are shown with the same symbol because they have very similar bulk REE compositions. Normalizing values are from Anders & Grevesse (1989). Also reported for comparison are the compositional fields of External Liguride garnet pyroxenites (Montanini et al., 2012), and Alpine-Apennine (A-A) gabbros (Borghini et al., 2007; Rampone et al., 1998; Rampone et al., 2014).

Figure 6. Variation of Mg# vs Al (a.p.f.u.) in clinopyroxene (a) and orthopyroxene (b) from pyroxenites. Filled symbols refer to spinel-facies porphyroclasts, open symbols refer to plagioclase-facies neoblasts (see the legend in figure).

Figure 7. Mg# vs Cr# (a), and Cr# vs Ti x 1000 (a.pf.u.) (b) in spinel from pyroxenites. Filled symbols refer to core of large spinel-facies porphyroclasts, open symbols refer to small relicts of plagioclase-facies spinel intensely replaced by the plagioclase-facies assemblage.

Figure 8. Chondrite-normalized REE patterns of clinopyroxene porphyroclasts from (a) HREE-enriched pyroxenites, (b) pyroxenites with rather flat MREE-HREE spectra, (c) samples GV8, GV12 and GV14 (details in text). (d) Representative chondrite-normalized REE patterns of clinopyroxene spinel-facies porphyroclast, and neoblasts of clinopyroxene, plagioclase and amphibole in pyroxenite BG13. Normalizing values are from Anders & Grevesse (1989).

Figure 9. Sc, Zr and REE abundance in clinopyroxene porphyroclasts along profile A-B analyzed in pyroxenite layer GV10, showing alternating px-rich and sp-rich zones (Suppl. Table 2). Data collected by in-situ laser ablation. Normalizing values for REE are from Anders & Grevesse (1989). Grey fields in the Sc diagram define the Sc content variations in garnet and its equilibrium clinopyroxene documented in garnet peridotites by Müntener et al. (2010).

Figure 10. Present-day $^{87}Sr/^{86}Sr$ versus $^{143}Nd/^{144}Nd$ measured on clinopyroxene separates from studied pyroxenites, compared to isotope data of pyroxenites from literature: Cr-Di websterites and Sp pyroxenites from Balmuccia (Ivrea Zone, Italy, Voshage et al., 1988; Mukasa & Shervais, 1999); pyroxenite, websterites and gnt-pyroxenites from Beni Boussera (BB, North Morocco, Pearson et al., 1993; Kumar et al., 1996); gnt-pyroxenites from (LA, Lowe Austria, Becker et al., 1996); websterites from Ronda (South Spain, Marchesi et al., 2012). The field of mid-ocean-ridge basalts (MORB) is from Class & Lehnert (2012); the field of ocean island basalts (OIB) is from GEOROC database (http://georoc.mpch-mainz.gwdg.de/georoc/).

Figure 11. (a) Present-day $^{143}Nd/^{144}Nd$ versus $^{147}Sm/^{144}Nd$ in clinopyroxenes from pyroxenites that define an errochron (dashed line) giving an age of 433 ± 51 Ma. Empty symbols refer to spatially controlled pyroxenite – wall-rock profiles, and relative isochrones (continuous lines), reported in Borghini et al. (2013). Data of EL garnet pyroxenites from Montanini et al. (2012) are reported for comparison. (b) Sm-Nd internal isochrons defined by whole rock (wr), plagioclase (plag) and clinopyroxene (cpx) from four pyroxenite samples (BG13, BG14, GV8 and BG5, this latter only based on clinopyroxene and plagioclase analyses). Ages and initial Nd isotopic ratios for the internal isochrons are: 178±11 Ma, initial $^{143}Nd/^{144}Nd$ = 0.512961 (±24), MSWD = 0.22 for BG13; 177±13 Ma, initial $^{143}Nd/^{144}Nd$ = 0.512837 (±20), MSWD = 0.69 for BG14; 174±25 Ma, initial $^{143}Nd/^{144}Nd$ = 0.512727 (±34), MSWD = 0.0024 for GV8; 183±14 Ma, initial $^{143}Nd/^{144}Nd$ = 0.512827 (±17) for BG5.

Figure 12. Whole-rock normative compositions of studied pyroxenites projected from Diopside within the (CMAS) triangle forsterite (Fo) - calcium tschermak (CaTs) - quartz (Qz)

(O'Hara, 1968). The compositional fields of EL garnet pyroxenites (EL gnt-pyrox, Montanini et al., 2012), Type-1 pyroxenites from Horoman (Takazawa et al., 1999), and Beni Boussera garnet pyroxenites (BB-gnt-pyrox, Gysi et al., 2011), are also shown for comparison. In the smaller CMAS triangle to the right, pyroxenite compositions are plotted together with the compositions of experimental partial melts from hybrid mafic-peridotite sources (Yaxley & Green, 1998; Kogiso et al., 1998; Takahashi & Nakajima, 2002), and the compositional field of melts in the eclogite-peridotite reaction experiments by Mallik & Dasgupta (2012)(tick-marks on the black arrow indicate the amount in wt% of eclogitic melt added to peridotite).

Figure 13. Bulk-rock Sm_N/Yb_N resulting from mass balance calculations compared to the Sm_N/Yb_N values measured in each pyroxenite sample (detailed explanation in the text). Open circles are the values calculated by using mineral compositions from Beni Boussera garnet pyroxenites (Gysi et al., 2011), open squares are obtained adopting in the calculation mineral compositions from Pyrenees garnet pyroxenites (Bodinier et al., 1987a).

Figure 14. Variation of bulk-rock Mg-number versus thickness (cm) of the studied pyroxenite layers and lens. Close to the symbols are also shown the Ni contents (ppm) of each pyroxenite sample.

Figure 15. (a) Chondrite-normalized REE patterns of clinopyroxene porphyroclasts in wall-rock peridotites from three profiles investigated by Borghini et al. (2013). (b) Computed melts in equilibrium with wall-rock clinopyroxenes shown in (a), using partition coefficients from Ionov et al. (2002). Also reported are the composition of average N-MORB (Hofmann, 1988), and average E-MORB from Mid-Atlantic Ridge 10-24°N (Hémond et al., 2006). The compositional fields refer to: 1) E-MORBs from South Atlantic Mid-Ocean-Ridge 5-11°S (A3 Seamount; Hoernle et al., 2011), 2) tholeiitic lavas (both olivine- and quartz-normative) from Iceland plume (Icelandic tholeiites; Hémond et al., 1993), 3) East Pacific Rise 9-10°N (Waters et al., 2011). Normalizing values are from Anders & Grevesse (1989).

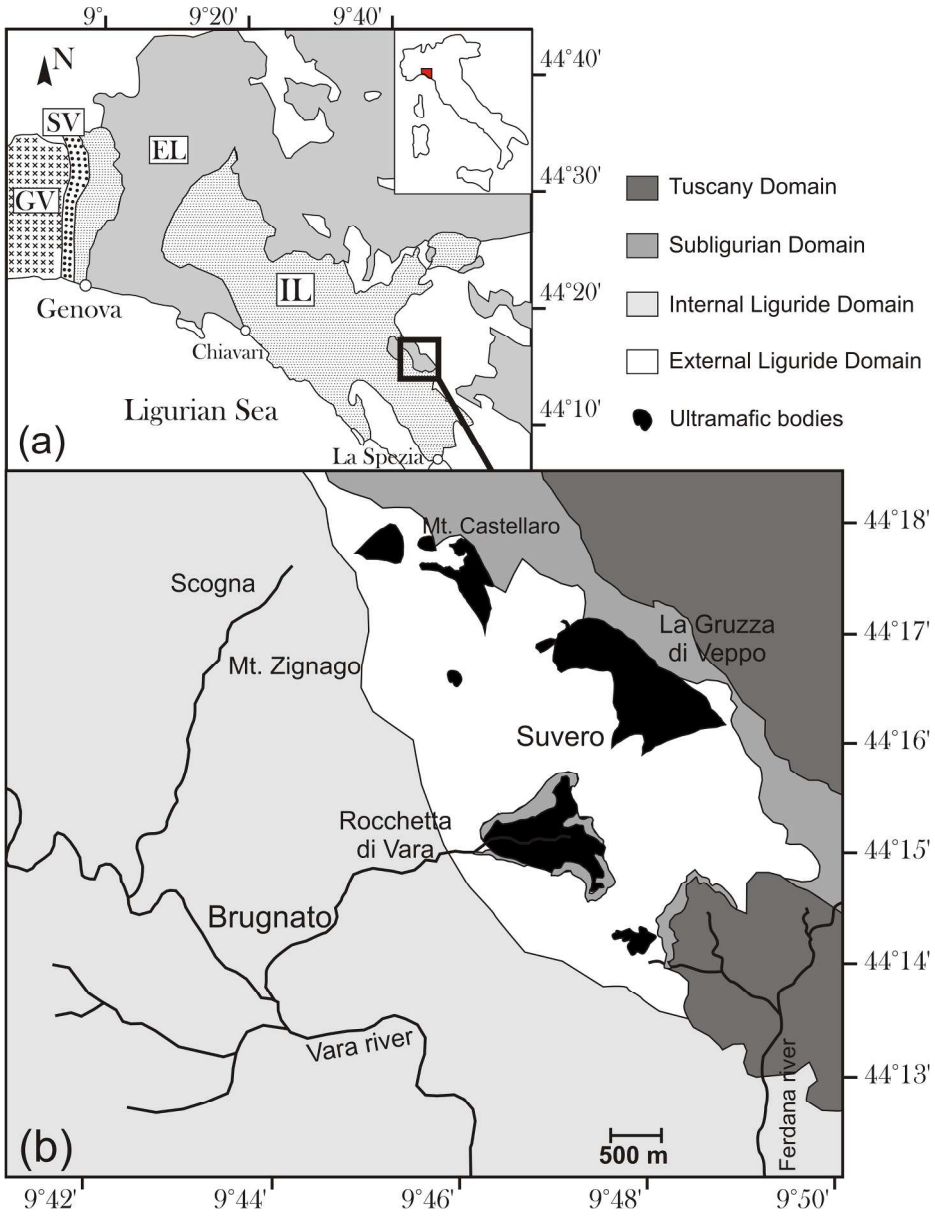

206x268mm (300 x 300 DPI)

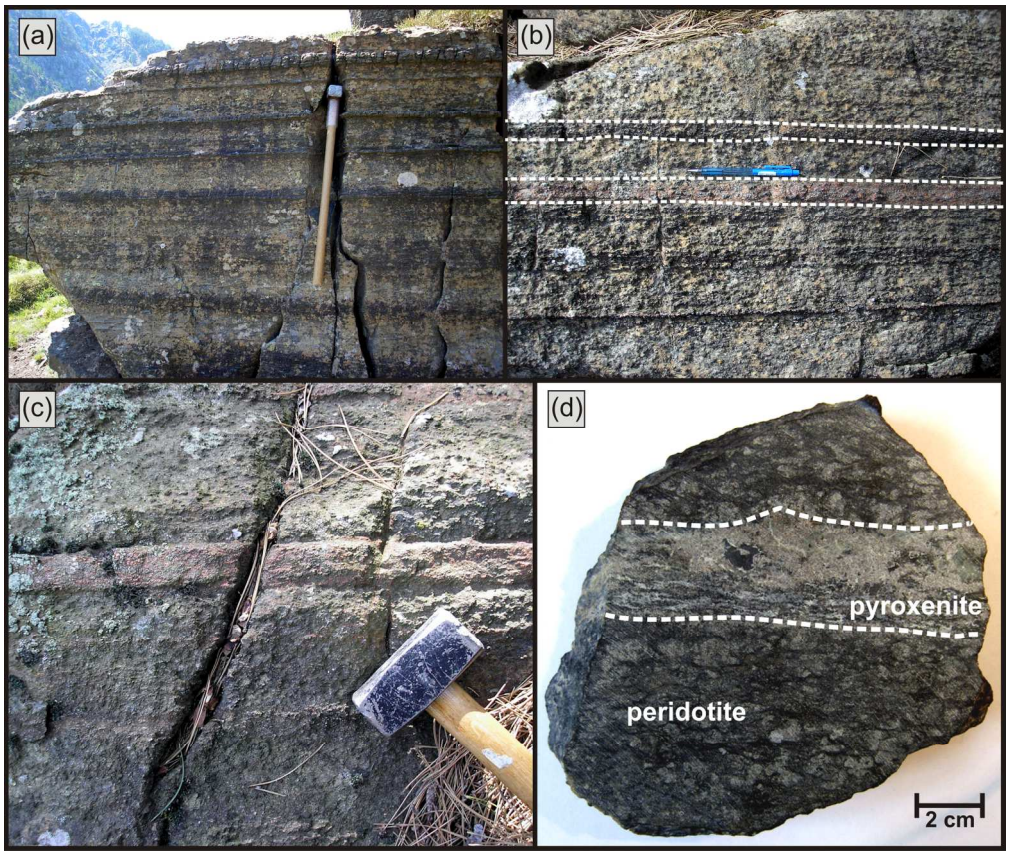

160x135mm (300 x 300 DPI)

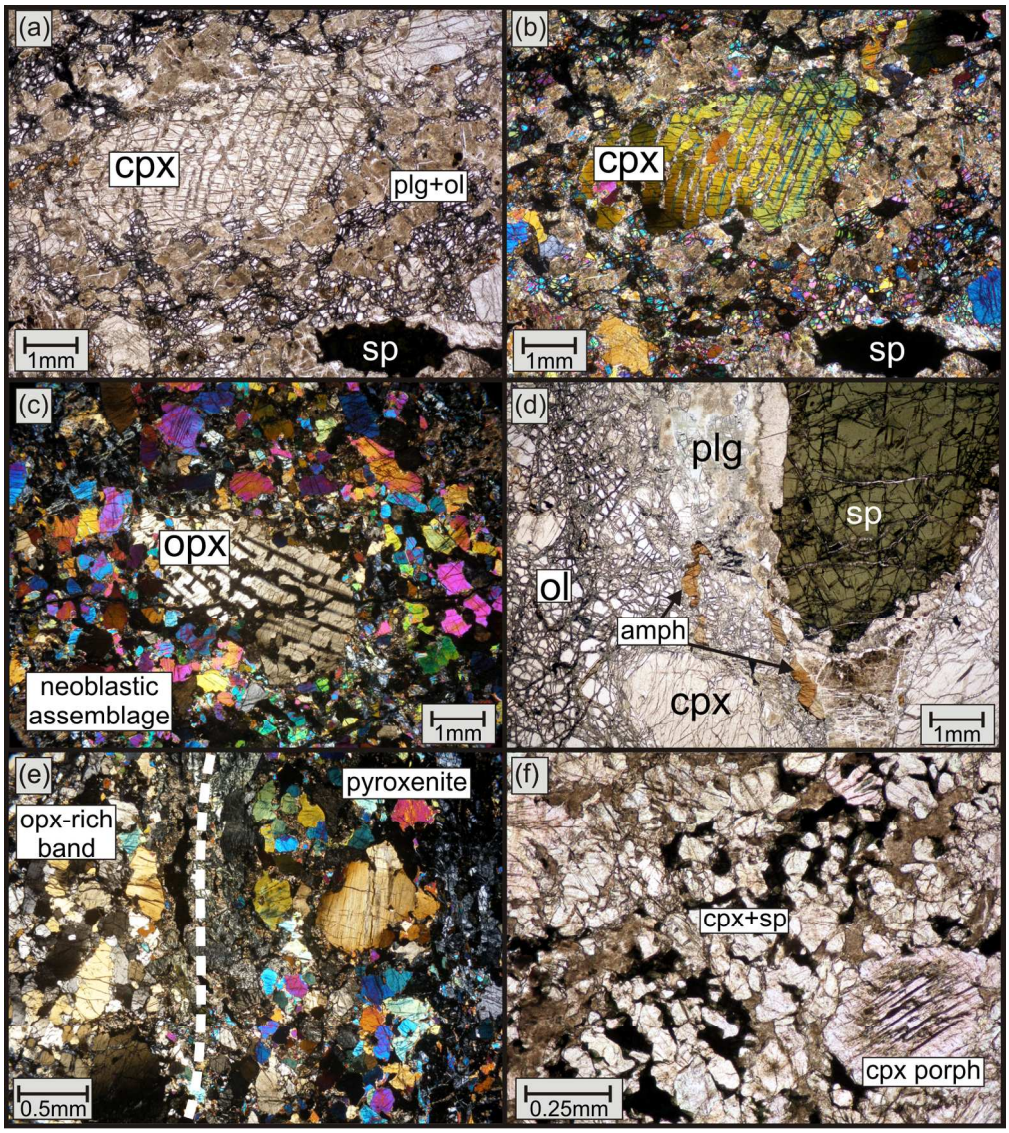

155x174mm (300 x 300 DPI)

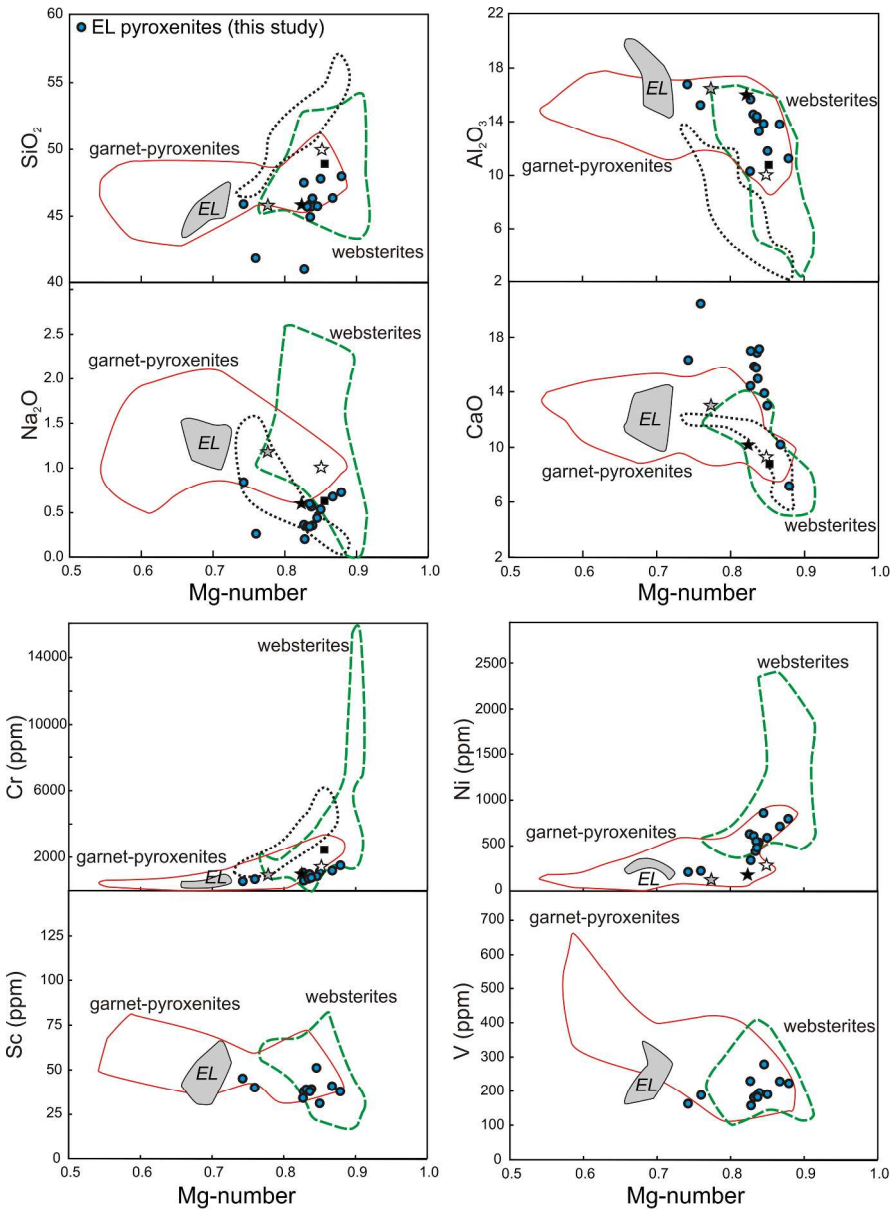

235x320mm (300 x 300 DPI)

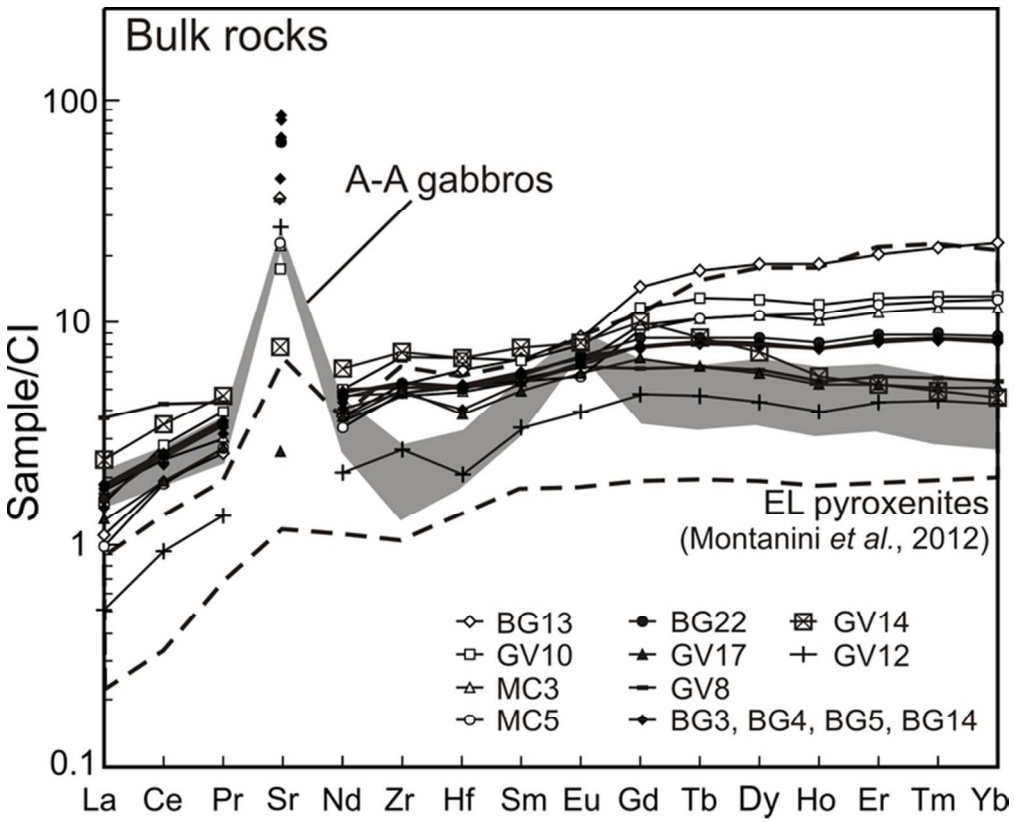

65x53mm (300 x 300 DPI)

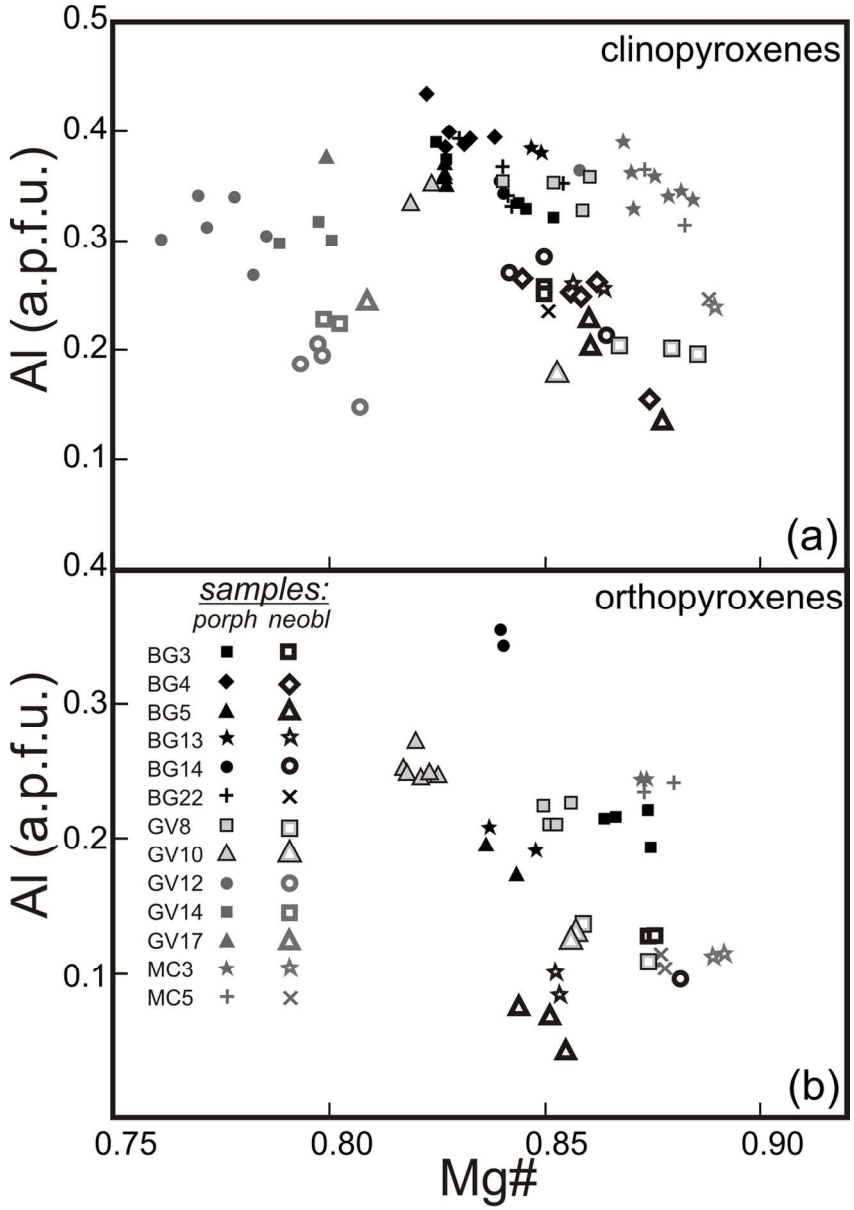

117x168mm (300 x 300 DPI)

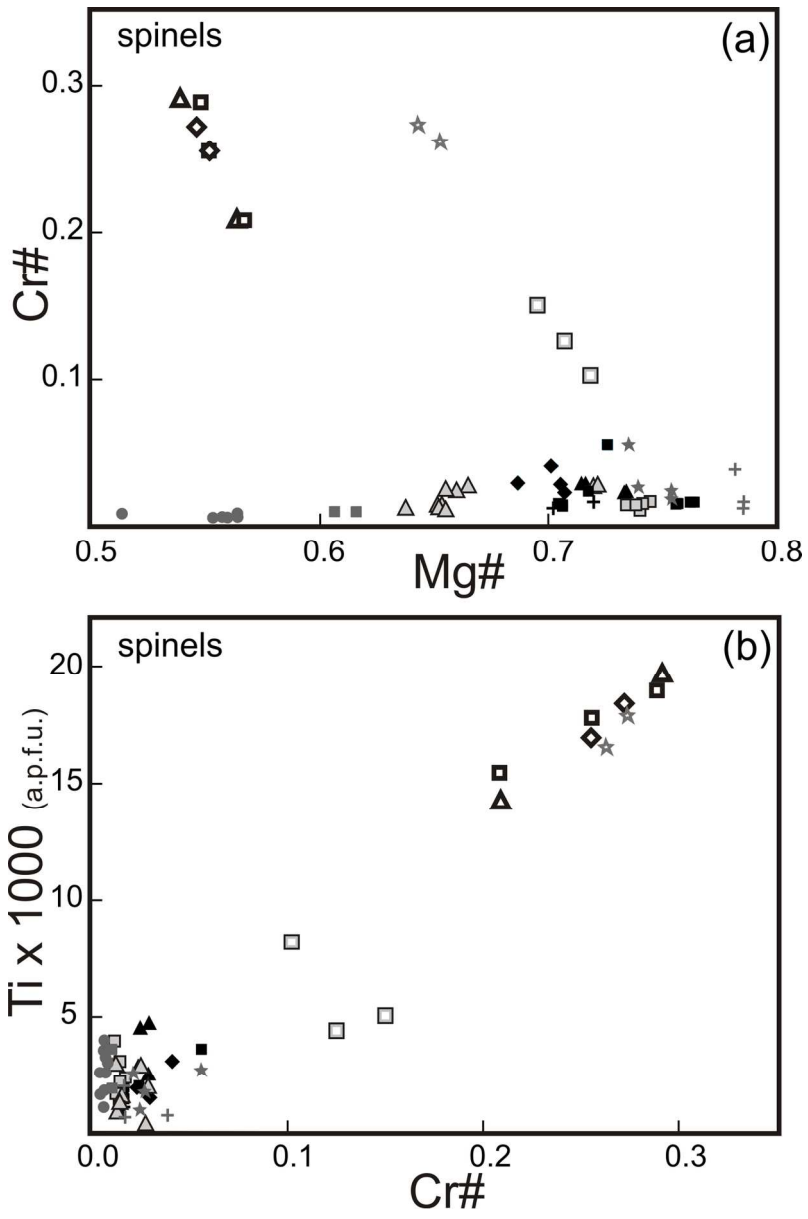

124x188mm (300 x 300 DPI)

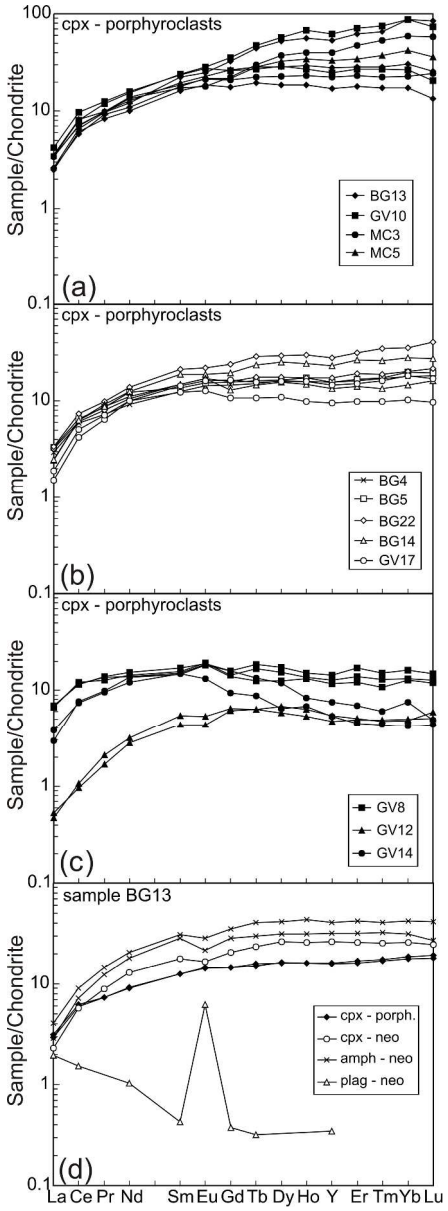

236x654mm (300 x 300 DPI)

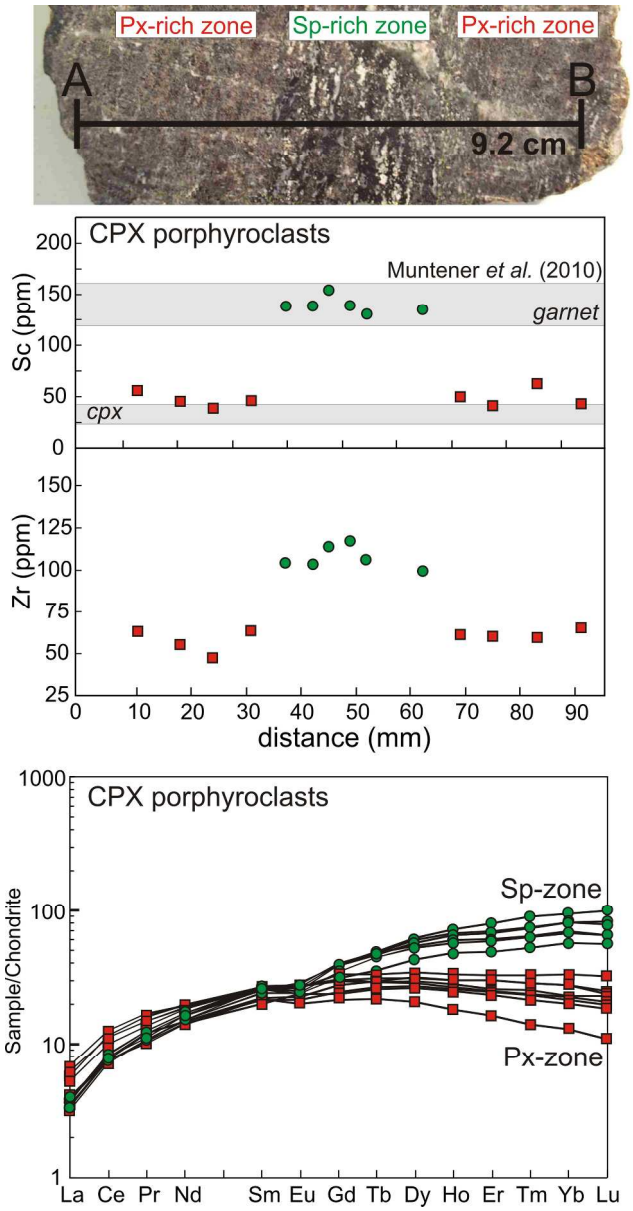

154x292mm (300 x 300 DPI)

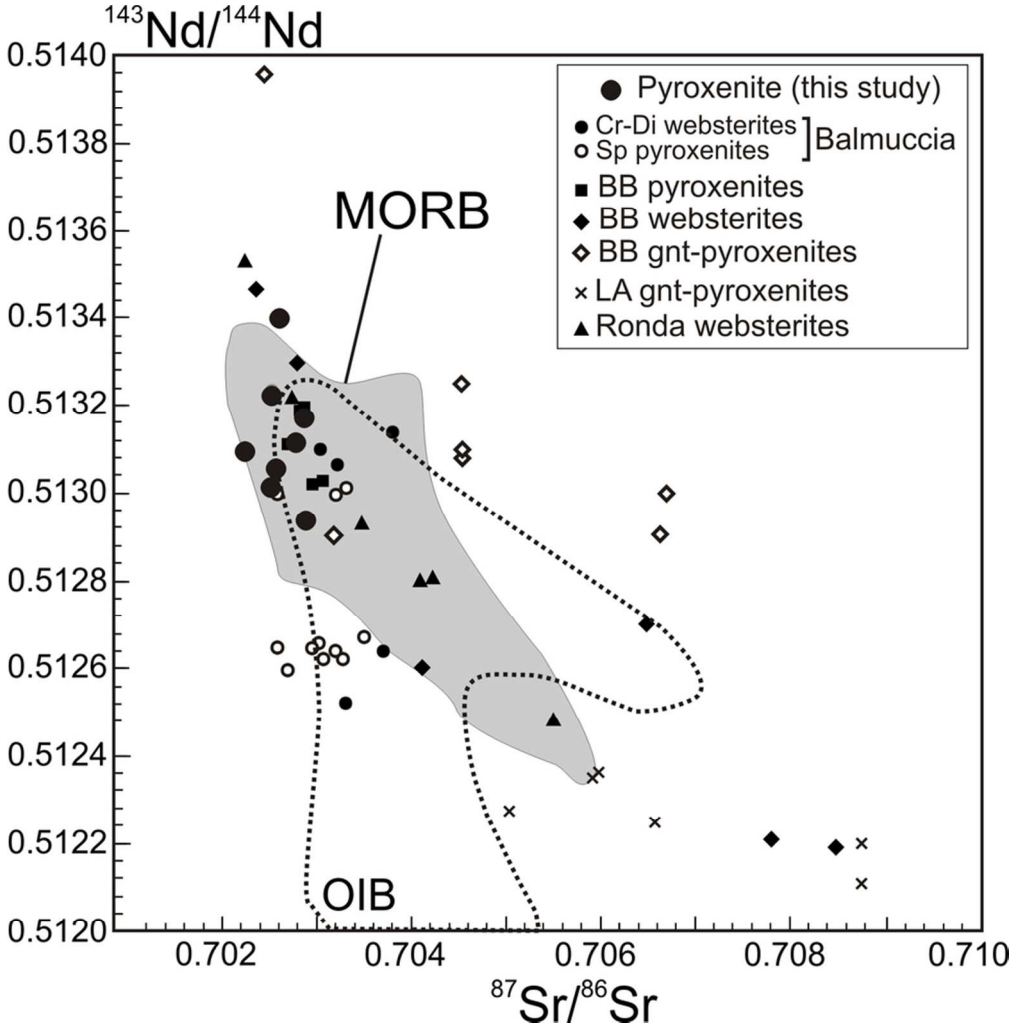

81x83mm (300 x 300 DPI)

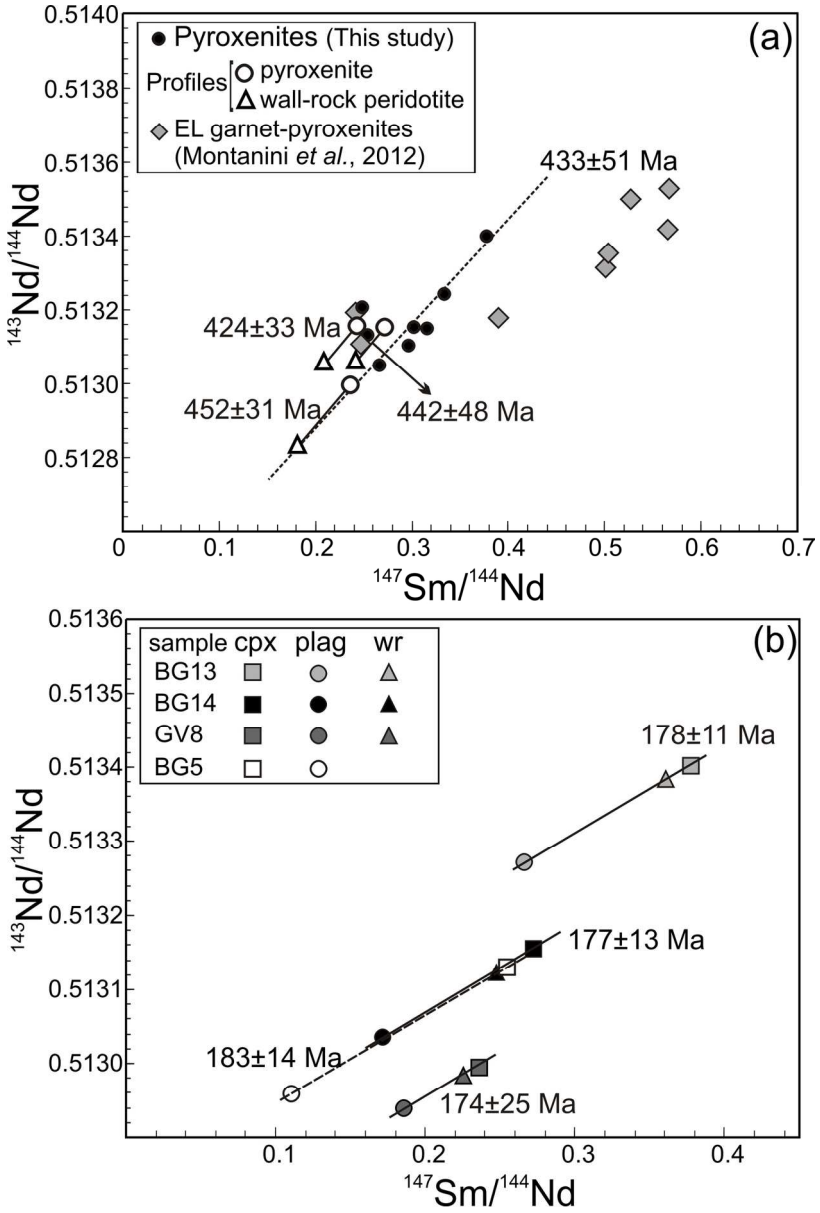

138x205mm (300 x 300 DPI)

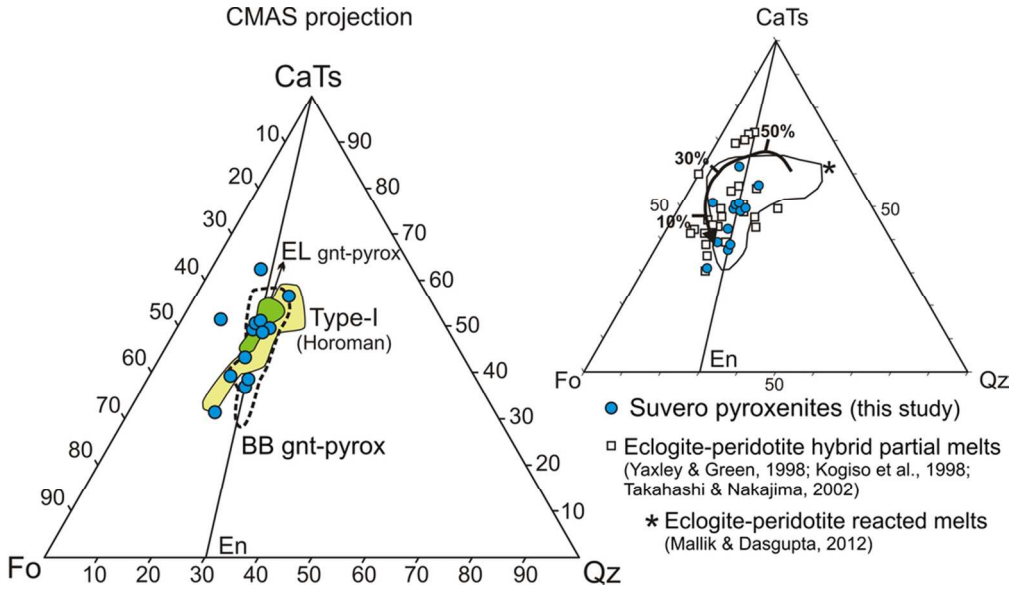

90x51mm (300 x 300 DPI)

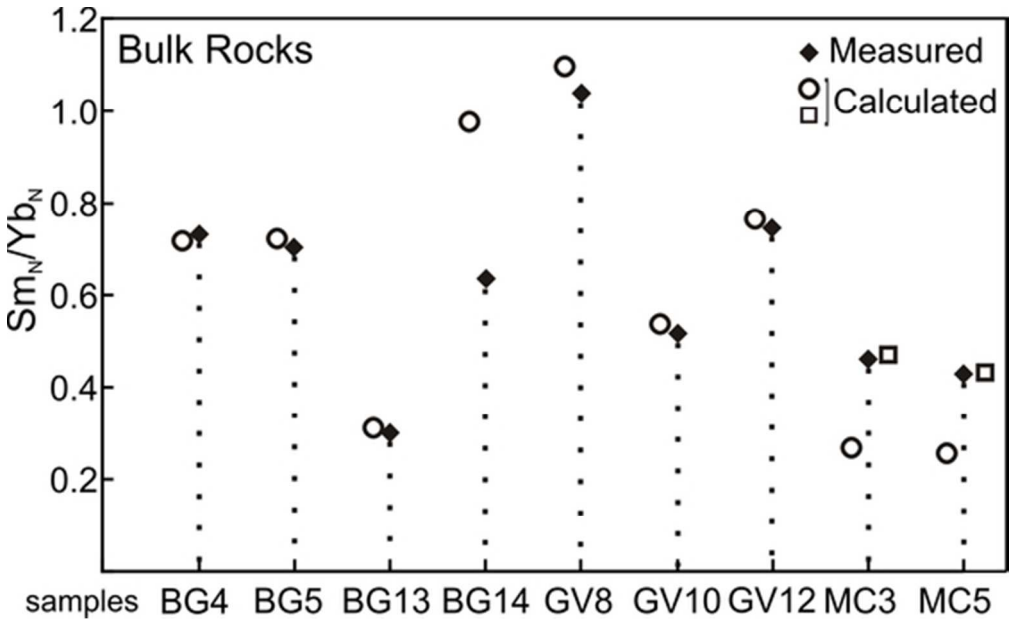

49x30mm (300 x 300 DPI)

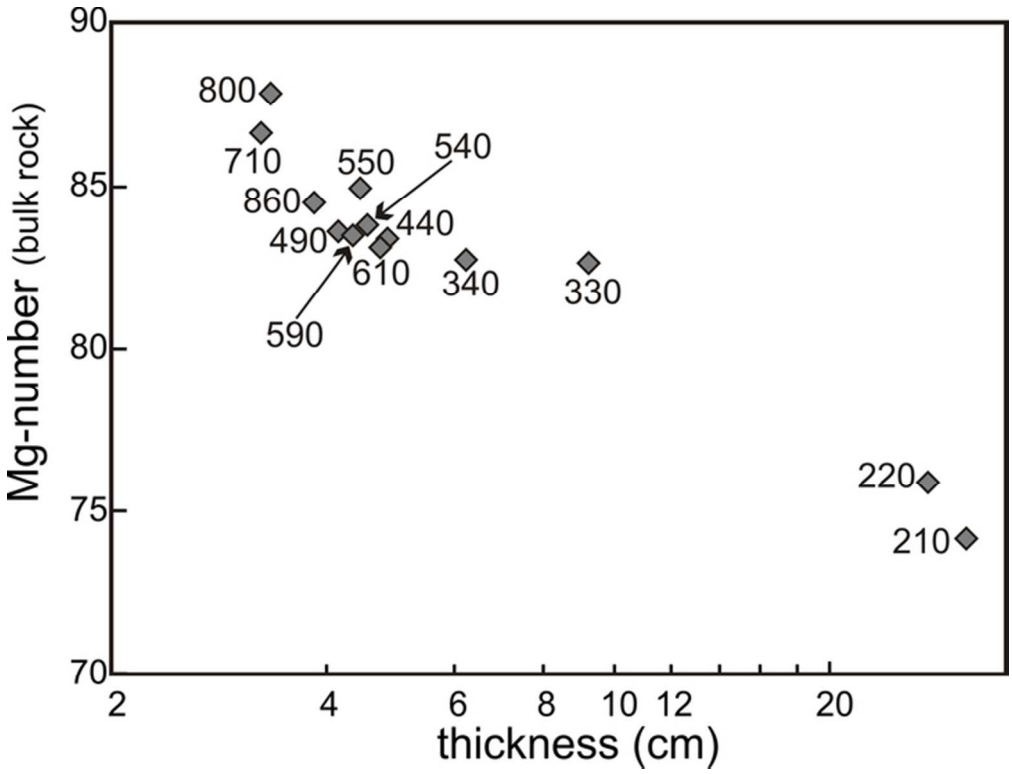

61x46mm (300 x 300 DPI)

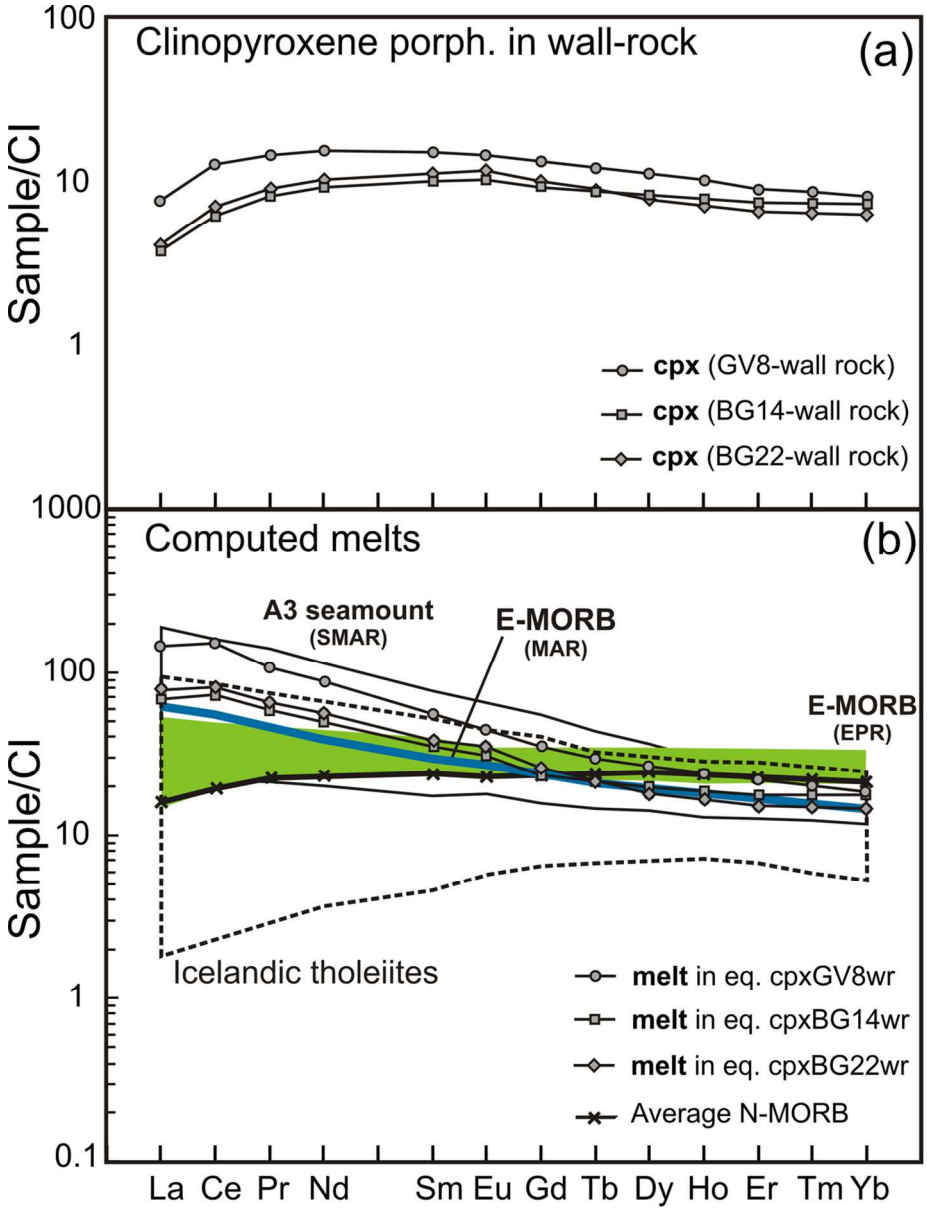

106x139mm (300 x 300 DPI)

Table 1: Localization, characteristics and texture of pyroxenites

Sample	*latitude*	*longitude*	*Geometry*	*Rock-type*	*Texture*
BG3P	44°16'44.68"	9°47'49.96"	4.3 cm layer	cpx-rich websterite	porphyroclastic sp+pxs; plag-bearing neobalstic assemblage
BG4'''	44°16'44.36"	9°47'49.08"	4.1 cm layer	clinopyroxenite	porphyroclastic sp+cpx; plag-bearing neobalstic assemblage
BG5	44°16'44.57"	9°47'48.64"	4.8 cm layer	cpx-rich websterite	porphyroclastic sp+pxs; plag-bearing neobalstic assemblage
BG13	44°16'45.93"	9°47'48.93"	3.8 cm layer	cpx-rich websterite	porphyroclastic sp+pxs; plag-bearing neobalstic assemblage
BG14	*44°16'44.15"*	*9°47'50.15"*	4.7 cm layer	cpx-rich websterite	porphyroclastic sp+pxs; plag-bearing neobalstic assemblage
BG22	*44°16'44.69"*	*9°47'49.57"*	4.5 cm layer	cpx-rich websterite	porphyroclastic sp+pxs; plag-bearing neobalstic assemblage
GV8	*44°16'15.65"*	*9°48'27.76"*	4.4 cm layer	websterite	porphyroclastic sp+pxs; plag-bearing neobalstic assemblage
GV10	*44°16'15.86"*	*9°48'26.82"*	9.2 cm layer	websterite	porphyroclastic sp+pxs; plag-bearing neobalstic assemblage
GV12	*44°16'15.95"*	*9°48'27.14"*	31 cm lens	clinopyroxenite	clusters and seams of dark green sp + cpx + plg on cpx porph.
GV14	*44°16'15.95"*	*9°48'27.14"*	27 cm lens	clinopyroxenite	porphyroclastic sp+cpx; plag-bearing neobalstic assemblage
GV17	*44°16'28.53"*	*9°48'17.59"*	6.2 cm layer	clinopyroxenite	porphyroclastic sp+cpx; plag-bearing neobalstic assemblage
MC3	*44°17'38.25"*	*9°45'42.58"*	3.2 cm layer	websterite	porphyroclastic sp+pxs; plag-bearing neobalstic assemblage
MC5	*44°17'37.54"*	*9°45'48.54"*	3.3 cm layer	websterite	porphyroclastic sp+pxs; plag-bearing neobalstic assemblage

Table 2: Bulk-rock major and trace element compositions

Sample	BG3P	BG4'''	BG5	BG13	BG14*	BG22*	GV8*	GV10	GV12	GV14	GV17	MC3	MC5
SiO_2	43.05	43.96	44.04	43.84	43.62	44.38	46.46	45.99	45.05	39.93	37.76	43.19	45.19
TiO_2	0.35	0.35	0.36	0.42	0.34	0.35	0.45	0.44	0.25	0.57	0.34	0.44	0.39
Al_2O_3	13.67	13.70	13.83	13.28	13.86	12.75	11.50	9.94	16.46	14.59	14.44	12.87	10.61
Fe_2O_3	6.25	6.40	6.19	6.55	6.35	5.98	6.71	7.77	8.11	8.14	7.05	6.18	6.52
MnO	0.14	0.14	0.14	0.19	0.14	0.14	0.14	0.16	0.14	0.15	0.16	0.17	0.17
MgO	15.99	16.52	15.73	18.06	15.80	15.65	19.17	18.53	11.78	12.98	17.04	20.29	23.91
CaO	16.16	14.37	15.14	13.33	15.13	16.41	12.64	13.96	16.03	19.52	15.68	9.52	6.77
Na_2O	0.33	0.55	0.57	0.42	0.33	0.34	0.52	0.48	0.83	0.25	0.19	0.63	0.68
K_2O	0.23	0.62	0.53	0.20	0.28	0.18	0.07	0.10	0.14	0.00	0.00	0.31	0.36
P_2O_5	0.02	0.02	0.02	0.02	0.03	0.02	0.04	0.00	0.00	0.02	0.00	0.02	0.00
LOI	4.73	3.75	3.62	4.48	4.98	4.66	3.13	2.82	1.62	4.83	6.43	5.98	5.41
Tot	100.92	100.38	100.17	100.79	100.86	100.86	100.83	100.35	100.41	100.98	99.09	99.59	100.02
Mg-no	83.51	83.64	83.42	84.52	83.13	83.82	84.98	82.53	74.06	76.11	82.72	86.67	87.90
Cr	980	810	740	890	920	820	1140	1090	560	720	610	1230	1530
Ni	550	490	440	860	610	540	590	630	210	220	340	710	800
Sr	340	486	648	331	602	491	274	132	196	57	19	166	173
Y	11.4	12.2	12.5	27.7	11.8	12.5	8.2	18.5	6.2	8.4	7.8	15.5	17
Zr	18	18	20	20	18	20	19	26	10	28	18	18	19
La	0.44	0.42	0.43	0.26	0.34	0.38	0.87	0.36	0.12	0.56	0.3	0.42	0.23
Ce	1.53	1.53	1.55	1.16	1.39	1.53	2.6	1.67	0.56	2.09	1.15	1.48	1.13
Pr	0.3	0.32	0.32	0.23	0.28	0.31	0.39	0.35	0.12	0.42	0.24	0.27	0.24
Nd	1.98	2.21	2.17	1.69	1.84	2.1	2.1	2.27	0.95	2.79	1.64	1.71	1.51
Sm	0.78	0.89	0.85	1.01	0.78	0.86	0.83	1	0.49	1.13	0.72	0.8	0.8
Eu	0.371	0.385	0.392	0.487	0.357	0.394	0.352	0.443	0.222	0.453	0.33	0.363	0.321
Gd	1.55	1.53	1.5	2.84	1.54	1.66	1.22	2.28	0.93	1.97	1.34	1.9	1.83
Tb	0.3	0.29	0.29	0.62	0.29	0.31	0.23	0.47	0.17	0.31	0.23	0.38	0.38
Dy	1.95	1.89	1.92	4.44	1.93	2.05	1.48	3.08	1.07	1.77	1.44	2.59	2.59
Ho	0.42	0.42	0.42	1.02	0.42	0.45	0.3	0.67	0.22	0.32	0.29	0.57	0.61
Er	1.28	1.32	1.3	3.21	1.32	1.4	0.91	2.04	0.69	0.84	0.83	1.77	1.93
Tm	0.201	0.207	0.199	0.522	0.205	0.213	0.137	0.316	0.108	0.118	0.124	0.282	0.301
Yb	1.32	1.34	1.33	3.68	1.35	1.41	0.88	2.12	0.7	0.75	0.83	1.91	2.05
Lu	0.208	0.197	0.211	0.665	0.208	0.223	0.141	0.355	0.103	0.113	0.128	0.301	0.331
Hf	0.5	0.5	0.5	0.6	0.4	0.5	0.5	0.7	0.2	0.7	0.4	0.5	0.5
Sc	38	38	38	51	39	39	31	34	45	40	38	41	38
V	187	183	186	280	182	195	191	231	163	190	159	230	225

(*) data are from Borghini et al. (2013). Major elements are in wt%; trace elements in ppm. Mg-no is the Mg-number.

Table 3: Average major element compositions of clinopyroxene in pyroxenites

sample	BG3		BG4		BG5		BG13		BG14		BG22		GV8	
p.to an.	porph	neobl	porph	neobl	porph	neobl	porph	neobl	porph	neobl	porph	neobl	porph	neobl
N. an.	5	3	6	5	7	3	5	2	3	3	5	1	7	3
SiO_2	49.88 (43)	51.16 (15)	49.01 (17)	50.79 (69)	49.22 (11)	51.42 (11)	48.95 (5)	50.58 (64)	49.53 (2)	50.69 (94)	49.63 (69)	51.07	49.58 (43)	51.40 (14)
TiO_2	0.84 (13)	0.99 (9)	0.69 (7)	1.09 (19)	0.67 (3)	1.07 (45)	1.02 (2)	0.95 (3)	0.92 (9)	0.97 (5)	0.77 (10)	0.71	1.20 (7)	1.30 (18)
Al_2O_3	8.21 (70)	5.96 (8)	9.29 (42)	5.5 (108)	8.32 (18)	4.41 (112)	8.84 (7)	5.98 (14)	8.18 (15)	5.95 (83)	8.33 (50)	5.45	8.13 (29)	4.67 (11)
Cr_2O_3	0.13 (2)	0.17 (10)	0.20 (7)	0.34 (10)	0.15 (4)	0.24 (6)	0.17 (3)	0.18 (9)	0.10 (5)	0.12 (5)	0.15 (10)	0.19	0.20 (3)	0.19 (13)
FeO	4.80 (30)	4.65 (1)	4.86 (17)	4.42 (26)	4.93 (3)	4.22 (18)	4.16 (7)	4.16 (28)	4.68 (3)	4.55 (24)	4.65 (28)	4.56	4.32 (24)	3.78 (33)
MgO	14.01 (48)	14.76 (2)	13.29 (20)	15.13 (53)	13.19 (6)	15.35 (75)	13.01 (6)	14.32 (36)	13.76 (15)	14.72 (60)	13.87 (28)	14.60	14.01 (44)	15.18 (18)
MnO	0.17 (3)	0.18 (1)	0.21 (3)	0.20 (6)	0.00	0.00	0.24 (1)	0.22 (1)	0.22 (1)	0.20 (2)	0.20 (5)	0.19	0.12 (7)	0.13 (4)
CaO	22.08 (43)	22.22 (9)	21.95 (39)	21.84 (56)	21.88 (11)	22.36 (23)	21.86 (13)	22.04 (42)	22.24 (14)	22.30 (18)	21.89 (29)	22.28	22.01 (34)	22.19 (36)
Na_2O	0.77 (6)	0.73 (1)	0.69 (19)	0.65 (8)	0.79 (3)	0.65 (4)	0.86 (4)	0.63 (2)	0.83 (3)	0.67 (4)	0.81 (5)	0.64	0.70 (7)	0.60 (6)
Total	100.89	100.83	100.19	99.95	99.15	99.72	99.17	99.15	100.46	100.17	100.24	99.70	100.25	99.44
Mg#	0.84	0.85	0.83	0.86	0.83	0.87	0.85	0.86	0.84	0.85	0.84	0.85	0.85	0.88

sample	GV10		GV12		GV14		GV17		MC3		MC5	
p.to an.	porph	neobl	porph	neobl	porph	neobl	porph	neobl	porph	neobl	porph	neobl
N. an.	11	1	6	4	5	2	1	1	7	1	5	1
SiO_2	49.20 (15)	51.32	50.37 (38)	51.59 (25)	49.73 (26)	50.63 (3)	48.58	50.06	49.45 (43)	50.26	49.31 (52)	50.31
TiO_2	1.13 (3)	0.86	0.43 (7)	0.39 (5)	1.13 (19)	0.81 (2)	0.70	0.75	1.17 (18)	1.58	1.03 (10)	1.65
Al_2O_3	8.02 (30)	4.15	7.18 (63)	4.23 (58)	7.06 (25)	5.18 (6)	8.75	5.65	8.25 (44)	5.62	8.08 (67)	5.70
Cr_2O_3	0.30 (7)	0.18	0.04 (2)	0.05 (3)	0.08 (4)	0.05 (2)	0.14	0.19	0.22 (10)	0.23	0.13 (7)	0.21
FeO	5.44 (24)	4.81	7.00 (65)	6.58 (25)	6.14 (22)	6.28 (5)	6.80	6.32	3.59 (15)	3.36	3.72 (32)	3.38
MgO	14.02 (29)	15.64	13.47 (79)	14.66 (20)	13.38 (18)	14.14 (36)	15.18	14.99	14.16 (34)	15.11	14.12 (47)	15.08
MnO	0.22 (15)	0.18	0.16 (5)	0.19 (1)	0.22 (2)	0.19 (3)	0.23	0.22	0.13 (2)	0.12	0.17 (2)	0.12
CaO	21.78 (35)	22.38	20.27 (96)	21.29 (35)	21.55 (20)	21.39 (33)	19.32	21.40	22.04 (38)	22.15	22.31 (2)	22.13
Na_2O	0.59 (45)	0.43	0.70 (7)	0.54 (4)	0.67 (6)	0.70 (5)	0.24	0.37	0.86 (11)	0.72	0.80 (3)	0.77
Total	100.70	99.95	99.63	99.51	99.95	99.37	99.94	99.95	99.88	99.15	99.68	99.35
Mg#	0.82	0.85	0.77	0.80	0.80	0.80	0.80	0.81	0.88	0.89	0.87	0.89

N. an., number of analyses. Values in parentheses represent 2σ standard deviation of the last unit cited. Abbreviations: porph = porphyroclast, neobl = neoblast.

Table 4: Average major element compositions of orthopyroxene in pyroxenites

sample	BG3	BG3	BG5	BG5	BG13	BG13	BG14	BG14	GV8	GV8	GV10	GV10	MC3	MC3	MC5	MC5
p.to an.	porph	neobl	porph	neobl	porph	neobl	porph	neobl	porph	neobl	porph	neobl	porph	neobl	porph	neobl
N. an.	4	2	2	3	2	2	2	2	4	2	10	3	3	2	2	3
SiO_2	54.57 (43)	55.28 (11)	54.51 (24)	55.81 (33)	54.37 (28)	55.22 (13)	54.56 (8)	55.44 (3)	53.52 (17)	55.08 (40)	53.19 (29)	55.34 (12)	54.12 (10)	55.90 (2)	53.05 (21)	55.23 (11)
TiO_2	0.22 (2)	0.28 (4)	0.23 (1)	0.17 (2)	0.23 (3)	0.36 (1)	0.16 (1)	0.16 (1)	0.23 (3)	0.29 (4)	0.24 (6)	0.21 (3)	0.17 (2)	0.28 (1)	0.21 (3)	0.29 (2)
Al_2O_3	5.26 (29)	3.21 (1)	4.61 (40)	1.64 (42)	4.95 (25)	2.36 (30)	4.85 (41)	2.50 (8)	5.34 (23)	3.10 (47)	6.55 (55)	3.23 (9)	6.04 (3)	2.90 (6)	5.84 (14)	2.77 (11)
Cr_2O_3	0.24 (6)	0.25 (2)	0.12 (1)	0.09 (3)	0.12 (1)	0.11 (9)	0.35 (3)	0.32 (1)	0.10 (2)	0.26 (7)	0.16 (7)	0.13 (2)	0.34 (3)	0.22 (1)	0.08 (2)	0.12 (1)
FeO	8.38 (38)	8.26 (1)	10.33 (30)	9.94 (20)	10.05 (27)	9.51 (3)	7.89 (13)	7.84 (6)	9.26 (15)	8.70 (67)	10.41 (99)	9.30 (7)	8.10 (4)	7.08 (10)	7.94 (30)	8.07 (5)
MgO	31.32 (21)	32.10 (6)	30.36 (23)	31.64 (76)	30.11 (93)	30.93 (8)	32.22 (7)	32.58 (2)	29.96 (24)	31.66 (45)	29.25 (69)	31.26 (9)	31.09 (7)	32.32 (5)	31.55 (18)	32.25 (29)
MnO	0.17 (2)	0.19 (1)	0.17 (5)	0.09 (9)	0.17 (10)	0.41 (1)	0.18 (4)	0.20 (1)	0.21 (5)	0.23 (1)	0.21 (6)	0.17 (2)	0.16 (6)	0.20 (0)	0.22 (7)	0.27 (2)
CaO	0.72 (5)	0.42 (2)	0.71 (23)	0.59 (18)	0.72 (21)	0.52 (6)	0.64 (17)	0.49 (5)	0.94 (18)	0.51 (3)	0.69 (11)	0.36 (2)	0.72 (4)	0.49 (4)	0.50 (12)	0.50 (1)
Na_2O	0.02 (1)	0.02 (1)	0.15 (10)	0.01 (1)	0.13 (9)	0.04 (2)	0.02 (2)	0.01 (1)	0.04 (3)	0.02 (2)	0.03 (2)	0.00	0.01 (0)	0.03 (1)	0.05 (1)	0.02 (0)
Total.	100.90	100.01	101.20	99.99	100.84	99.47	100.88	99.55	99.61	99.83	100.72	99.99	100.75	99.47	99.43	99.51
Mg#	0.87	0.87	0.84	0.85	0.84	0.85	0.88	0.88	0.85	0.87	0.83	0.86	0.87	0.89	0.88	0.88

N. an., number of analyses. Values in parentheses represent 2σ standard deviation of the last unit cited. Abbreviations as in Table 3.

Table 5: Representative major element compositions of spinel in pyroxenites

sample	BG3	BG3	BG4	BG4	BG5	BG5	BG22	GV8	GV8	GV10	GV12	GV14	MC3	MC3	MC5
p.to an.	porph	neobl	porph	neobl	porph	neobl	porph	porph	neobl	porph	porph	porph	porph	neobl	porph
N. an.	9	3	4	2	4	2	4	10	5	10	8	2	4	3	4
TiO_2	0.09 (4)	0.81 (7)	0.11 (4)	0.82 (4)	0.19 (6)	0.78 (16)	0.08 (4)	0.10 (5)	0.29 (10)	0.10 (5)	0.12 (4)	0.14 (6)	0.11 (4)	0.81 (4)	0.06 (4)
Al_2O_3	62.99 (143)	39.28 (327)	61.87 (74)	38.90 (91)	59.85 (74)	38.85 (478)	63.52 (144)	61.56 (16)	52.00 (224)	61.84 (105)	61.26 (66)	57.85 (60)	63.92 (158)	38.35 (28)	62.60 (111)
Cr_2O_3	2.01 (125)	19.54 (263)	2.93 (70)	20.78 (78)	2.47 (28)	19.20 (362)	1.40 (19)	1.35 (15)	11.16 (194)	1.91 (68)	0.62 (12)	0.91 (4)	3.17 (154)	21.01 (64)	2.26 (124)
FeO	15.37 (155)	26.70 (61)	16.62 (53)	26.44 (4)	17.19 (40)	27.00 (117)	16.72 (2)	15.07 (34)	16.23 (68)	19.51 (161)	22.22 (65)	23.39 (34)	12.89 (21)	23.94 (4)	12.36 (22)
MgO	19.28 (78)	13.21 (48)	18.27 (28)	13.06 (14)	18.70 (28)	13.09 (76)	18.64 (6)	18.79 (12)	17.32 (52)	17.26 (84)	13.85 (55)	15.16 (18)	19.57 (48)	15.56 (14)	20.30 (19)
MnO	0.00	0.12 (2)	0.00	0.12 (1)	0.00	0.00	0.15 (2)	0.12 (2)	0.11 (3)	0.17 (5)	0.15 (4)	0.19 (1)	0.12 (2)	0.12 (1)	0.13 (2)
NiO	0.00	0.00	0.00	0.00	0.00	0.00	0.33 (5)	0.39 (4)	0.33 (3)	0.44 (13)	0.18 (5)	0.19 (2)	0.34 (4)	0.00	0.33 (8)
Total	99.74	99.66	99.80	100.11	98.39	98.92	100.87	97.38	97.44	101.23	98.40	97.84	100.12	99.78	98.04
Mg#	0.73	0.56	0.70	0.55	0.72	0.55	0.71	0.74	0.71	0.67	0.55	0.61	0.75	0.65	0.78
Cr#	0.02	0.25	0.03	0.26	0.03	0.25	0.01	0.01	0.13	0.02	0.01	0.01	0.03	0.27	0.02
Tix1000	1.80	17.38	2.08	17.63	3.68	16.96	1.58	2.00	5.85	1.86	2.46	2.76	2.06	17.23	1.23

N. an., number of analyses. Values in parentheses represent 2σ standard deviation of the last unit cited. Abbreviations as in Table 3.

Table 6: Representative major element compositions of olivine in pyroxenites

sample	BG3	BG4	BG5	BG13	BG14	BG22	GV8	GV10	MC3	MC5
N. an.	6	4	5	7	4	6	6	4	4	5
SiO_2	40.17 (6)	39.94 (28)	40.04 (37)	40.09 (43)	40.45 (8)	40.21 (3)	40.22 (15)	39.80 (14)	40.74 (40)	40.53 (10)
FeO	14.60 (11)	14.92 (95)	15.31 (85)	14.72 (29)	14.78 (4)	14.75 (9)	12.69 (5)	18.13 (16)	12.47 (29)	12.22 (12)
MgO	44.72 (8)	44.69 (69)	44.61 (64)	44.46 (48)	45.46 (15)	45.37 (16)	46.64 (13)	42.60 (40)	46.19 (96)	47.17 (2)
MnO	0.43 (1)	0.44 (5)	0.34 (8)	0.47 (5)	0.27 (2)	0.26 (6)	0.22 (1)	0.40 (3)	0.23 (3)	0.22 (3)
NiO	0.26 (1)	0.28 (0)	0.35 (12)	0.27 (10)	0.12 (2)	0.12 (1)	0.32 (1)	0.25 (5)	0.26 (1)	0.25 (2)
CaO	0.03 (1)	0.04 (1)	0.03 (0)	0.01 (1)	0.02 (1)	0.02 (1)	0.02 (1)	0.03 (1)	0.01 (1)	0.01 (0)
Total	100.21	100.28	100.69	100.04	101.12	100.74	100.11	101.22	99.91	100.41
Fo	0.85	0.84	0.84	0.84	0.85	0.85	0.87	0.81	0.87	0.87

N. an., number of analyses. Values in parentheses represent 2σ standard deviation of the last unit cited.

Table 7: Average major element compositions of plagioclase in pyroxenites

sample	BG4		BG5		BG13	GV8		GV10	GV12		MC3	MC5
site	core	rim	core	rim	core	core	rim	core	core	rim	core	core
N. an.	5	3	7	5	3	4	3	5	6	5	5	4
SiO_2	52.21 (97)	47.80 (31)	52.27 (51)	47.70 (5)	52.78 (57)	53.61 (60)	49.85 (6)	53.59 (63)	52.60 (60)	47.84 (3)	53.52 (31)	53.61 (40)
TiO_2	0.02 (2)	0.02 (0)	0.02 (2)	0.03 (2)	0.04 (1)	0.06 (6)	0.00	0.01 (1)	0.01 (2)	0.04 (1)	0.02 (2)	0.04 (5)
Al_2O_3	30.70 (61)	33.24 (17)	30.16 (20)	33.45 (11)	30.61 (45)	29.20 (43)	31.89 (4)	30.12 (41)	29.70 (46)	33.00 (13)	29.90 (31)	28.91 (22)
FeO	0.21 (10)	0.39 (8)	0.21 (6)	0.33 (15)	0.18 (2)	0.12 (1)	0.40 (4)	0.14 (3)	0.33 (15)	0.33 (10)	0.19 (4)	0.17 (7)
MgO	0.00	0.12 (2)	0.03 (3)	0.10 (7)	0,01 (1)	0.01 (1)	0.00	0.02 (1)	0.01 (1)	0.01 (1)	0.01 (1)	0.01 (1)
CaO	13.12 (16)	16.28 (21)	13.05 (16)	16.59 (15)	12.43 (37)	12.33 (17)	15.51 (8)	12.00 (41)	13.36 (36)	16.65 (7)	12.19 (66)	11.87 (60)
Na_2O	4.08 (12)	2.27 (10)	4.14 (13)	2.09 (7)	4.47 (20)	4.52 (14)	2.71 (11)	4.77 (23)	3.96 (20)	1.97 (5)	4.69 (44)	4.78 (37)
K_2O	0.02 (1)	0.01 (1)	0.00	0.00	0.05 (1)	0.01 (1)	0.01 (1)	0.02 (1)	0.03 (1)	0.02 (1)	0.02 (1)	0.02 (1)
Total	100.36	100.10	99.89	100.31	100.58	99.86	100.38	100.66	100.01	99.85	100.54	99.41
An	0.64	0.80	0.64	0.81	0.61	0.60	0.76	0.58	0.65	0.82	0.59	0.58

N. an., number of analyses. Values in parentheses represent 2σ standard deviation of the last unit cited.

Table 8: Representative major element compositions of amphibole in pyroxenites

sample	BG4		BG5		BG13		BG14	BG22	GV8		GV10		MC3		MC5	
	Ks	Ti-prg	Ti-prg	Ti-prg	Ks	Ks	Ks	Ti-prg	Ks	Ti-prg	Ks	Ti-prg	Ks	Ks	Ks	Ks
SiO_2	42.07	42.94	42.61	42.36	41.47	40.56	41.96	42.25	41.62	42.33	41.12	41.49	42.22	41.76	41.51	41.98
TiO_2	4.66	4.37	4.43	4.56	4.90	5.01	4.84	3.89	5.25	4.33	5.00	3.74	5.41	5.60	5.44	5.31
Al_2O_3	12.45	12.3	12.84	12.42	14.23	13.79	13.37	13.78	12.09	11.77	12.84	14.58	13.47	13.75	12.34	12.36
Cr_2O_3	0.53	0.68	1.1	0.57	0.67	0.74	0.56	0.53	0.21	0.22	0.28	0.28	0.54	0.57	0.27	0.62
FeO	6.9	6.68	6.93	6.73	5.92	6.10	6.47	7.01	6.29	6.11	8.01	7.51	5.50	5.25	5.25	5.10
MgO	15.66	15.78	15.06	15.5	15.47	15.10	15.06	15.31	15.22	15.84	14.75	14.75	15.75	15.39	15.50	15.61
MnO	0.22	0.25	0.07	0.19	0.15	0.24	0.11	0.15	0.08	0.08	0.20	0.08	0.12	0.09	0.10	0.08
CaO	11.78	11.76	12.18	11.48	12.02	11.89	11.82	11.94	11.69	11.88	11.92	11.81	11.89	11.96	11.75	11.55
Na_2O	3.88	3.44	2.91	3.68	2.86	3.28	3.42	3.27	3.24	3.13	3.37	3.42	3.54	3.47	3.39	3.61
K_2O	0.14	0.15	0.03	0.13	0.22	0.29	0.17	0.21	0.07	0.07	0.05	0.03	0.07	0.07	0.04	0.02
Total	98.29	98.35	98.16	97.62	97.91	97.00	97.77	98.34	95.76	95.76	97.54	97.69	98.51	97.92	95.59	96.25
Mg#	0.80	0.81	0.79	0.80	0.82	0.82	0.81	0.80	0.81	0.82	0.77	0.78	0.84	0.84	0.84	0.85

Ks = Kaersutite, Ti-prg = Titanian pargasite.

Table 9: Representative trace element compositions (ppm) of minerals in pyroxenites

sample	BG13							GV10		MC3		MC5	GV17	
mineral type	cpx porph	cpx porph	plag neobl	cpx neobl	amph neobl	amph neobl	cpx porph	cpx porph	cpx porph	cpx porph	cpx porph	cpx porph	cpx porph	cpx porph
Sc	38.2	65.3	0.827	127	244	192	59.5	42.4	162	58.4	98.8	71.7	86.5	36.8
V	516	535	0.803	557	1017	751	506	430	522	333	322	419	275	280
Sr	4.75	6.95	196	5.06	66.5	20.8	3.84	5.68	7.51	3.20	3.65	7.64	3.39	3.79
Y	26.5	82.5	0.538	41.1	63.7	49.6	43.4	38.5	97.4	34.9	62.3	51.6	22.8	14.9
Zr	25.9	44.9	0.054	54.8	75.9	58.7	33.1	51.4	77.0	38.2	39.8	44.7	37.2	25.9
Nb	0.154	0.094		0.106	9.24	4.98	0.058	0.095	0.027	0.128	0.1705	0.347	0.178	0.390
La	0.585	0.620	0.456	0.544	0.962	0.677	0.601	0.996	0.805	0.807	0.795	0.843	0.360	0.446
Ce	3.68	3.99	0.917	3.48	5.50	4.37	3.54	5.82	4.85	4.25	4.31	4.91	2.55	3.09
Pr	0.737	0.862	0.078	0.796	1.31	1.11	0.822	1.12	1.06	0.874	0.888	0.886	0.577	0.637
Nd	4.56	5.52	0.467	5.85	9.30	8.09	4.99	7.25	6.94	6.31	6.03	5.76	4.58	4.56
Sm	2.38	3.27		2.59	4.52	4.15	2.64	3.44	3.51	2.71	2.53	2.89	2.11	1.81
Eu	1.03	1.40	0.349	0.922	1.59	1.20	1.20	1.54	1.59	1.19	1.01	1.28	0.900	0.720
Gd	3.48	6.43	0.074	4.03	6.94	5.60	4.28	5.12	6.91	4.11	4.39	5.18	3.22	2.10
Tb	0.714	1.61	0.012	0.849	1.47	1.08	1.04	0.975	1.71	0.816	1.09	1.04	0.567	0.390
Dy	4.50	12.7	0.121	6.41	10.12	7.60	6.93	6.96	13.8	5.54	8.99	7.93	3.88	2.64
Ho	1.04	3.10	0.029	1.45	2.40	1.75	1.63	1.50	3.79	1.29	2.22	1.91	0.890	0.550
Er	2.87	9.94		4.08	6.64	5.06	4.54	4.26	11.4	3.68	7.58	5.43	2.42	1.56
Tm	0.417	1.59		0.617	0.980	0.785	0.685	0.650	1.81	0.542	1.28	0.899	0.390	0.238
Yb	2.81	14.2		4.16	6.83	5.08	4.90	4.34	14.1	3.70	9.65	6.83	2.98	1.66
Lu	0.327	2.04		0.596	1.007	0.657	0.626	0.501	1.80	0.594	1.41	0.880	0.414	0.237
Hf	0.523	1.02		1.24	2.68	2.24	1.01	1.54	2.25	0.827	0.910	0.927	0.621	0.662

sample	BG4		BG5	BG14		BG22		GV8			GV12		GV14	
mineral type	cpx porph	cpx porph	cpx porph	cpx porph	cpx porph	cpx porph	cpx porph	cpx porph	cpx porph	cpx porph	cpx porph	cpx porph	cpx porph	cpx porph
Sc	61.7	62.2	39.8	84.9	57.3	66.5	72.4	88	62	50.5	74	94	44	33
V	288	274	280	379	344	276	286	339	324	273	183	230	289	257
Sr	11.4	13.1	3.56	7.16	5.67	7.25	4.22	18.69	10.63	14.1	4.1	3.83	4.14	5.94
Y	24.6	24.9	24.3	36.1	21.1	27.0	43.5	28.53	22.53	20.0	8.44	23.31	11.71	8.35
Zr	29.4	27.6	30.9	47.3	30.6	33.6	49.8	54.6	44.9	33.2	7.90	18.2	43.3	28.3
Nb	0.495	0.638	0.500	0.286	0.435	0.595	0.628	0.105	0.270	0.275	0.061	0.287	0.186	0.251
La	0.692	0.738	0.782	0.579	0.587	0.761	0.788	1.34	1.62	1.56	0.124	0.274	0.698	0.896
Ce	3.58	3.74	3.99	3.86	3.85	3.68	4.45	7.74	6.98	7.28	0.577	1.31	4.62	4.47
Pr	0.649	0.656	0.775	0.821	0.780	0.722	0.874	1.375	1.233	1.14	0.150	0.273	0.878	0.852
Nd	4.15	4.08	5.55	5.70	5.08	4.75	6.25	7.12	6.91	6.55	1.28	2.11	6.20	5.44
Sm	1.85	1.86	2.02	2.76	2.20	2.18	3.13	3.10	2.51	2.31	0.647	1.32	2.15	2.17
Eu	0.803	0.813	0.863	1.066	0.949	0.947	1.23	1.20	1.06	1.07	0.243	0.371	1.01	0.742
Gd	2.86	2.85	3.06	3.87	2.56	3.11	4.70	4.55	3.11	2.82	1.20	2.68	3.13	1.86
Tb	0.550	0.570	0.591	0.848	0.529	0.638	1.05	0.772	0.672	0.607	0.230	0.590	0.489	0.321
Dy	3.96	3.90	3.97	6.17	3.82	4.29	7.12	5.28	4.20	3.73	1.66	4.06	2.90	1.57
Ho	0.890	0.890	0.965	1.36	0.823	0.968	1.65	1.11	0.848	0.755	0.353	0.899	0.463	0.378
Er	2.57	2.68	2.64	4.22	2.24	3.04	4.99	3.37	2.69	2.22	0.810	2.56	1.10	0.717
Tm	0.409	0.420	0.422	0.631	0.327	0.455	0.843	0.463	0.366	0.312	0.116	0.420	0.146	0.072
Yb	2.89	3.01	3.22	4.52	2.36	3.31	5.72	4.02	2.65	2.16	0.782	2.99	1.23	0.685
Lu	0.441	0.465	0.475	0.663	0.393	0.528	0.990	0.403	0.360	0.308	0.145	0.466	0.120	0.106
Hf	0.685	0.617	0.439	0.799	0.867	0.691	0.730	1.65	1.18	1.05	0.23	0.266	1.21	0.988

Abbreviations: cpx = clinopyroxene, plag = plagioclase, amph = amphibole.

Table 10: Temperature estimates for pyroxene porphyroblasts and neoblasts within pyroxenites

sample		T(°C)Ca-in-opx B&K(1990)	T(°C)Ca-in-opx Corrected*	T(°C)2-pyrox B&K(1990)	T(°C)2-pyrox Taylor(1998)
BG3	*porph*	986 ± 21	971	978 ± 33	939 ± 31
	neobl	856 ± 27	810	895 ± 36	826 ± 35
BG5	*porph*	1018 ± 19	1008	856 ± 38	839 ± 36
	neobl	868 ± 23	826	869 ± 42	833 ± 40
BG13	*porph*	1018 ± 32	1008	863 ± 29	841 ± 29
	neobl	891 ± 22	855	817 ± 44	768 ± 42
BG14	*porph*	986 ± 17	971	881 ± 36	830 ± 33
	neobl	880 ± 14	841	894 ± 41	828 ± 38
GV8	*porph*	1107 ± 28	1107	965 ± 21	942 ± 20
	neobl	887 ± 23	850	846 ± 38	797 ± 36
GV10	*porph*	1018 ± 21	1008	933 ± 35	913 ± 33
	neobl	830 ± 16	776	900 ± 31	862 ± 30
MC3	*porph*	986 ± 12	971	913 ± 25	873 ± 24
	neobl	880 ± 25	841	878 ± 33	794 ± 32
MC5	*porph*	932 ± 27	906	867 ± 24	845 ± 25
	neobl	891± 29	855	871 ± 26	791 ± 25

sample	T(°C)cpx N&T(2010) *porph*	*neobl*
BG3	927 ± 28	840 ± 32
BG4	957 ± 33	794 ± 21
BG5	828 ± 37	856 ± 41
BG13	819 ± 27	775 ± 38
BG14	830 ± 32	848 ± 36
BG22	936 ± 31	835 ± 33
GV8	924 ± 21	803 ± 31
GV10	934 ± 34	882 ± 31
GV12	953 ± 33	900 ± 28
GV14	907 ± 21	859 ± 17
GV17	1136 ± 19	989 ± 24
MC3	905 ± 23	814 ± 32
MC5	817 ± 25	808 ± 25

(*) correction of average T according to Nimis & Grutter (2010)

Table 11: Sm-Nd isotope data determined on bulk-rock, clinopyroxene and plagioclase from pyroxenites

	bulk rocks				clinopyroxenes				plagioclases			
sample	Sm (ppm)	Nd (ppm)	147Sm/144Nd^	143Nd/144Nd (±2σ x 10^6)†	Sm (ppm)	Nd (ppm)	147Sm/144Nd^	143Nd/144Nd (±2σ x 10^6)†	Sm (ppm)	Nd (ppm)	147Sm/144Nd^	143Nd/144Nd (±2σ x 10^6)†
BG13	0.946	1.586	0.3608	0.513383 ± 06	3.054	4.888	0.3778	0.513401 ± 07	0.086	0.195	0.2663	0.513272 ± 06
BG14	0.765	1.867	0.2478	0.513123 ± 06	1.992	4.426	0.2721	0.513155 ± 07	0.138	0.488	0.1714	0.513037 ± 06
GV8	0.757	2.029	0.2255	0.512984 ± 06	2.596	6.657	0.2358	0.512995 ± 09	0.250	0.812	0.1860	0.512939 ± 05
BG5					1.585	3.766	0.2545	0.513131 ± 09	0.038	0.202	0.1106	0.512959 ± 09

Note: All data by isotope dilution.

† Internal precision.

^Estimated error is 0.3%.

Table 12: Phase abundances of model spinel- and garnet-facies assemblages by mass balance

sample	BG3	BG4	BG5	BG13	BG14	BG22	GV8	GV10	GV12	GV14	GV17	MC3	MC5
spinel-facies assemblage(*):													
CPX	77	80	74	64	75	80	59	63	87	85	74	47	31
OPX	12	0	14	24	13	10	32	30	0	0	0	42	61
OL	0	11	0	0	0	0	0	0	0	0	9	0	0
SP	11	9	12	12	12	10	9	7	13	15	17	11	8
R2	0.15	0.21	0.27	0.18	0.23	0.22	0.21	0.16	0.24	0.33	0.41	0.16	0.18
garnet-facies assemblage(§):													
CPX	---	77	81	55	78	---	62	61	69	---	---	45	30
GNT	---	17	12	40	11	---	23	18	31	---	---	40	29
OPX	---	0	0	5	0	---	15	21	---	---	---	5	31
OL	---	0	0	0	0	---	0	0	---	---	---	10	10
SP	---	6	7	0	11	---	0	0	---	---	---	0	0
R2	---	0.57	0.61	0.35	0.45	---	0.45	0.55	0.56	---	---	0.35	0.48

(*) modal abundances obtained by mass balance calculation using bulk rock analyses and average mineral compositions measured on spinel-facies porphyroclasts in each sample.

(§) modal abundances obtained by mass balance calculation using bulk rock analyses and mineral compositions from garnet-bearing assemblages documented in selected orogenic garnet pyroxenites (see text and supplementary files for details).